FACULTY OF SCIENCE
UNIVERSITY OF COPENHAGEN

Master Thesis

Rasmus Westphal Rasmussen

Determination of the neutrino mixing angle θ_{23} octant and differentiation among flavour symmetries

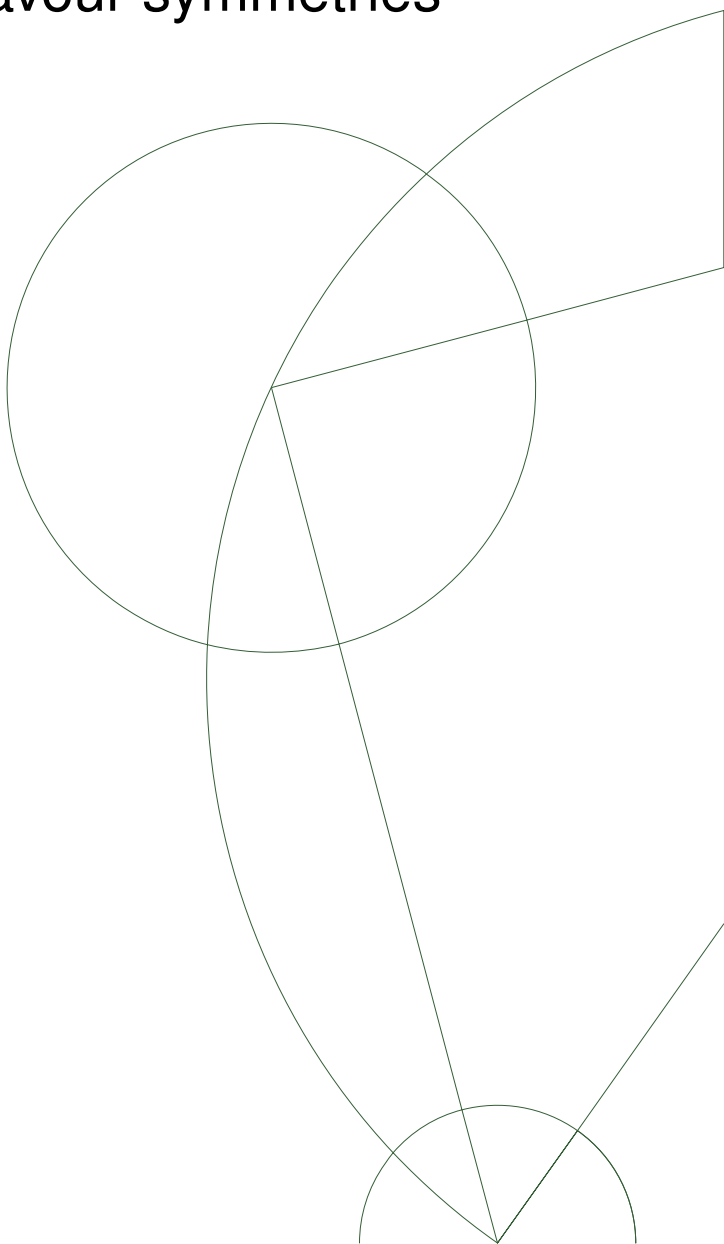

Academic supervision by Subir Sarkar

Friday, August 1st, 2014

1

Preface

1.1 Abstract

This thesis studies the potential/reach for the Proposed IceCube Next Generation Upgrade (PINGU) with respect to the determination of the octant of the atmospheric mixing angle θ_{23}. In the neutrino sector, this is one of the still unknown parameters which have to be determined by future experiments. Present measurements of θ_{23} are not precise enough to establish whether this mixing is maximal or not. If it is non-maximal, there are two solutions to the neutrino oscillation data in that θ_{23} can either be below or above 45 degrees, i.e. it lies in the first or second octant.

From Monte Carlo simulations the event rates of neutrinos in PINGU were calculated and a chi square fit was done, assuming the theoretical predicted event rates were fitted in the wrong octant of the atmospheric angle. This provides a way to constrain this mixing parameter. In turn this can potentially differentiate among various flavour symmetries which can underly the neutrino mixing matrix and thereby the oscillation parameters. By implementing multiple flavour symmetries in the simulations, a comparison of the sensitivities to the various models could be made. This in priciple provides a way to experimentally determine the flavour symmetry for neutrinos.

1.2 Acknowledgements

I want to thank Subir Sarkar for his guidance and helpful discussions. Without his supervision, this thesis would not have existed at all. He was so kind as to arrange a trip in November 2013 to Oxford where I had the opportunity to meet Graham Ross and Jim Talbert. I hope this is the start for future collaboration between Jim and myself. In June 2014, I had the privilege to join the PhD school at NBI where the topic was neutrinos. This was an interesting week and I met a lot of new people (mostly students, but also lecturers) and learned about new topics in neutrino physics.

Also, I should mention Poul H. Damgaard and Christine Hartmann with whom I have had a lot of discussions about physics and other related questions. A special thanks goes to the IceCube-PINGU group at the institute: Jason Koskinen, Michael Larson, Morten Medici and Joakim Sandroos plus Jenni Adams (who was here on sabbatical leave for a year) for letting me participate in the weekly journal club. A big thanks goes to Jochen Heinrich who helped me with LaTeX issues and the layout of the thesis and presentation. Last but not least, thanks to all the people at NBI who I have met daily, at coffee/tea breaks, lunches etc.

I want to dedicate this thesis to my beloved friend, Anne-Lise Westphal Skovstrøm. She died the 1st June 2014 (just 2.5 month before the thesis defense) which was all so sudden. I was devastated to hear about her death and it was a difficult time for me. I would have loved it for her to be at my defense and see me graduate. I will always cherish the memories of her and I will always miss her.

My family was supporting and loving throughout the thesis period and I am glad for them always standing by my side.

Contents

1 Preface **iii**
1.1 Abstract . . . iii
1.2 Acknowledgements . . . iii

Contents **v**

2 Introduction **1**

3 The Standard Model of particle physics **3**
3.1 The V-A theory of the weak interaction . . . 3
3.2 Gauge theories . . . 5
3.2.1 The gauge principle . . . 5
3.2.2 Global symmetries . . . 5
3.2.3 Local (=gauge) symmetries . . . 6
3.2.4 Non-Abelian gauge theories (=Yang-Mills theories) . . . 7
3.3 Renormalization . . . 8
3.4 Effective field theory . . . 11
3.5 The Glashow-Weinberg-Salam model . . . 14
3.5.1 Spontaneous symmetry breaking and the Higgs mechanism . . . 17
3.5.2 Number of neutrino flavours from the width of the Z^0 . . . 19

4 Neutrino mass: Beyond the Standard Model **23**
4.1 Helicity and chirality . . . 23
4.2 Charge conjugation . . . 25
4.3 Parity transformation . . . 26
4.4 Dirac and Majorana mass terms . . . 26
4.5 See-saw mechanism . . . 30
4.5.1 The type I see-saw mechanism . . . 31
4.5.2 The type II see-saw mechanism . . . 31
4.5.3 The type III see-saw mechanism . . . 31

5 Neutrino oscillations **33**
5.1 General formalism . . . 33
5.2 CP and T violation in neutrino oscillations . . . 35
5.3 Oscillations with two flavours . . . 35
5.4 The case for three flavours . . . 36
5.5 Experimental consideration . . . 39
5.6 Neutrino mass hierarchy, θ_{23} octant and matter effects . . . 40
5.6.1 Neutrino oscillation in matter . . . 41
5.6.2 Evolution equation . . . 41

5.6.3 Constant density case 43

6 Atmospheric neutrinos **45**
6.1 Cosmic rays 45
6.2 Interactions within the atmosphere 46
6.3 Neutrino cross-section 49
6.4 Experimental consideration 51
6.5 The Earth's matter density profile 51
6.6 Atmospheric neutrino oscillations 52

7 Sensitivity of PINGU to the octant of θ_{23} **55**
7.1 Earth matter effects in oscillation probabilities 55
7.2 Description of numerical analysis 56
7.3 Neutrino flux 57
7.4 GENIE cross-section 58
7.5 Contour plots from global data 58
7.6 Event rates 59
7.7 Sensitivity to the octant of the atmospheric angle θ_{23} 61
7.8 Systematic uncertainties 64
7.9 Another relevant systematic uncertainty 64

8 Impact of different flavour symmetries on the analysis **69**
8.1 Group theory 69
8.1.1 Group presentation 70
8.1.2 Character table 70
8.1.3 Kronecker products and Chebsch-Gordan coefficients 71
8.1.4 Finite groups with triplet representations 73
8.2 Flavour symmetries 74
8.2.1 A μ-τ symmetric mass matrix 75
8.2.2 C_3 and $S_2 \times S_2$ symmetry 75
8.2.3 Tetrahedral symmetry A_4 76
8.3 Comparison between flavour symmetries 78
8.4 Flavour symmetry comparison over multiple of years 80

9 Conclusion **85**

Appendices **87**

Appendix A Plots of octant sensitivity **89**

Appendix B Plots of systematic uncertainties **93**

Appendix C Plots including particle identification uncertainty **97**

Appendix D Introduction to A_4 **101**

Appendix E Plots of flavour symmetries **105**

Appendix F Plots of flavour symmetries over time **111**

Bibliography **117**

2

Introduction

The neutrino was proposed by W. Pauli in 1930 [1] and first detected by C. Cowan and F. Reines in 1956 [2]. Later the solar neutrino deficit [3], the atmospheric neutrino anomaly [4], and other neutrino oscillation results [5] have revealed that the neutrino masses are non-zero. However essential questions concerning the absolute scale of their masses, their type (whether Dirac or Majorana), etc. still remain unanswered.

Besides the reactor [6], Gallium [[7], [8]] and a few other neutrino anomalies, the available neutrino data can be explained within the phenomenological model of three light neutrinos with two mass splittings (squared mass differences): $\Delta m_{21} \sim 10^{-5}\,\mathrm{eV}^2$ and $|\Delta m_{31}| \sim 10^{-3}\,\mathrm{eV}^2$ [5]. We call it the conventional neutrino theory (CNT). In case of Majorana (Dirac) neutrinos the masses and mixings are generically parameterized in CNT by 9 (7) free parameters: 3 masses, 3 mixing angles and 3 phases (1 phase).

The latest set of data from the reactor-based experiments Daya Bay [9], RENO [10] and Double Chooz [11] have confirmed beyond all doubt what the accelerator-based experiments T2K [12] and MINOS [13] had indicated earlier - namely the value of the neutrino mixing parameter $\sin^2(2\theta_{13}) \simeq 0.1$. The implications of this discovery has far reaching implications in neutrino physics. On the phenomenological front, this opens up the possibility for the determination of the two missing links in the neutrino oscillation physics, namely (i) the magnitude of CP violation in the lepton sector, and (ii) the sign of Δm^2_{31}, i.e. the neutrino 'mass hierarchy'. Next generation neutrino oscillation experiments are being proposed to elucidate these two remaining issues. The optimal design of such experiments will determine just how well they can measure CP violation and the neutrino mass hierarchy, given that we now know that θ_{13} is much larger than previously thought. The fact that the sensitivity of the proposed experiment to one of these parameters could be restricted by the uncertainty of the other parameter makes the designing of the experiments all the more challenging.

Of the two unknowns mentioned above, measurement of CP violation is trickier for a variety of reasons. CP violation in neutrino oscillations is necessarily a sub-leading effect and is expected to be in the θ_{13}-driven appearance channel, $P(\nu_\mu \to \nu_e)$. Indeed, the CP phase δ_{CP} would be unphysical and hard to determine if θ_{13} were zero. However, the fact that θ_{13} has turned to be relatively large might prove counter-productive for the CP violation searches. Because CP violation effects in the appearance channel become even more sub-dominant compared to the main CP independent θ_{13} driven oscillations for such large values of θ_{13}. This makes the latter an irreducible background, thereby decreasing thereby the sensitivity of the experiment for CP searches [14]. The uncertainty regarding the neutrino mass hierarchy introduces another limitation on these experiments through the δ_{CP}-mass hierarchy parameter degeneracy, further deteriorating the sensitivity of the experiment to the CP phase.

Measurements of the neutrino mass hierarchy on the other hand certainly becomes easier as the value of θ_{13} increases. This parameter is expected to be measured using the effects of propagation through the Earth on neutrino oscillations. The Earth matter

effect increases monotonically with the value of θ_{13}, making their detection in terrestrial experiments easier for larger θ_{13}. The atmospheric neutrino experiments could play a crucial role in the field of neutrino physics in this regard. The possibility of measuring the neutrino mass hierarchy in atmospheric neutrino experiments has been widely considered in the literature. Upcoming detectors for atmospheric neutrinos include the magnetized Iron CALorimeter detector at the India-based Neutrino Observatory (ICAL@INO), the megaton-class water Cherenkov detectors such as the proposed Hyper-Kamiokande project, large liquid argon detectors, as well as the giant ice detector PINGU (Proposed IceCube Next Generation Upgrade).

PINGU [15] has been proposed as a low energy extension of the already existing and successfully running IceCube detector. While the energy threshold of the full IceCube detector is 100 GeV, PINGU is envisioned to have an energy threshold of a few GeV, thereby allowing it to function as a low energy atmospheric neutrino experiment, with an effective fiducial mass in the multi-megaton range. The plan is to increase the number of strings, increasing the optical module density, hence increasing the photo-coverage of the region. This will reduce the energy threshold for the detection of various particles. The large fiducial mass gives PINGU an edge over other competitive experiments due to the statistical amount of neutrino events.

Amongst the other issues in neutrino physics that remains to be probed, is the determination of the octant of θ_{23} mixing angle, in case it is different from maximal. Various ways have been suggested in the literature to determine the octant of θ_{23} in the current and next generation neutrino oscillation experiments. One way is to combine the data from reactor experiments with the ν_e-appearance data from conventional accelerator experiments [16]. The reactor experiments return a pure measurement of the mixing angle $\sin^2(2\theta_{13})$, while the ν_e-appearance data from conventional accelerator experiments measure the combination $\sin^2(\theta_{23})\sin^2(2\theta_{13})$, at leading order. Using this combined analysis, one could then extract information on the octant of θ_{23}.

Another approach studied in the literature has been to combine the ν_e-appearance channel in long baseline experiments with the ν_μ-disappearance channel [[17], [18]]. The upshot of this reasoning is that the best-fit θ_{23} preferred by the appearance channel is different from the best-fit θ_{23} favored by the disappearance channel. This generates a synergy between the two data sets in the long baseline experiment, leading to an octant sensitivity.

The third way is to use Δm^2_{21} dependent terms in the oscillation probability, which depends on either $\sin^2(\theta_{23})$ or $\cos^2(\theta_{23})$, leading to θ_{23} octant sensitivity. This was shown in the context of sub-GeV ν_e-events from atmospheric neutrinos at a water Cherenkov experiment like Super-Kamiokande where the Δm^2_{21} driven oscillatory terms brings in an octant of θ_{23} dependence in the low energy electron event sample. Finally, one can use the octant of θ_{23} dependence in the Earth matter effects in the $P(\nu_\mu \to \nu_\mu)$ channel to get a measure on this parameter. In particular, the issue of determining the octant of θ_{23} was briefly discussed in [19].

Disclaimer: I have used Mathematica to plot various figures. Mathematica has the tendency to squeeze words together in the plots as I am exporting them to pdf causing spelling errors.

3

The Standard Model of particle physics

An important feature of the Standard Model (SM) is that "it works": It is consistent with, or verified by, all available data, with only a few compelling evidence for physics beyond. Secondly, it is a unified description, in terms of "gauge theories" of all the interactions of known particles (except gravity). The joint description of the electromagnetic and the weak interaction by a single theory certainly is one of major achievements of the physical science in this century. The model proposed by Glashow, Salam and Weinberg in the middle sixties has been extensively tested during the last 40 years. In this chapter the basic features of the current Standard Model of elementary particle physics are discussed. As the subject concerns neutrinos, the main focus of this chapter will consider the electroweak interaction.

3.1 The V-A theory of the weak interaction

Historically, the first theoretical description of the weak interaction as an explanation of the β-decay was given in the classical paper by Fermi [20]. Nowadays, we rate this as a low-energy limit of the Glashow-Weinberg-Salam (GWS) model but it is still valid to describe most of the weak processes. Fermi chose an ansatz quite similar to that in quantum electrodynamics (QED). In QED, the interaction of a proton with an electromagnetic field A_μ is described by a Hamiltonian

$$H_{\text{em}} = e \int d^3x \bar{p}(x)\gamma^\mu p(x) A_\mu(x) \tag{3.1.1}$$

where $p(x)$ is the Dirac field-operator of the proton. In analogy, Fermi introduced an interaction Hamiltonian for β-decay:

$$H_\beta = \frac{G_F}{\sqrt{2}} \int d^3x (\bar{p}(x)\gamma^\mu n(x))(\bar{e}(x)\gamma_\mu \nu(x)) + h.c. \tag{3.1.2}$$

The new fundamental constant G_F is called the Fermi constant which is determined experimentally to be $G_F = 1.16637(1) \cdot 10^{-5}$ GeV^{-2}. If we stay with a four-fermion interaction, the following question arises: How many Lorentz-invariant combinations of the two currents involved can be built? The weak Hamiltonian H_β can be deduced from the Lagrangian $\mathcal{L}$:

$$H_\beta = -\int d^3x \mathcal{L}(x) \tag{3.1.3}$$

The most general Lagrangian for β-decay, which transforms as a scalar under a Lorentz transformation, is [21]

$$\mathcal{L}(x) = \sum_{j=1}^{5} [g_j \bar{p}(x) O_j n(x) \bar{e}(x) O'_j \nu(x) + g'_j \bar{p}(x) O_j n(x) \bar{e}(x) O'_j \gamma_5 \nu(x)] + h.c. \tag{3.1.4}$$

Operator	Transformation properties($\Psi_f O \Psi_i$)	Representation with γ matrices
O_S (S)	scalar	$\mathbb{1}$
O_V (V)	vector	γ_μ
O_T (T)	tensor	$\gamma_\mu\gamma_\nu - \gamma_\nu\gamma_\mu$
O_A (A)	axial vector	$i\gamma_\mu\gamma_5$
O_P (P)	pseudo-scalar	γ_5

Table 3.1.1: *Possible operators and their transformation properties as well as their representation.*

with g_j, g'_j as arbitrary complex coupling constants and O_j, O'_j as operators. The possible invariants for the operators O are listed in table 3.1.1. The kind of coupling realized in Nature was revealed by investigating allowed β-decay transitions. From the absence of Fierz interference terms, it could be concluded that Fermi transitions are either of S or V type, while Gamow-Teller transitions could only be due to T or A type operators. P-type operators do not permit allowed transitions at all. After the discovery of parity violation, the measurement of electron-neutrino angular correlations in β-decay and the Goldhaber experiment, it became clear that the combination $\gamma_\mu(1-\gamma_5)$ represented all the data accurately. This is the (V-A) structure of weak interactions. After losing its leading role as a tool for probing weak interactions, current investigations of nuclear β-decay are used for searches S- and T-type contributions motivated by theories beyond the Standard Model and searches for a non-vanishing rest mass of the neutrino. Models with charged Higgs particles, leptoquarks and supersymmetry might lead to such S, T contributions. In summary, classical β-decay can be written in the form of two currents J (current-current coupling)

$$\mathcal{L}(x) = \frac{G_F}{\sqrt{2}} J_L \cdot J_H \tag{3.1.5}$$

where the leptonic current is given by (e, ν as spinor fields)

$$J_L = \bar{e}(x)\gamma_\mu(1-\gamma_5)\nu(x) \tag{3.1.6}$$

and the hadronic current by (using u, d quarks instead of proton and neutron)

$$J_H = \bar{u}(x)\gamma^\mu(1-\gamma_5)d(x). \tag{3.1.7}$$

As we go from the quark level to nucleons, eq. 3.1.7 must be rewritten due to renormalization effects in strong interactions as:

$$J_H = \bar{p}(x)\gamma^\mu(g_V - g_A\gamma_5)n(x) \tag{3.1.8}$$

The coupling constants G_F, $g_V = I_W^3 - 2\sin^2(\theta_W)Q_f$ and $g_A = I_W^3$, where I_W^3 and Q_f are, respectively, the third component of the weak isospin and the charge of fermions. Measurements of G_F in muon decay are in good agreement with those in nuclear β-decay and lead to the concept of common current couplings (lepton universality), also justified in measurements of τ-decays. The total leptonic current is

$$J_L = J_e + J_\mu + J_\tau \tag{3.1.9}$$

each of them having the form of eq. 3.1.6. The formalism allows most of the observed weak interactions to be described. It contains maximal parity violation, lepton universality and describes charged current interactions. How this picture is modified and embedded in the current understanding of gauge theories will be discussed next

3.2 Gauge theories

All modern theories of elementary particles are gauge theories. We will attempt to indicate the fundamental characteristics of such theories without going into the details of a complete presentation.

3.2.1 The gauge principle

The gauge principle can be explained by the example of classical electrodynamics. It is based on the Maxwell equations and the electric and magnetic fields - measureable quantities which can be represented as the components of the field-strength tensor $F_{\mu\nu} = \partial_\mu A_\nu - \partial_\nu A_\mu$. Here the four-potential A_μ is given by $A_\mu = (\phi, \boldsymbol{A})$, and the field strengths are derived from it as $E = \nabla\phi - \partial_t \boldsymbol{A}$ and $B = \nabla \times \boldsymbol{A}$. If $\rho(t, \boldsymbol{x})$ is a well-behaved, differentiable real function, it can be seen that under a transformation of the potential such as

$$\phi'(t, \boldsymbol{x}) = \phi(t, \boldsymbol{x}) + \partial_t \rho(t, \boldsymbol{x}) \tag{3.2.1}$$

$$\boldsymbol{A}'(t, \boldsymbol{x}) = \boldsymbol{A}(t, \boldsymbol{x}) + \nabla\rho(t, \boldsymbol{x}) \tag{3.2.2}$$

all observable quantities remain invariant. The fixing of ϕ and $\boldsymbol{A}$ to particular values in order to simplify the equations of motion is called *fixing the gauge*. In gauge theories, this gauge freedom for certain quantities is raised to a fundamental principle. The existence and structure of interactions is determined by the demand for such gauge-fixable but physically undetermined quantities. The inner structure of the gauge transformation is specified through a symmetry group. As mentioned before, symmetries and behavior under symmetry operations play a crucial role and will be considered next.

3.2.2 Global symmetries

Internal symmetries can be subdivided into discrete and continuous symmetries. We will concentrate on continuous symmetries. In quantum mechanics a physical state is described by a wavefunction $\psi(\boldsymbol{x}, t)$. However, only the modulus squared appears as a measurable quantity. This means that as well as $\psi(\boldsymbol{x}, t)$ the functions

$$\psi'(\boldsymbol{x}, t) = e^{i\alpha}\psi(\boldsymbol{x}, t) \tag{3.2.3}$$

are also solutions of the Schrödinger equation, where α is a real (space and time independent) function. This is called a *global symmetry* and relates to the space and time independence of α. Consider the wavefunction of a charged particle such as the electron. The relativistic equation of motion is the Dirac equation:

$$(i\gamma^\mu\partial_\mu - m)\psi_e(\boldsymbol{x}, t) = 0 \tag{3.2.4}$$

The invariance under the global transformation

$$\psi_e'(\boldsymbol{x}, t) = e^{ie\alpha}\psi_e(\boldsymbol{x}, t) \tag{3.2.5}$$

where e is a constant (for example, the electric charge) is clear

$$e^{ie\alpha} i\gamma^\mu\partial_\mu\psi_e(\boldsymbol{x}, t) = e^{ie\alpha} m\psi_e(\boldsymbol{x}, t) \tag{3.2.6}$$

$$i\gamma^\mu\partial_\mu e^{ie\alpha}\psi_e(\boldsymbol{x}, t) = me^{ie\alpha}\psi_e(\boldsymbol{x}, t) \tag{3.2.7}$$

$$i\gamma^\mu \partial_\mu \psi'_e(\boldsymbol{x}, t) = m\psi'_e(\boldsymbol{x}, t). \tag{3.2.8}$$

Instead of discussing symmetries of the equations of motion, the Lagrangian $\mathcal{L}$ is often used. The equations of motion of a theory can be derived from the Lagrangian $\mathcal{L}(\phi, \partial_\mu \phi)$ with the help of the principle of least action [22]. For example, consider a real scalar field $\phi(x)$. Its free Lagrangian is:

$$\mathcal{L}(\phi, \partial_\mu \phi) = \frac{1}{2}\left(\partial_\mu \phi \partial^\mu \phi - m^2 \phi^2\right) \tag{3.2.9}$$

From the requirement that the action integral $\mathcal{S}$ is stationary

$$\delta \mathcal{S}[x] = 0 \quad \text{with} \quad \mathcal{S}[x] = \int \mathcal{L}(\phi, \partial_\mu \phi) dx \tag{3.2.10}$$

the equations of motion can be obtained

$$\partial_\alpha \frac{\partial \mathcal{L}}{\partial(\partial_\alpha \phi)} - \frac{\partial \mathcal{L}}{\partial \phi} = 0. \tag{3.2.11}$$

The Lagrangian clearly displays certain symmetries of the theory. In general, it can be shown that the invariance of the field $\phi(x)$ under certain symmetry transformations results in the conservation of a four-current:

$$\partial_\alpha \mathcal{J}^\alpha = \partial_\alpha \left(\frac{\partial \mathcal{L}}{\partial(\partial_\alpha \phi)} \delta\phi \right) = 0 \tag{3.2.12}$$

This is generally known as *Noether's theorem*. Using this expression, time, translation and rotation invariance imply the conservation of energy, momentum and angular momentum respectively. We proceed to consider local symmetries, in which α in eq. 3.2.3 is no longer a constant function but shows a space and time dependence.

3.2.3 Local (=gauge) symmetries

If the requirement for space and time independence of α is dropped, the symmetry becomes a local symmetry. It is obvious that under transformations such as

$$\psi'_e(x) = e^{ie\alpha(x)} \psi_e(x) \tag{3.2.13}$$

the Dirac equation 3.2.4 does not remain invariant

$$\begin{aligned} \left(i\gamma^\mu \partial_\mu - m\right) \psi'_e(x) &= e^{ie\alpha(x)} \left[(i\gamma^\mu \partial_\mu - m)\psi_e(x) + e(\partial_\mu \alpha(x))\gamma^\mu \psi_e(x)\right] \\ &= e(\partial_\mu \alpha(x))\gamma^\mu \psi'_e(x) \neq 0. \end{aligned} \tag{3.2.14}$$

The field $\psi'_e(x)$ is, therefore, not a solution of the free Dirac equation. If it were possible to compensate the additional term, the original invariance could be restored. This can be achieved by introducing a gauge field A_μ, which transforms itself in such a way that it compensates for the extra term. In order to achieve this, it is necessary to introduce a covariant derivative D_μ:

$$D_\mu = \partial_\mu - ieA_\mu \tag{3.2.15}$$

The invariance can be restored if all partial derivatives ∂_μ are replaced by the covariant derivative D_μ. The Dirac equation becomes:

$$i\gamma^\mu D_\mu \psi_e(x) = i\gamma^\mu (\partial_\mu - ieA_\mu)\psi_e(x) = m\psi_e(x) \tag{3.2.16}$$

If one uses the transformed field $\psi'_e(x)$, it is easy to see that the original invariance of the Dirac equation can be restored if the gauge field transforms itself according to:

$$A_\mu \rightarrow A_\mu + \partial_\mu \alpha(x) \tag{3.2.17}$$

The equations 3.2.13 and 3.2.17 describe the transformation of the wavefunction and the gauge field. They are called *gauge transformations*. The whole of electrodynamics can be described in this way as a consequence of the invariance of the Lagrangian $\mathcal{L}$ or, equivalently, the equations of motion under phase transformations $e^{ie\alpha(x)}$. The resulting conserved quantity is the electric charge, e. The corresponding theory is called quantum electrodynamics (QED) and, as a result of its enormous success, it has become a paradigm of a gauge theory.

In the transition to classical physics, the gauge field A_μ becomes the classical vector potential of electrodynamics. The gauge field can be associated with the photon, which takes over the role of an exchange particle. It is found that generally in all gauge theories the gauge fields have to be massless. This is logical because a photon mass term would be proportional to $m_\gamma^2 A_\mu A^\mu$, which is obviously not invariant. Any required masses have to be built in subsequently. The case discussed here corresponds to the gauge theoretical treatment of electrodynamcis. Group-theoretically, the multiplication with a phase factor can be described by a unitary transformation, in this case the U(1) group. It has the unity operator as generator. The gauge principle can easily be generalized for Abelian gauge groups, i.e. groups whose generators commute with each other. It becomes somewhat more complex in the case of non-Abelian groups, as we will see in the next section

3.2.4 Non-Abelian gauge theories (=Yang-Mills theories)

Non-Abelian means that the generators of the groups no longer commute, but are subject to certain commutator relations which constructs non-Abelian gauge theories. One example for commutator relations are the Pauli spin matrices σ_i

$$[\sigma_i, \sigma_j] = 2i\sigma_k \tag{3.2.18}$$

which act as generators for the SU(2) group. Generally SU(N) groups possess $N^2 - 1$ generators. A representation of the SU(2) group is all unitary 2×2 matrices with determinant +1. Consider the electron and neutrino as an example. Apart from their electric charge and their mass these two particles behave identically with respect to the weak interaction, and one can imagine transformations

$$\begin{pmatrix} \psi_e(x) \\ \psi_\nu(x) \end{pmatrix}' = U(x) \begin{pmatrix} \psi_e(x) \\ \psi_\nu(x) \end{pmatrix} \tag{3.2.19}$$

where the transformation can be

$$U(a_1, a_2, a_3) = e^{i\frac{1}{2}(a_1\sigma_1 + a_2\sigma_2 + a_3\sigma_3)} = e^{i\frac{1}{2}\boldsymbol{a}(x)\boldsymbol{\sigma}}. \tag{3.2.20}$$

The particles are generally arranged in multiplets of the corresponding group (in eq. 3.2.19 they are arranged as doublets). Considering the Dirac equation and substituting a covariant derivative of the normal derivative by introducing a gauge field $\boldsymbol{W}_\mu(x)$ and a quantum number g in analogy to eq. 3.2.15

$$D_\mu = \partial_\mu + \frac{ig}{2}\boldsymbol{W}_\mu(x) \cdot \boldsymbol{\sigma} \tag{3.2.21}$$

does *not* lead to gauge invariance. The gauge field $\boldsymbol{W}_\mu(x)$ also needs to transform in addition to the introduction of the covariant derivative to have gauge invariance. However,

because of the non-commutation of the generators, an additional term results, an effect which did not appear in the electromagnetic interaction. Only transformations of the gauge fields as

$$\boldsymbol{W}'_\mu = \boldsymbol{W}_\mu + \frac{1}{g}\partial_\mu \boldsymbol{a}(x) - \boldsymbol{W}_\mu \times \boldsymbol{a}(x) \tag{3.2.22}$$

supply the desired invariance (note the difference compared with eq. 3.2.17). The non-commutation of the generators causes the exchange particles to carry 'charge' themselves (contrary to the case of the photon, which does not carry electric charge) because of this additional term. Among other consequences, this results in a self-coupling of the exchange fields.

3.3 Renormalization

When introducing loops in a quantum field theory, they most likely are divergent and more importantly, they might not be normalizable. In a renormalizable quantum field theory, however, an amplitude involving divergent diagrams can get a finite result through renormalization. The renormalization is done using regulators to obtain the physical masses and coupling constants, that will not depend on these regulators. The resulting expression for the amplitude is then finite for the cutoff $\Lambda \to \infty$. In a ϕ^4 theory, the Lagrangian is defined as:

$$\mathcal{L}_0 = \frac{1}{2}(\partial_\mu \phi)^2 - \frac{1}{2}m_0^2\phi^2 - \frac{\lambda_0}{4!}\phi^4 \tag{3.3.1}$$

We now write m_0 and λ_0 as the bare mass and coupling constant, not the values measured in experiments. Since the theory is invariant under $\phi \to -\phi$, all amplitudes with an odd number of external legs vanish. The only divergent amplitudes are therefore

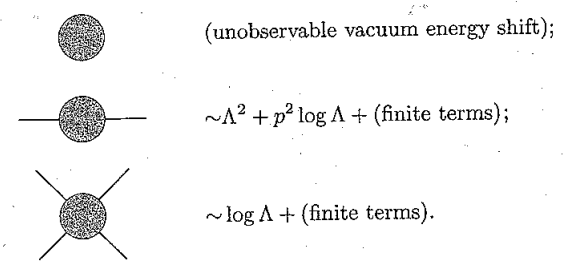

Ignoring the vacuum diagram, these amplitudes contain three infinite constants. Our goal is to absorb these constants into the three unobservable parameters of the theory: The bare mass, the bare coupling constant and the field strength. To accomplish this goal, it is convenient to reformulate the perturbation expansion so that these unobservable quantities do not appear explicitly in the Feynman rules. First we will eliminate the shift in the field strength. The exact two-point function has the form

$$\int d^4x \langle\Omega|T\phi(x)\phi(0)|\Omega\rangle e^{ip\cdot x} = \frac{iZ}{p^2 - m^2} + (\text{terms regular at } p^2 = m^2) \tag{3.3.2}$$

where m is the physical mass. We can eliminate the awkward residue Z from the equation by rescaling the field:

$$\phi = Z^{1/2}\phi_r \tag{3.3.3}$$

This transformation changes the values of correlation functions by a factor of $Z^{-1/2}$ for each field. The Lagrangian is much uglier after the rescaling:

$$\mathcal{L} = \frac{1}{2}Z(\partial_\mu \phi_r)^2 - \frac{1}{2}m_0^2 Z\phi_r^2 - \frac{\lambda_0}{4!}Z^2\phi_r^4 \tag{3.3.4}$$

The bare mass and coupling constant still appear in $\mathcal{L}$, but they can be eliminated as follows. Define

$$\delta_Z = Z - 1 \quad \delta_m = m_0^2 Z - m^2 \quad \delta_\lambda = \lambda_0 Z^2 - \lambda \tag{3.3.5}$$

where m and λ are the physically measured mass and coupling constant. Then the Lagrangian becomes:

$$\mathcal{L} = \frac{1}{2}(\partial_\mu \phi_r)^2 - \frac{1}{2}m^2\phi_r^2 - \frac{\lambda}{4!}\phi_r^4 + \frac{1}{2}\delta_Z(\partial_\mu\phi_r)^2 - \frac{1}{2}\delta_m\phi_r^2 - \frac{\delta_\lambda}{4!}\phi_r^4 \tag{3.3.6}$$

The first three terms now looks like the familiar ϕ^4-theory Lagrangian, but is written in terms of the physical mass and coupling. The terms afterwards, known as *counterterms*, have absorbed the infinite but unobservable shifts between the bare parameters and the physical parameters. It is tempting to say that we have "added" these counterterms to the Lagrangian, but in fact we have merely split each term into two pieces. The definition in eq. 3.3.5 are not useful unless we give precise definitions of the physical mass and coupling constant. Equation 3.3.2 defines m^2 as the location of the pole in the propagator. There is no obviously best definition of λ, but a perfectly good suggestion would be obtained by setting λ equal to the magnitude of the scattering amplitude at zero momentum. Thus we have the two defining relations:

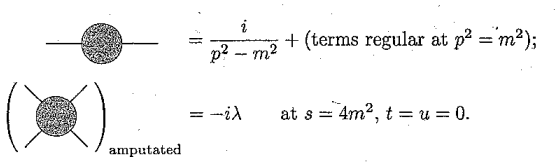

These equations are called *renomarlization conditions*. Our new Lagrangian gives a new set of Feynman rules. The propagator and the first vertex comes from the first few terms in eq. 3.3.6, and are identical to the old rules except for the appearance of the physical mass and coupling in place of the bare values. The counterterms give two vertices. We can use these new Feynman rules to compute any amplitude in ϕ^4 theory. The procedure is as follows. Compute the desired amplitude as the sum of all possible diagrams created from the propagator and vertices. The loop integrals in the diagrams will often diverge, so one must introduce a regulator. The result of this computation will be a function of the three unknown parameters δ_Z, δ_m and δ_λ. Adjust (or "renormalize") these three parameters as necessary to maintain the renormalization conditions. After this adjustment, the expression for the amplitude should be finite and independent of the regulator. To make more sense of the renormalization procedure, let us carry out explicitly at the one-loop level. First consider the basic two-particle scattering amplitude:

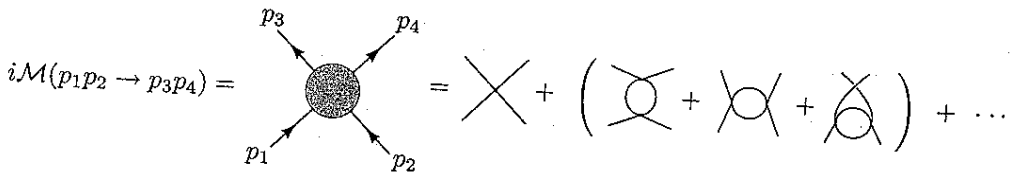

If we define $p = p_1 + p_2$, then the second diagram is:

$$\frac{(-i\lambda)^2}{2}\int \frac{d^4k}{(2\pi)^4}\frac{i}{k^2 - m^2}\frac{i}{(k+p)^2 - m^2} \equiv (-i\lambda)^2 \cdot iV(p^2) \tag{3.3.7}$$

Note that p^2 is equal to the Mandelstam variable s. The next two diagrams are identical, except that s will be replaced by t and u. The entire amplitude is therefore:

$$i\mathcal{M} = -i\lambda + (-i\lambda)^2[iV(s) + iV(t) + iV(u)] - i\delta_\lambda \tag{3.3.8}$$

According to our renormalization conditions, this amplitude should equal $-i\lambda$ at $s = 4m^2$ and $t = u = 0$. We must therefore set:

$$\delta_\lambda = -\lambda^2[V(4m^2) + 2V(0)] \tag{3.3.9}$$

We can compute $V(p^2)$ explicitly using dimensional regularization. Introduce a Feynman parameter, shift the integration variable, rotate to Euclidian space and perform the momentum integral. We obtain

$$\begin{aligned} V(p^2) &= \frac{i}{2}\int_0^1 dx \int \frac{d^dk}{(2\pi)^d}\frac{1}{(k^2+2xk\cdot p + xp^2 - m^2)^2} \\ &= \frac{i}{2}\int_0^1 dx \int \frac{d^d\ell}{(2\pi)^d}\frac{1}{(\ell^2 + x(1-x)p^2 - m^2)^2} \qquad (\ell = k + xp) \\ &= -\frac{1}{2}\int_0^1 dx \int \frac{d^d\ell_E}{(2\pi)^d}\frac{1}{(\ell_E^2 + x(1-x)p^2 + m^2)^2} \qquad (\ell_E^0 = -i\ell^0) \\ &= -\frac{1}{2}\int_0^1 dx \frac{\Gamma(2-d/2)}{(4\pi)^{d/2}}\frac{1}{(m^2 - x(1-x)p^2)^{2-d/2}} \\ &\xrightarrow{d\to 4} -\frac{1}{32\pi^2}\int_0^1 dx \left(\frac{2}{\epsilon} - \gamma + \log(4\pi) - \log(m^2 - x(1-x)p^2)\right) \end{aligned} \tag{3.3.10}$$

where $\epsilon = 4 - d$. The shift in the coupling constant is therefore:

$$\begin{aligned} \delta_\lambda &= \frac{\lambda^2}{2}\frac{\Gamma(2-d/2)}{(4\pi)^{d/2}}\int_0^1 dx \left(\frac{1}{(m^2 - x(1-x)4m^2)^{2-d/2}} + \frac{2}{(m^2)^{2-d/2}}\right) \\ &\xrightarrow{d\to 4} \frac{\lambda^2}{32\pi^2}\int_0^1 dx \left(\frac{6}{\epsilon} + 3\gamma + 3\log(4\pi) - \log(m^2 - x(1-x)4^2) - 2\log(m^2)\right) \end{aligned} \tag{3.3.11}$$

These expressions are divergent as $d \to 4$. But if we combine them according to 3.3.8, we obtain the finite (if rather complicated) result:

$$\begin{aligned} i\mathcal{M} = -i\lambda - \frac{i\lambda^2}{32\pi^2}\int_0^1 dx \Bigg[&\log\left(\frac{m^2 - x(x-x)s}{m^2 - x(1-x)4m^2}\right) + \log\left(\frac{m^2 - x(1-x)t}{m^2}\right) \\ &+\log\left(\frac{m^2 - x(1-x)u}{m^2}\right)\Bigg] \end{aligned} \tag{3.3.12}$$

To determine δ_Z and δ_m we must compute the two-point function. We define $-iM^2(p^2)$ as the sum of all one-particle-irreducible insertions into the propagator:

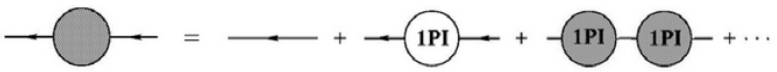

Then the full two-point function is given by the geometric series:

$$\frac{i}{p^2 - m^2 - M^2(p^2)} \tag{3.3.13}$$

The renormalization conditions require that the pole in this full propagator occur at $p^2 = m^2$ and have residue 1. These two conditions are equivalent, respectively, to:

$$M^2(p^2)|_{p^2=m^2} = 0 \quad \text{and} \quad \frac{d}{dp^2}M^2(p^2)|_{p^2=m^2} = 0 \tag{3.3.14}$$

Explicitly, to one-loop order:

$$\begin{aligned} -iM^2(p^2) &= -i\lambda\frac{1}{2}\int\frac{d^dk}{(2\pi)^d}\frac{i}{k^2-m^2} + i(p^2\delta_Z - \delta_m) \\ &= -\frac{i\lambda}{2}\frac{1}{(4\pi)^{d/2}}\frac{\Gamma(1-d/2)}{(m^2)^{1-d/2}} + i(p^2\delta_Z - \delta_m) \end{aligned} \tag{3.3.15}$$

Since the first term is independent of p^2, the result is rather trivial: Setting

$$\delta_Z = 0 \quad \text{and} \quad \delta_m = -\frac{\lambda}{2(4\pi)^{d/2}}\frac{\Gamma(1-d/2)}{(m^2)^{1-d/2}} \tag{3.3.16}$$

yields $M^2(p^2) = 0$ for all p^2, satisfying both of the renormalization conditions. The vanishing of δ_Z at one-loop order is a special feature of ϕ^4 theory, which does not occur in more general theories of scalar fields. Yukawa theory gives an explicit example of a one-loop correction for which the counterterm is required. Renormalization has presented a constraint to the Standard Model, which does not allow non-renormalizable interactions. However, when expanding the Standard Model, thus often being forced to introduce these non-renormalizable interactions, a new approach has to be used, namely an effective field theory approach.

3.4 Effective field theory

When a field theory is non-renormalizable, we have to make use of effective field theory approach. When the Standard Model is extended to describe new physics, higher dimensional operators are occasionally introduced and thus bring with them non-renormalizability. To generate neutrino masses, a dimension 5 operator is commonly used, see eq. 4.5.1. However, the effective field theory approach takes care of this. It is a realistic theory used to describe physics at accessible energies, being a low energy approximation that includes an infinite number of non-renormalizable interactions. We make use of the Wilsonian approach to illustrate how a theory becomes effective. In this functional integral approach, the degrees of freedom of the quantum fields are variables of the integration. In a ϕ^4 theory, the generating functional, that is the partition function, is:

$$Z[J] = \int \mathcal{D}\phi e^{i\int[\mathcal{L}+J\phi]} = \left(\prod_k \int d\phi(k)\right) e^{i\int[\mathcal{L}+J\phi]} \tag{3.4.1}$$

Imposing a sharp ultraviolet cutoff Λ, we restrict the number of the integration variables. That is, we integrate only over $\phi(k)$ with $|k| \leq \Lambda$, and set $\phi(k) = 0$ for $|k| > \Lambda$. This modification of the functional integral suggests a method for neglecting the influence of the quantum fluctuations at very short distances or very large momenta. The cutoff is imposed in Euclidian space to avoid the light-like very large momenta with very small $|k|^2$. After the cutoff has been applied, and $J = 0$, the partition function is:

$$Z[J=0] = \int [\mathcal{D}\phi]_{|k|<\Lambda} \exp\left[-\int d^dx \left[\frac{1}{2}(\partial_\mu\phi)^2 + \frac{1}{2}m^2\phi^2 + \frac{\lambda}{4!}\phi^4\right]\right] \tag{3.4.2}$$

In the Lagrangian of eq. 3.4.2, m and λ are the bare parameters, and so there are no counterterms and also $(\partial_\mu\phi)^2 = (\frac{\partial\phi}{\partial\tau})^2 + (\triangle\phi)^2$. We now divide the integration variables $\phi(k)$ into two groups. Choose a fraction $b < 1$. The variables $\phi(k)$ with $b\Lambda \leq |k| \leq \Lambda$ are the high-momentum degrees of freedom that we will integrate over. To label these degrees of freedom, let us define:

$$\hat{\phi}(k) = \left\{ \begin{pmatrix} \phi(k) & \text{if } b\Lambda \leq |k| < \Lambda \\ 0 & \text{otherwise} \end{pmatrix} \right\} \tag{3.4.3}$$

Next, let us define a new scalar $\phi(k)$, which is identical to the old for $|k| < b\Lambda$ and zero for $|k| > b\Lambda$. Then we can replace the old ϕ in the Lagrangian with $\phi + \hat{\phi}$, and rewrite eq. 3.4.2 as:

$$\begin{aligned} Z &= \int \mathcal{D}\phi \int \mathcal{D}\hat{\phi} \exp\left(-\int d^d x \left[\frac{1}{2}(\partial_\mu \phi + \partial_\mu \hat{\phi})^2 + \frac{1}{2}m^2(\phi+\hat{\phi})^2 + \frac{\lambda}{4!}(\phi+\hat{\phi})^4\right]\right) \\ &= \int \mathcal{D}\phi e^{-\int \mathcal{L}(\phi)} \int \mathcal{D}\hat{\phi} \exp\left(-\int d^d x \left[\frac{1}{2}(\partial_\mu \hat{\phi})^2 + \frac{1}{2}m^2\hat{\phi}^2 + \lambda\left(\frac{1}{6}\phi^3\hat{\phi} + \frac{1}{4}\phi^2\hat{\phi}^2 + \frac{1}{6}\phi\hat{\phi}^3 + \frac{1}{4!}\hat{\phi}^4\right)\right]\right) \end{aligned} \tag{3.4.4}$$

In the final expression we have gathered all terms independent of $\hat{\phi}$ into $\mathcal{L}(\phi)$. Note that quadratic terms of the form $\phi\hat{\phi}$ vanish, since Fourier components of different wavelengths are orthogonal. After the integration over $\hat{\phi}$ is performed, we have:

$$Z = \int [\mathcal{D}\phi]_{b\Lambda} \exp\left(-\int d^d x \mathcal{L}_{\text{eff}}\right) \tag{3.4.5}$$

This new effective Lagrangian, which contains only momenta below $b\Lambda$, can be found carrying out the integrals over $\hat{\phi}$. We will see that $\mathcal{L}_{\text{eff}}(\phi) = \mathcal{L}(\phi)$ plus corrections proportional to powers of λ. These correction terms compensate for the removal of the large-k Fourier components $\hat{\phi}$, by supplying the interactions among the remaining $\phi(k)$ that were previously mediated by fluctuations of the $\hat{\phi}$. The integration over $\hat{\phi}$ is done perturbatively since $m^2 << \Lambda$. Then the leading-order term in the portion of the Lagrangian involving $\hat{\phi}$ is:

$$\int \mathcal{L}_0 = \frac{1}{2}\int_{b\Lambda \le |k| < \Lambda} \frac{d^d k}{(2\pi)^d} \hat{\phi}^*(k) k^2 \hat{\phi}(k) \tag{3.4.6}$$

This term leads to a propagator

$$\langle \hat{\phi}(k)\hat{\phi}(p)\rangle = \frac{\int \mathcal{D}\hat{\phi} e^{-\int \mathcal{L}_0} \hat{\phi}(k)\hat{\phi}(p)}{\int \mathcal{D}\hat{\phi} e^{-\int \mathcal{L}_0}} = \frac{1}{k^2}(2\pi)^d \delta^d(k+p)\Theta(k) \tag{3.4.7}$$

where $\Theta(k) = 1$ for $b\Lambda \le |k| < \Lambda$ and 0 otherwise. We will regard the remaining $\hat{\phi}$ terms in eq. 3.4.4 as perturbations, and expand the exponential. The various contributions from these perturbations can be evaluated by using Wick's theorem with eq. 3.4.7 as the propagator. First consider the term that results from expanding to one power of the $\phi^2\hat{\phi}^2$ term in the exponent of eq. 3.4.4. We find

$$-\int d^d x \frac{\lambda}{4}\phi^2\hat{\phi}\hat{\phi} = -\frac{1}{2}\int \frac{d^d k_1}{(2\pi)^d} \Delta m^2 \phi(k_1)\phi(-k_1) \tag{3.4.8}$$

where the coefficient Δm^2 is the result of contracting the two $\hat{\phi}$ fields

$$\Delta m^2 = \frac{\lambda}{2}\int_{b\Lambda \le |k| < \Lambda} \frac{d^d k}{(2\pi)^d}\frac{1}{k^2}. \tag{3.4.9}$$

The integral from this term therefore has the form:

$$\exp\left(-\int d^d x \frac{1}{2}\Delta m^2 \phi^2 + ...\right) \tag{3.4.10}$$

We will soon see that the rest of the perturbation series also organizes itself into this form. The coefficient Δm^2 therefore gives a positive correction to the m^2 term in $\mathcal{L}$. The higher orders of the perturbation theory in the correction terms can be worked out in a similar way. As in our derivation of the standard perturbation theory for ϕ^4 theory,

it is useful to adopt a diagrammatic notation. Represent the propagator eq. 3.4.7 by a double line. This propagator will connect pairs of fields $\hat{\phi}$ from the various quadratic interactions. Represent the fields ϕ in these interactions, which are not integrated over, as single external lines. Then, for example, the contribution of eq. 3.4.8 corresponds to the following in figure 3.4.1:

Figure 3.4.1: *Order λ contribution to the effective Lagrangian.*

At order λ^2, we will have, among other contributions, terms involving the contractions of two interaction terms $\lambda\phi^2\hat{\phi}^2$. Each term corresponds to a vertex connecting two single lines and two double lines. There are two possible contractions:

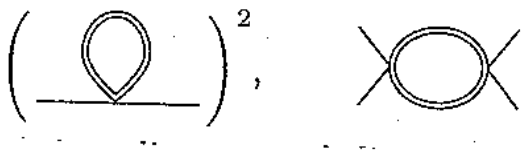

Figure 3.4.2: *Order λ^2 contribution to the effective Lagrangian.*

Of these, the first, which is a disconnected diagram, supplies the order-λ^2 term in the exponential in eq. 3.4.10. The second is a new contribution, which will become a correction to the ϕ^4 interaction in $\mathcal{L}(\phi)$. Let us now evaluate this second contribution. For simplicity, we consider the limit in which the external momenta carried by the factors ϕ are very small compared to $b\Lambda$, so we can ignore them. Then this diagram has the value

$$-\frac{1}{4!}\int d^dx \Delta\lambda\phi^4 \tag{3.4.11}$$

where

$$\Delta\lambda = -4!\frac{2}{2!}\left(\frac{\lambda}{4}\right)^2\int_{b\Lambda\leq|k|<\Lambda}\frac{d^dk}{(2\pi)^d}\left(\frac{1}{k^2}\right)^2. \tag{3.4.12}$$

The effective Lagrangian is:

$$\mathcal{L}_{\text{eff}} = \frac{1}{2}(\partial_\mu\phi)^2 + \frac{1}{2}m^2\phi^2 + \frac{\lambda}{4!}\phi^4 + \text{sum of connected terms} \tag{3.4.13}$$

Higher order contributions can be done similarly. Starting out with a partition function for all k lower than a cutoff Λ

$$Z = \int \mathcal{D}\phi_{|k|<\Lambda}\exp\left[-\int d^dx\left[\frac{1}{2}(\partial_\mu\phi)^2 + \frac{1}{2}m^2\phi^2 + \frac{\lambda}{4!}\phi^4\right]\right] \tag{3.4.14}$$

a rescaling can be made, so that

$$k' = k/b \qquad x' = xb. \tag{3.4.15}$$

The integration of

$$\int d^dx\left[\frac{1}{2}(1+\Delta Z)(\partial_\mu\phi)^2 + \frac{1}{2}(m^2+\Delta m^2)\phi^2 + \frac{1}{4}(\lambda+\Delta\lambda)\phi^4 + \Delta C(\partial_\mu\phi)^4 + \Delta D\phi^6 + ...\right] \tag{3.4.16}$$

can then be done for $|k'| > \Lambda$, which is the same as $|k| > b\Lambda$, leaving the integration over $|k'| < \Lambda$, that is, the function

$$\int d^d x \mathcal{L}_{\text{eff}} = \int d^d x' \left[\frac{1}{2}(\partial'_\mu \phi')^2 + \frac{1}{2}(m')^2(\phi')^2 + \frac{1}{4}\lambda'(\phi')^4 + C'(\partial'_\mu \phi')^4 + D'(\phi')^6 + .. \right] \tag{3.4.17}$$

where the new field is given by

$$\phi' = [b^{2-d}(1 + \Delta Z)]^{1/2}\phi. \tag{3.4.18}$$

The new parameters of the Lagrangian are

$$(m')^2 = (m^2 + \Delta m^2)(1 + \Delta Z)^{-1} b^{-2} \qquad \lambda' = (\lambda + \Delta\lambda)(1 + \Delta Z)^{-2} b^{d-4} \tag{3.4.19}$$

$$C' = (C + \Delta C)(1 + \Delta Z)^{-2} b^d \qquad D' = (D + \Delta D)(1 + \Delta Z)^{-3} b^{2d-6} \tag{3.4.20}$$

plus higher order. The original Lagrangian had $C = D = 0$, but the same equations would apply if the initial values of C and D were non-zero. If the perturbation condition is justified these corrections are very small and finite. This transformation can then be continued over another shell of momentum space, which transforms the Lagrangian once again, and so forth. This leads to an iteration of transformation, so that if $b \to 1$, the transformations become continuous. This is the Renormalization group.

The Wilsonian approach to effective field theory is therefore to define a quantum field theory through an action with a momentum cutoff. This cutoff can then be lowered by integrating out the higher momenta degrees of freedom and from this change the coefficients in the effective action. At an energy much lower than the initial cutoff, the results can then be approximated to the same as those for a renormalized perturbation theory up to small correction proportional to the energy over the initial cutoff. As a result, every Lagrangian, as long as the couplings are significantly weak, can be described at the energies of experiments by an effective Lagrangian. This is the effective field theory approach. It is used when higher mass-dimensional operators are introduced to describe physics beyond the Standard Model. We now proceed to discuss in more detail the non-Abelian gauge theories of the electroweak interaction, which are unified in the *Standard Model of elementary particle physics*. The main interest of this thesis lies in neutrinos. Therefore, we concentrate on the electroweak part of the Standard Model.

3.5 The Glashow-Weinberg-Salam model

We now consider a treatment of electroweak interactions in the framework of gauge theories. Theoretically, the Standard Model group corresponds to a direct product of three groups, SU(3) ⊗ SU(2) ⊗ U(1), where SU(3) belongs to the color group of quantum chromodynamics (QCD), SU(2) to the weak isospin and U(1) belongs to the hypercharge. The elementary particles are arranged as doublets for chiral left-handed fields and singlets for right-handed fields in the form:

$$\begin{array}{cccccccccc} \begin{pmatrix} u \\ d' \end{pmatrix}_L & \begin{pmatrix} c \\ s' \end{pmatrix}_L & \begin{pmatrix} t \\ b' \end{pmatrix}_L & \begin{pmatrix} e \\ \nu_e \end{pmatrix}_L & \begin{pmatrix} \mu \\ \nu_\mu \end{pmatrix}_L & \begin{pmatrix} \tau \\ \nu_\tau \end{pmatrix}_L \\ u_R & d_R & s_R & c_R & b_R & t_R & e_R & \mu_R & \tau_R \end{array} \tag{3.5.1}$$

We discuss the theory taking the first generation of the three known chiral lepton fields e_R, e_L and ν_{eL} as an example. An extension to all three generations and quarks is straightforward. Neglecting any mass and switching off weak interactions and electromagnetism

the Lagrangian for the free Dirac fields can be written as:

$$\mathcal{L}(x) = (\bar{\nu}_{eL}(x), \bar{e}_L(x))(i\gamma^\mu \partial_\mu) \begin{pmatrix} \nu_{eL}(x) \\ e_L(x) \end{pmatrix} + \bar{e}_R(x) i\gamma^\mu \partial_\mu e_R(x) \tag{3.5.2}$$

This Lagrangian is invariant with respect to global SU(2) transformations on the fields ν_{eL} and e_L. Going to a local SU(2) transformation, the Lagrangian clearly is not invariant but we can compensate for that by introducing a corresponding number of gauge vector fields. In the case of SU(2) we have three generators and, therefore, we need three vector fields called W^1_μ, W^2_μ and W^3_μ. The Lagrangian including the W-fields can then be written as:

$$\begin{aligned} \mathcal{L}(x) = &- \frac{1}{2}\mathrm{Tr}(W_{\mu\rho}(x) W^{\mu\rho}(x)) + (\bar{\nu}_{eL}(x), \bar{e}_L(x)) i\gamma^\mu (\partial_\mu + igW_\mu) \begin{pmatrix} \nu_{eL}(x) \\ e_L(x) \end{pmatrix} \\ &+ \bar{e}_R(x) i\gamma^\mu \partial_\mu e_R(x) \end{aligned} \tag{3.5.3}$$

The introduced gauge group SU(2) is called the weak isospin. Introducing the fields $W^\pm_\mu$ as

$$W^\pm_\mu = \frac{1}{\sqrt{2}}(W^1_\mu \mp i W^2_\mu) \tag{3.5.4}$$

from eq. 3.5.3 the ν-e-W coupling term can be obtained as

$$\begin{aligned} \mathcal{L} = &- g(\bar{\nu}_{eL}, \bar{e}_L)\gamma^\mu W_\mu \frac{\sigma}{2} \begin{pmatrix} \nu_{eL} \\ e_L \end{pmatrix} = -g(\bar{\nu}_{eL}, \bar{e}_L)\gamma^\mu \frac{1}{2} \begin{pmatrix} W^3_\mu & \sqrt{2}W^+_\mu \\ \sqrt{2}W^-_\mu & -W^3_\mu \end{pmatrix} \begin{pmatrix} \nu_{eL} \\ e_L \end{pmatrix} \\ = &- \frac{g}{2}[W^3_\mu(\bar{\nu}_{eL}\gamma^\mu \nu_{eL} - \bar{e}_L \gamma^\mu e_L) + \sqrt{2}W^+_\mu \bar{\nu}_{eL}\gamma^\mu e_L + \sqrt{2}W^-_\mu \bar{e}_L \gamma^\mu \nu_{eL}] \end{aligned} \tag{3.5.5}$$

with σ as the Pauli matrices. This looks quite promising because the last two terms already have the $\gamma^\mu(1-\gamma_5)$ structure. Hence, by finding a method to make the W-boson very massive, at low energy the theory reduces to the Fermi four-point interaction. Before discussing masses we want to add electromagnetism. The easiest assumption for associating the remaining field W^3_μ with the photon field does not work, because W^3_μ couples to neutrinos and not to e_R in contrast to the photon. Going to eq. 3.5.3 beside the SU(2) invariance one can recognize an additional invariance under two further U(1) transformations with quantum numbers y_L, y_R:

$$\begin{aligned} \begin{pmatrix} \nu_{eL}(x) \\ e_L(x) \end{pmatrix} &\to e^{+iy_L \chi} \begin{pmatrix} \nu_{eL}(x) \\ e_L(x) \end{pmatrix} \\ e_R(x) &\to e^{+iy_R \chi} e_R(x) \end{aligned} \tag{3.5.6}$$

However, this would result in two 'photon-like' gauge bosons in contrast to Nature from which we know there is only one. Therefore, we can restrict ourselves to one special combination of these phase transitions resulting in one U(1) transformation by choosing:

$$y_L = -\frac{1}{2} \tag{3.5.7}$$

y_R is fixed later. This U(1) group is called the weak hypercharge Y. We can make this U(1) into a gauge group as in QED, where the charge Q is replaced by the weak hypercharge Y. Between charge, hypercharge and the third component of the weak isospin, the following relation holds:

$$Q = I_3 + \frac{Y}{2} \tag{3.5.8}$$

The necessary real vector field is called B_μ and the corresponding gauge coupling constant g'. Now we are left with two massless neutral vector fields W^3_μ, B_μ and the question

arises as to whether we can combine them in a way to account for weak neutral currents and electromagnetism. Let us define two orthogonal linear combinations resulting in normalized fields Z_μ and A_μ:

$$Z_\mu = \frac{1}{\sqrt{g^2 + g'^2}}(gW_\mu^3 - g'B_\mu) \tag{3.5.9}$$

$$A_\mu = \frac{1}{\sqrt{g^2 + g'^2}}(gW_\mu^3 + g'B_\mu) \tag{3.5.10}$$

By writing

$$\sin(\theta_W) = \frac{g'}{\sqrt{g^2 + g'^2}} \tag{3.5.11}$$

$$\cos(\theta_W) = \frac{g}{\sqrt{g^2 + g'^2}} \tag{3.5.12}$$

we can simplify the expressions to

$$Z_\mu = \cos(\theta_W)W_\mu^3 - \sin(\theta_W)B_\mu \tag{3.5.13}$$

$$A_\mu = \sin(\theta_W)W_\mu^3 + \cos(\theta_W)B_\mu. \tag{3.5.14}$$

The angle $\sin(\theta_W)$ is called the Weinberg angle and is one of the fundamental parameters of the Standard Model. Replacing the fields W_μ^3, B_μ in eq. 3.5.5 by Z_μ, A_μ results in:

$$\begin{aligned}\mathcal{L} = &- \frac{g}{\sqrt{2}}(W_\mu^+ \bar{\nu}_{eL}\gamma^\mu e_L + W_\mu^- \bar{e}_L\gamma^\mu \nu_{eL}) \\ &- \sqrt{g^2 + g'^2}Z_\mu \left[\frac{1}{2}\bar{\nu}_{eL}\gamma^\mu\nu_{eL} - \frac{1}{2}\bar{e}_L\gamma^\mu e_L - \sin^2(\theta_W)(-\bar{e}_L\gamma^\mu e_L + y_R\bar{e}_R\gamma^\mu e_R)\right] \\ &- \frac{gg'}{\sqrt{g^2 + g'^2}}A_\mu(-\bar{e}_L\gamma^\mu e_L + y_R\bar{e}_R\gamma^\mu e_R)\end{aligned} \tag{3.5.15}$$

One can note that the Z_μ coupling results in neutral currents. However, A_μ no longer couples neutrinos and is, therefore, a good candidate to be associated with the photon field. To reproduce electromagnetism we have to choose the following

$$y_R = -1 \qquad \frac{gg'}{\sqrt{g^2 + g'^2}} = e \tag{3.5.16}$$

which immediately yields another important relation by using eq. 3.5.11

$$\sin(\theta_W) = \frac{e}{g}. \tag{3.5.17}$$

This finally allows us to write the Lagrangian using electromagnetic, charged and neutral currents

$$\mathcal{L} = - e\left[A_\mu J_{\text{em}}^\mu + \frac{1}{\sqrt{2}\sin(\theta_W)}(W_\mu^+ \bar{\nu}_{eL}\gamma^\mu e_L + W_\mu^- \bar{e}_L\gamma^\mu\nu_{eL}) + \frac{1}{\sin(\theta_W)\cos(\theta_W)}Z_\mu J_{NC}^\mu\right] \tag{3.5.18}$$

with the currents

$$J_{\text{em}}^\mu = -\bar{e}_L\gamma^\mu e_L - \bar{e}_R\gamma^\mu e_R = -\bar{e}\gamma^\mu e \tag{3.5.19}$$

$$J_{NC}^\mu = \frac{1}{2}\bar{\nu}_{eL}\gamma^\mu\nu_{eL} - \frac{1}{2}\bar{e}_L\gamma^\mu e_L - \sin^2(\theta_W)J_{\text{em}}^\mu. \tag{3.5.20}$$

3.5.1 Spontaneous symmetry breaking and the Higgs mechanism

In the formulation of the theory all particles have to be massless to guarantee gauge invariance. The concept of spontaneous symmetry breaking is then used for particles to receive mass through the so-called *Higgs mechanism*. Spontaneous symmetry breaking results in the ground state of a system having no longer the full symmetry corresponding to the underlying Lagrangian. Consider the following classical Lagrangian

$$\mathcal{L} = (\partial_\mu \Phi)^\dagger (\partial^\mu \Phi) - \mu^2 \Phi^\dagger \Phi - \lambda (\Phi^\dagger \Phi)^2 \tag{3.5.21}$$

where $\Phi(x)$ is a complex scalar field. $\mathcal{L}$ is invariant under the group U(1) of *global* transformations equivalent to eq. 3.2.3. The kinetic energy term is positive and can vanish only if Φ = constant. The ground state of the system will be obtained when the value of the constant corresponds to the minimum of the potential:

$$V(\Phi) = \mu^2 \Phi^\dagger \Phi + \lambda (\Phi^\dagger \Phi)^2 \tag{3.5.22}$$

If $\mu^2 > 0$ and $\lambda > 0$, a minimum configuration occurs at the origin and we have a symmetric ground-state configuration. If, however, $\mu^2 < 0$, the minimum is at

$$\rho = \Phi \Phi^\dagger = -\mu^2 / 2\lambda \tag{3.5.23}$$

which means that there is a whole ring of radius

$$|\Phi| \equiv \frac{v}{\sqrt{2}} = \sqrt{-\mu^2/2\lambda} \tag{3.5.24}$$

in the complex plane. There are infinitely many ground states, degenerate with each other but none shows the original symmetry of the Lagrangian any longer. The symmetry is broken spontaneously. Generally, it can be shown that spontaneous symmetry breaking is connected with the degeneracy of the ground state. Now we impose invariance under a *local* gauge transformation, as it is implemented in the Standard Model. In the electroweak model the simplest way of spontaneous symmetry breaking is achieved by introducing a doublet of complex scalar fields, one charged, one neutral

$$\phi = \begin{pmatrix} \phi^\dagger \\ \phi^0 \end{pmatrix} \tag{3.5.25}$$

where the complex fields are given by:

$$\phi^\dagger = \frac{\phi_1 + i\phi_2}{\sqrt{2}} \qquad \phi^0 = \frac{\phi_3 + i\phi_4}{\sqrt{2}} \tag{3.5.26}$$

Adding a kinetic term to the potential eq. 3.5.22 leads to the following expression for the Lagrangian:

$$\mathcal{L}_{\text{Higgs}} = (\partial_\mu \phi)^\dagger (\partial^\mu \phi) - \mu^2 \phi^\dagger \phi - \lambda (\phi^\dagger \phi)^2 \tag{3.5.27}$$

Proceeding as before, the potential $V(\phi)$ has a minimum for $\mu^2 < 0$ at:

$$\phi^\dagger \phi = \frac{-\mu^2}{2\lambda} = \frac{v^2}{2} \tag{3.5.28}$$

Here again the minima, corresponding to the vacuum expectation values for ϕ lie on a circle with $\langle \phi \rangle \equiv v/\sqrt{2} = \sqrt{-\mu^2/2\lambda}$. This ground state is degenerate and its orientation in two-dimensional isospin space is not defined. It can choose the same radius in any

orientation between $[0, 2\pi]$. From this infinite number of possible orientations we choose a particular field configuration which is defined as the vacuum state as

$$\phi_0 = \frac{1}{\sqrt{2}} \begin{pmatrix} 0 \\ v \end{pmatrix} \tag{3.5.29}$$

which is no longer invariant under SU(2) transformations. The upper component is motivated by the fact that a vacuum is electrically neutral. The field $\phi(x)$ can now be expanded around the vacuum

$$\phi = \frac{1}{\sqrt{2}} \begin{pmatrix} 0 \\ v + H(x) \end{pmatrix} \tag{3.5.30}$$

where a perturbation theory for $H(x)$ can be formulated as usual. Now consider the coupling of this field to fermions first. Fermions get their masses through coupling to the vacuum expectation value (VEV) of the Higgs field. To conserve isospin invariance of the coupling, the Higgs doublet has to be combined with a fermion doublet and singlet. The resulting coupling is called Yukawa coupling and has the typical form (given here for the case of electrons):

$$\begin{aligned} \mathcal{L}_{\text{Yuk}} &= -c_e \bar{e}_R \phi^\dagger \begin{pmatrix} \nu_{eL} \\ e_L \end{pmatrix} + h.c. \\ &= -c_e \left[\bar{e}_R \phi_0^\dagger \begin{pmatrix} \nu_{eL} \\ e_L \end{pmatrix} + (\bar{\nu}_{eL}, \bar{e}_L) \phi_0 e_R \right] \\ &= -c_e \left[\bar{e}_R \frac{1}{\sqrt{2}} v e_L + \bar{e}_L \frac{1}{\sqrt{2}} v e_R \right] \\ &= -c_e v \frac{1}{\sqrt{2}} (\bar{e}_R e_L + \bar{e}_L e_R) \\ &= -c_e \frac{v}{\sqrt{2}} \bar{e} e \end{aligned} \tag{3.5.31}$$

Here c_e is an arbitrary coupling constant. This corresponds exactly to mass term for the electron with an electron mass:

$$m_e = c_e \frac{v}{\sqrt{2}} \tag{3.5.32}$$

The same strategy holds for the other charged leptons and quarks with their corresponding coupling constant c_i. In this way fermions obtain their masses within the GWS model. Neutrinos remain massless because with the currently accepted particle content there are no right-handed ν_R singlet states and one cannot write down couplings like in eq. 3.5.31. With the evidence for massive neutrinos, one is forced to generate the masses in another way such as using Higgs triplets or adding right-handed neutrino singlets. Substituting the covariant derivative for the normal derivative in $\mathcal{L}$ as in eq. 3.2.15 leads directly to the coupling of the Higgs field with the gauge fields. The gauge bosons then acquire masses of

$$m_W^2 = \frac{g^2 v^2}{4} = \frac{e^2 v^2}{4 \sin^2(\theta_W)} \tag{3.5.33}$$

$$m_Z^2 = \frac{(g^2 + g'^2) v^2}{4} = \frac{e^2 v^2}{4 \sin^2(\theta_W) \cos^2(\theta_W)} \tag{3.5.34}$$

resulting in

$$\frac{m_W}{m_Z} = \cos(\theta_W). \tag{3.5.35}$$

The gauge bosons has been determined accurately with given values:

$$m_Z = 91.1874 \pm 0.0021 \quad \mathrm{GeV/c^2} \quad \text{and} \quad m_W = 80.452 \pm 0.091 \quad \mathrm{GeV/c^2} \tag{3.5.36}$$

An estimate for v can be given by eq. 3.5.33 resulting in:

$$v = (\sqrt{2}G_F)^{-1/2} \approx 246 \quad \mathrm{GeV} \tag{3.5.37}$$

The inclusion of spontaneous symmetry breaking with the help of a complex scalar field doublet has another consequence, namely the existence of a new scalar particle called the Higgs boson, with a mass of m_H, such that:

$$m_H^2 = 2\lambda v^2 \tag{3.5.38}$$

This particle was recently discovered by CMS ($m_H = 125.5 \pm 0.4(\mathrm{stat}) \pm 0.5(\mathrm{sys})$ GeV/c^2) and ATLAS ($m_H = 126.0 \pm 0.4(\mathrm{stat}) \pm 0.4(\mathrm{sys})$ GeV/c^2) independently at the LHC-ring. The discussion at the moment is whatever it is a Standard Model Higgs or a more exotic Higgs [[23], [24], [25]]

3.5.2 Number of neutrino flavours from the width of the Z^0

The number N_ν of light ($m_\nu < m_Z/2$) and active neutrinos was determined at LEP by measuring the total decay width of the Z^0 resonance. Calling the hadronic decay width Γ_{had} (consisting of $Z^0 \to q\bar{q}$) and assuming lepton universality (implying that there is a common partial width Γ_ℓ for the decay into charged lepton pairs $\ell^+\ell^-$), the invisible width Γ_{inv} is [26]:

$$\Gamma_{\mathrm{inv}} = \Gamma_Z - \Gamma_{\mathrm{had}} - 3\Gamma_\ell \tag{3.5.39}$$

As the invisible width corresponds to

$$\Gamma_{\mathrm{inv}} = N_\nu \cdot \Gamma_\nu \tag{3.5.40}$$

where the number of neutrino flavours N_ν can be determined. The partial widths of decays in fermions $\mathrm{Z} \to f\overline{f}$ are given in electroweak theory by [27]

$$\Gamma_f = \frac{G_F m_Z^3}{6\sqrt{2}\pi} c_f [(g_V)^2 + (g_A)^2] = \Gamma_0 c_f [(g_V)^2 + (g_A)^2] \tag{3.5.41}$$

with

$$\Gamma_0 = \frac{G_F m_Z^3}{6\sqrt{2}\pi} = 0.332 \text{ GeV}. \tag{3.5.42}$$

In this equation c_f corresponds to a color factor ($c_f = 1$ for leptons, $c_f = 3$ for quarks) and g_V and g_A are the vector and axial-vector coupling constants respectively. They are closely related to the Weinberg angle $\sin^2(\theta_W)$ and the third component of weak isospin I_3 via

$$g_V = I_3 - 2Q\sin^2(\theta_W) \tag{3.5.43}$$

$$g_A = I_3 \tag{3.5.44}$$

with Q being the charge of the particle. Therefore, the different branching ratios [5] are:

$$\Gamma(Z^0 \to u\bar{u}, c\bar{c}) = \left(\frac{3}{2} - 4\sin^2(\theta_W) + \frac{16}{3}\sin^4(\theta_W)\right)\Gamma_0 = 0.286 \text{ GeV} \tag{3.5.45}$$

$$\Gamma(Z^0 \to d\bar{d}, s\bar{s}, b\bar{b}) = \left(\frac{3}{2} - 2\sin^2(\theta_W) + \frac{4}{3}\sin^4(\theta_W)\right)\Gamma_0 = 0.369 \text{ GeV} \tag{3.5.46}$$

$$\Gamma(Z^0 \to e^+e^-, \mu^+\mu^-, \tau^+\tau^-) = \left(\frac{1}{2} - 2\sin^2(\theta_W) + 4\sin^4(\theta_W)\right)\Gamma_0 = 0.084 \text{ GeV} \tag{3.5.47}$$

$$\Gamma(Z^0 \to \nu\bar{\nu}) = \frac{1}{2}\Gamma_0 = 0.166 \text{ GeV} \tag{3.5.48}$$

Summing all decay channels into quarks results in a total hadronic width $\Gamma_{\text{had}} = 1.687$ GeV. The different decay widths are determined from the reaction $e^+e^- \to f\bar{f}$ for $f \neq e$ whose cross-section as a function of the centre-of-mass energy $\sqrt{s}$ is measured ($\sqrt{s} \approx m_Z$) and is dominated by the Z^0 pole. The cross-section at the resonance is described in the

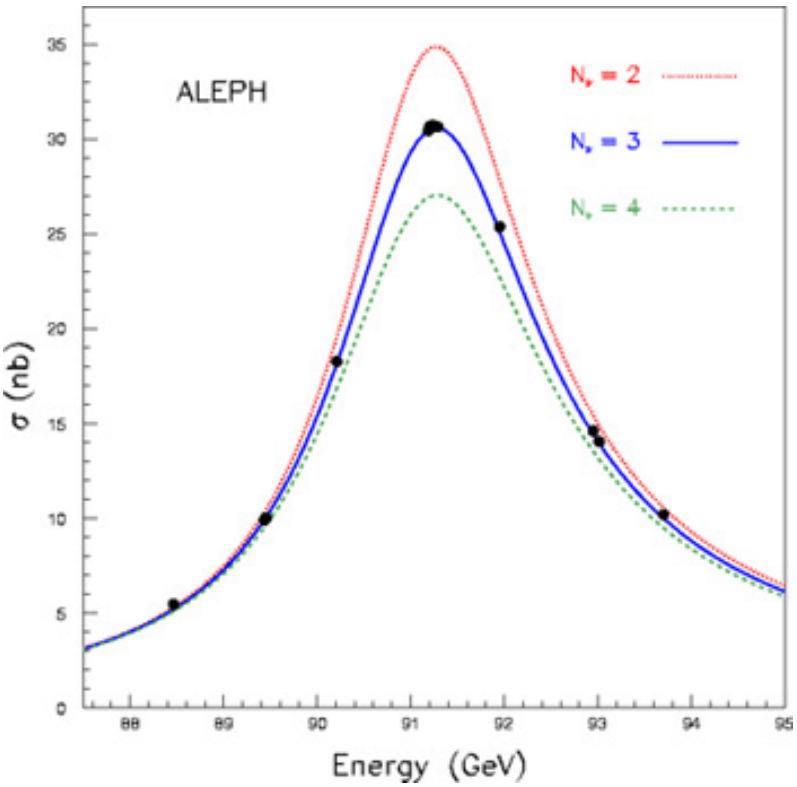

Figure 3.5.1: *Cross-section as a function of $\sqrt{s}$ for the reaction $e^+e^- \to$ hadron as obtained by the ALEPH detector at LEP. The different curves show the Standard Model predictions for two, three and four light neutrino flavours.*

Born approximation by a Breit-Wigner formula

$$\sigma(s) = \sigma^0 \frac{s\Gamma_Z^2}{(s - m_Z^2)^2 + s^2\Gamma_Z^2/m_Z^2} \quad \text{with} \quad \sigma^0 = \frac{12\pi}{m_Z^2}\frac{\Gamma_e\Gamma_f}{\Gamma_Z^2} \tag{3.5.49}$$

with σ^0 being the maximum of the resonance. Γ_Z can be determined from the width and $\Gamma_e\Gamma_f$ from the maximum of the observed resonance (figure 3.5.1). Experimentally, the Z^0 resonance is fitted with four different parameters, namely:

$$m_Z, \Gamma_Z, \sigma^0_{\text{had}} = \frac{12\pi}{m_Z^2}\frac{\Gamma_e\Gamma_{\text{had}}}{\Gamma_Z^2} \quad \text{and} \quad R_l = \frac{\Gamma_{\text{had}}}{\Gamma_\ell} \tag{3.5.50}$$

$\sigma^0_{\rm had}$ is determined from the maximum of the resonance in $e^+e^- \to$ hadrons. Assuming again lepton-universality, which is justified by the equality of the measured leptonic decay width, the number of neutrino flavours can be determined as:

$$N_\nu = \frac{\Gamma_{\rm inv}}{\Gamma_\ell}\left(\frac{\Gamma_\ell}{\Gamma_\nu}\right) = \left[\sqrt{\frac{12\pi R_\ell}{m_Z^2\sigma^0_{\rm had}}} - R_\ell - 3\right]\left(\frac{\Gamma_\ell}{\Gamma_\nu}\right) \tag{3.5.51}$$

Using the most recent fit to the data of the four LEP experiments a number of

$$N_\nu = 2.9841 \pm 0.0083 \tag{3.5.52}$$

which is in excellent agreement with the theoretical expectation of three.

4

Neutrino mass: Beyond the Standard Model

Neutrinos hold a special place in the Standard Model because they only interact through the weak force. Historically, the neutrino was first postulated by Pauli to explain energy non-conservation in beta decay. Reines and Cowan observed the first interactions of electron antineutrinos in 1953, for which Reines received the Nobel prize in 1995. In 1962, Lederman, Schwartz and Steinberger detected muon neutrino interactions showing that neutrinos come in at least two types; they received the Nobel prize for this work in 1988. Evidence for tau neutrino interactions was published in 2000, thus filling out the observation of the three neutrinos.

Two historical observations are particularly noteworthy. First, the observation of neutrino neutral current interactions was key in establishing the Standard Model and electroweak unification. The second was the observation of neutrino oscillations, first proposed by Pontecorvo in 1957 [28]. Neutrino oscillations imply massive neutrinos, which is the first indication of physics beyond the Standard Model. With this description, an introduction to neutrino physics is presented.

4.1 Helicity and chirality

In quantum field theory spin-$\frac{1}{2}$ particles are described by four-component wavefunctions $\psi(x)$ (spinors) which obey the Dirac equation. The four independent components of $\psi(x)$ correspond to particles and antiparticles with the two possible spin projections $J_Z = \pm 1/2$ equivalent to the two helicities $\mathcal{H} = \pm 1$. Neutrinos as fundamental leptons are spin-$\frac{1}{2}$ particles like other fermions; however, it is an experimental fact that only left-handed neutrinos ($\mathcal{H} = -1$) and right-handed antineutrinos ($\mathcal{H} = +1$) are observed. Therefore, a two-component spinor description should, in principle, be sufficient (Weyl spinors). In a four-component theory they are obtained by projecting out of a general spinor $\psi(x)$, the components with $\mathcal{H} = +1$ for particles and $\mathcal{H} = -1$ for antiparticles with the help of the operators $P_{L,R} = \frac{1}{2}(1 \mp \gamma_5)$. The Dirac equation is the relativistic wave equation for spin-$\frac{1}{2}$ particles:

$$(i\gamma_\mu \partial^\mu - m)\,\psi = 0 \tag{4.1.1}$$

Here ψ denotes a four-component spinor and the 4×4 γ-matrices are given in the form

$$\gamma_0 = \begin{pmatrix} 0 & 1 \\ 1 & 0 \end{pmatrix} \quad \gamma_i = \begin{pmatrix} 0 & \sigma_i \\ -\sigma_i & 0 \end{pmatrix} \tag{4.1.2}$$

where σ_i correspond to the 2×2 Pauli matrices. The matrix γ_5 is given by

$$\gamma_5 = i\gamma_0\gamma_1\gamma_2\gamma_3 = \begin{pmatrix} -1 & 0 \\ 0 & 1 \end{pmatrix} \tag{4.1.3}$$

and the following anticommutator relations hold

$$\{\gamma_\alpha, \gamma_\beta\} = 2g_{\alpha\beta} \tag{4.1.4}$$

$$\{\gamma_\alpha, \gamma_5\} = 0 \tag{4.1.5}$$

with $g_{\alpha\beta} = (+1, -1, -1, -1)$. Multiplying the Dirac equation from the left with γ_0 and using $\gamma_i = \gamma_0\gamma_5\sigma_i$ results in:

$$\left(i\gamma_0^2\partial^0 - i\gamma_0^2\gamma_5\sigma_i\partial^i - m\gamma_0\right)\psi = 0 \quad i = 1, 2, 3 \tag{4.1.6}$$

Another multiplication of eq. 4.1.6 from the left with γ_5 and using $\gamma_5\sigma_i = \sigma_i\gamma_5$ leads to ($\gamma_0^2 = 1, \gamma_5^2 = 1$):

$$\left(i\partial^0\gamma_5 - i\sigma_i\partial^i + m\gamma_0\gamma_5\right)\psi = 0 \tag{4.1.7}$$

Subtraction and addition of the last two equations results in the following system of coupled equations:

$$\left(i\partial^0(1+\gamma_5) - i\sigma_i\partial^i(1+\gamma_5) - m\gamma_0(1-\gamma_5)\right)\psi = 0 \tag{4.1.8}$$

$$\left(i\partial^0(1-\gamma_5) + i\sigma_i\partial^i(1-\gamma_5) - m\gamma_0(1+\gamma_5)\right)\psi = 0 \tag{4.1.9}$$

Now let us introduce left- and right-handed components by defining two projection operators P_L and P_R:

$$P_L = \frac{1}{2}(1-\gamma_5) \quad \text{and} \quad P_R = \frac{1}{2}(1+\gamma_5) \tag{4.1.10}$$

Because they are projectors, the following relations hold:

$$P_L P_R = 0 \quad P_L + P_R = 1 \quad P_L^2 = P_L \quad P_R^2 = P_R \tag{4.1.11}$$

With the definition

$$\psi_L = P_L\psi \quad \text{and} \quad \psi_R = P_R\psi \tag{4.1.12}$$

it is obviously valid that:

$$P_L\psi_R = P_R\psi_L = 0 \tag{4.1.13}$$

Then the following eigenequation holds:

$$\gamma_5\psi_{L,R} = \mp\psi_{L,R} \tag{4.1.14}$$

The eigenvalues ∓ 1 to γ_5 are called chirality and $\psi_{L,R}$ are called chiral projections of ψ. Any spinor ψ can be rewritten in chiral projections as:

$$\psi = (P_L + P_R)\psi = P_L\psi + P_R\psi = \psi_L + \psi_R. \tag{4.1.15}$$

The equations 4.1.8 and 4.1.9 can now be expressed in these projections as:

$$\left(i\partial^0 - i\sigma_i\partial^i\right)\psi_R = m\gamma_0\psi_L \tag{4.1.16}$$

$$\left(i\partial^0 + i\sigma_i\partial^i\right)\psi_L = m\gamma_0\psi_R \tag{4.1.17}$$

Both equations decouple in the case of a vanishing mass $m = 0$ and can be depicted as:

$$i\partial^0\psi_R = i\sigma_i\partial^i\psi_R \tag{4.1.18}$$

$$i\partial^0\psi_L = -i\sigma_i\partial^i\psi_L \tag{4.1.19}$$

But this is identical to the Schrödinger equation ($x_0 = t, \hbar = 1$)

$$i\frac{\partial}{\partial t}\psi_{L,R} = \mp i\sigma_i \frac{\partial}{\partial x_i}\psi_{L,R} \tag{4.1.20}$$

or in momentum space ($i\frac{\partial}{\partial t} = E, -i\frac{\partial}{\partial x_i} = p_i$)

$$E\psi_{L,R} = \pm\sigma_i p_i \psi_{L,R}. \tag{4.1.21}$$

The latter implies that the $\psi_{L,R}$ are also eigenfunctions to the helicity operator $\mathcal{H}$:

$$\mathcal{H} = \frac{\boldsymbol{\sigma}\cdot\boldsymbol{p}}{|\boldsymbol{p}|}. \tag{4.1.22}$$

ψ_L is an eigenspinor with helicity eigenvalues $\mathcal{H} = +1$ for particles and $\mathcal{H} = -1$ for antiparticles. Correspondingly ψ_R is the eigenspinor to the helicity eigenvalues $\mathcal{H} = -1$ for particles and $\mathcal{H} = +1$ for antiparticles. Therefore, in the case of massless particles, chirality and helicity are identical. For $m > 0$ the decoupling of equations 4.1.16 and 4.1.17 is no longer possible. This means that the chirality eigenspinors ψ_L and ψ_R no longer describe particles with fixed helicity and helicity is no longer a good conserved quantum number.

4.2 Charge conjugation

While for all fundamental fermions of the Standard Model a clear discrimination between particle and antiparticle can be made by their electric charge, for neutrinos it is not so obvious. If the particle and antiparticle are not identical, we call such a fermion a Dirac particle which has four independent components. If particle and antiparticle are identical, they are called Majorana particles. The latter requires that all additive quantum numbers (charge, strangeness, baryon number, lepton number etc.) have to vanish. Consequently, the lepton number is violated if neutrinos are Majorana particles. The operator connecting particle $f(x,t)$ and antiparticle $\bar{f}(x,t)$ is charge conjugation $\mathcal{C}$:

$$\mathcal{C}|f(\boldsymbol{x},t)\rangle = \eta_c|\bar{f}(\boldsymbol{x},t)\rangle \tag{4.2.1}$$

If $\psi(x)$ is a spinor field of a free neutrino then the corresponding charge conjugated field ψ^c is defined by

$$\psi \xrightarrow{\mathcal{C}} \psi^c \equiv \mathcal{C}\psi\mathcal{C}^{-1} = \eta_c\mathcal{C}\bar{\psi}^T \tag{4.2.2}$$

with η_c as a phase factor with $|\eta_c| = 1$. The 4×4 unitary charge conjugation matrix $\mathcal{C}$ obeys the following general transformations:

$$\mathcal{C}^{-1}\gamma_\mu\mathcal{C} = -\gamma_\mu^T \quad \mathcal{C}^{-1}\gamma_5\mathcal{C} = \gamma_5^T \quad \mathcal{C}^\dagger = \mathcal{C}^{-1} = \mathcal{C}^T = -\mathcal{C} \tag{4.2.3}$$

A possible representation is $\mathcal{C} = i\gamma_0\gamma_2$. Using the projection operators $P_{L,R}$, it follows that:

$$P_{L,R}\psi = \psi_{L,R} \xrightarrow{\mathcal{C}} P_{L,R}\psi^c = (\psi^c)_{L,R} = (\psi_{R,L})^c \tag{4.2.4}$$

It is easy to show that if ψ is an eigenstate of chirality, ψ^c is an eigenstate too but it has an eigenvalue of opposite sign. Furthermore, from eq. 4.2.4 it follows that the charge conjugation $\mathcal{C}$ transforms a left(right)-handed particle into a left(right)-handed antiparticle, leaving the helicity (chirality) untouched. Only the additional application of a parity transformation changes the helicity as well.

4.3 Parity transformation

A parity transformation $\mathcal{P}$ operation is defined as:

$$\psi(\boldsymbol{x},t) \xrightarrow{\mathcal{P}} \mathcal{P}\psi(\boldsymbol{x},t)\mathcal{P}^{-1} = \eta_p\gamma_0\psi(-\boldsymbol{x},t). \tag{4.3.1}$$

The phase factor η_p with $|\eta_p| = 1$ corresponds for real $\eta_p = \pm 1$ with the inner parity. Using eq. 4.2.2 for the charge conjugated field, it follows that:

$$\psi^c = \eta_c\mathcal{C}\bar{\psi}^T \xrightarrow{\mathcal{P}} \eta_c\eta_p^*\mathcal{C}\gamma_0^T\bar{\psi}^T = -\eta_p^*\gamma_0\psi^c \tag{4.3.2}$$

This implies that a fermion and its corresponding antifermion have opposite inner parity, i.e. for a Majorana particle $\psi^c = \pm\psi$ holds which results in $\eta_p = -\eta_p^*$. Therefore, an interesting point with respect to the inner parity occurs for Majorana neutrinos. A Majorana field can be written as

$$\psi_M = \frac{1}{\sqrt{2}}(\psi + \eta_c\psi^c) \quad \text{with} \quad \eta_c = \lambda_c e^{2i\phi}, \quad \lambda_c = \pm 1 \tag{4.3.3}$$

where λ_c is sometime called creation phase. By applying a phase transformation

$$\psi_M \to \psi_M e^{-i\phi} = \frac{1}{\sqrt{2}}(\psi e^{-i\phi} + \lambda_c\psi^c e^{i\phi}) = \frac{1}{\sqrt{2}}(\psi + \lambda_c\psi^c) \equiv \psi_M \tag{4.3.4}$$

it can be achieved that the field ψ_M is an eigenstate with respect to charge conjugation $\mathcal{C}$

$$\psi_M^c = \frac{1}{\sqrt{2}}(\psi^c + \lambda_c\psi) = \lambda_c\psi_M \tag{4.3.5}$$

with eigenvalues $\lambda_c = \pm 1$. This means the Majorana particle is identical to its antiparticle, i.e. ψ_M and ψ_M^c cannot be distinguished. With respect to CP, one obtains

$$\begin{aligned}\psi_M(\boldsymbol{x},t) \xrightarrow{\mathcal{C}} \psi_M^c = \lambda_c\psi_M \xrightarrow{\mathcal{P}} \frac{\lambda_c}{\sqrt{2}}(\eta_p\gamma_0\psi - \lambda_c\eta_p^*\gamma_0\psi^c) \\ = \lambda_c\eta_p\gamma_0\psi_M = \pm i\gamma_0\psi_M(-\boldsymbol{x},t)\end{aligned} \tag{4.3.6}$$

because $\eta_p^* = -\eta_p$. This means that the inner parity of a Majorana particle is imaginary, $\eta_p = \pm i$ if $\lambda_c = \pm 1$. Finally, from eq. 4.3.4 it follows that

$$(\gamma_5\psi_M)^c = \eta_c\mathcal{C}\gamma_5\bar{\psi}_M^T = -\eta_c\mathcal{C}\gamma_5^T\bar{\psi}_M^T = -\gamma_5\psi_M^c = -\lambda_c\gamma_5\psi_M \tag{4.3.7}$$

because $\gamma_5\bar{\psi}_M = (\gamma_5\psi_M)^\dagger\gamma_0 = \psi_M^\dagger\gamma_5\gamma_0 = -\bar{\psi}_M\gamma_5$. Since ψ and ψ^c obey the Dirac equation, ψ_M will also do so [29].

4.4 Dirac and Majorana mass terms

Consider the case of free fields without interactions and start with the Dirac mass. The Dirac equation can be deduced with the help of the Euler-Lagrange equation from a Lagrangian

$$\mathcal{L} = \bar{\psi}\left(i\gamma_\mu\partial^\mu - m_D\right)\psi \tag{4.4.1}$$

where the first term corresponds to the kinetic energy and the second is the mass term. The Dirac mass term is

$$\mathcal{L} = m_D\bar{\psi}\psi \tag{4.4.2}$$

where the combination $\bar{\psi}\psi$ has to be Lorentz invariant and Hermitian. Requiring $\mathcal{L}$ to be Hermitian as well, m_D must be real ($m_D^* = m_D$). Multiplying two arbitrary spinors ψ and ϕ with the same chirality gives

$$\begin{aligned}\bar{\psi}_L\phi_L &= \psi_L^\dagger\gamma_0 P_L\phi = \psi^\dagger\frac{1}{2}\left(1-\gamma_5\right)\gamma_0 P_L\phi \\ &= \psi^\dagger\gamma_0\frac{1}{2}\left(1+\gamma_5\right)P_L\phi = \bar{\psi}\frac{1}{2}\left(1+\gamma_5\right)P_L\phi = \bar{\psi}P_R P_L\phi = 0\end{aligned} \tag{4.4.3}$$

$$\bar{\psi}_R\phi_R = 0 \tag{4.4.4}$$

with $\gamma_5^\dagger = \gamma_5$ and $\gamma_5\gamma_0 = -\gamma_0\gamma_5$. It follows that:

$$\bar{\psi}\phi = (\bar{\psi}_L + \bar{\psi}_R)(\phi_L + \phi_R) = \bar{\psi}_L\phi_R + \bar{\psi}_R\phi_L \tag{4.4.5}$$

In this way the Dirac mass term can be written in its chiral components (Weyl spinors) as:

$$\mathcal{L} = m_D(\bar{\psi}_L\psi_R + \bar{\psi}_R\psi_L) \quad \text{and} \quad \bar{\psi}_R\psi_L = (\bar{\psi}_L\psi_R)^\dagger \tag{4.4.6}$$

Applying this to neutrinos, it requries both a left- and right-handed Dirac neutrino to produce such a mass term. In the Standard Model of particle physics only left-handed neutrinos exist, that is the reason why neutrinos remain massless.

In a more general treatment including ψ^c one might ask which other combinations of spinors behaving like Lorentz scalars can be produced. Three more are possible: $\bar{\psi}^c\psi^c$, $\bar{\psi}\psi^c$ and $\bar{\psi}^c\psi$; $\bar{\psi}^c\psi^c$ is also Hermitian and equivalent to $\bar{\psi}\psi$; $\bar{\psi}\psi^c$ and $\bar{\psi}^c\psi$ are Hermitian conjugates, which can be shown for arbitrary spinors

$$(\bar{\psi}\phi)^\dagger = (\psi^\dagger\gamma_0\phi)^\dagger = \phi^\dagger\gamma_0\psi = \bar{\phi}\psi \tag{4.4.7}$$

using the relation $\gamma_0^\dagger = \gamma_0$. With this we have an additional Hermitian mass term, called the Majorana mass term given by

$$\mathcal{L} = \frac{1}{2}(m_M\bar{\psi}\psi^c + m_M^*\bar{\psi}^c\psi) = \frac{1}{2}m_M\bar{\psi}\psi^c + h.c. \tag{4.4.8}$$

were m_M is called the Majorana mass. Now using the chiral projections with the notation

$$\psi^c_{L,R} = (\psi^c)_{R,L} = (\psi_{R,L})^c \tag{4.4.9}$$

one gets two Hermitian mass terms

$$\mathcal{L}^L = \frac{1}{2}m_L(\bar{\psi}_L\psi^c_R + \bar{\psi}^c_R\psi_L) = \frac{1}{2}m_L\bar{\psi}_L\psi^c_R + h.c. \tag{4.4.10}$$

$$\mathcal{L}^R = \frac{1}{2}m_R(\bar{\psi}^c_L\psi_R + \bar{\psi}_R\psi^c_L) = \frac{1}{2}m_R\bar{\psi}^c_L\psi_R + h.c. \tag{4.4.11}$$

with $m_{L,R}$ as real Majorana masses. Lets us define two Majorana fields

$$\phi_1 = \psi_L + \psi^c_R \qquad \phi_2 = \psi_R + \psi^c_L \tag{4.4.12}$$

which allows eq. 4.4.10 to be rewritten as

$$\mathcal{L}^L = \frac{1}{2}m_L\bar{\phi}_1\phi_1 \qquad \mathcal{L}^R = \frac{1}{2}m_R\bar{\phi}_2\phi_2. \tag{4.4.13}$$

While $\psi_{L,R}$ are interaction eigenstates, $\phi_{1,2}$ are mass eigenstates to $m_{L,R}$. The most general mass term (the Dirac-Majorana mass term) is a combination of equations 4.4.6 and 4.4.10

$$\begin{aligned} 2\mathcal{L} &= m_D(\bar{\psi}_L\psi_R + \bar{\psi}^c_L\psi^c_R) + m_L\bar{\psi}_L\psi^c_R + m_R\bar{\psi}^c_L\psi_R + h.c. \\ &= (\bar{\psi}_L, \bar{\psi}^c_L)\begin{pmatrix} m_L & m_D \\ m_D & m_R \end{pmatrix}\begin{pmatrix} \psi^c_R \\ \psi_R \end{pmatrix} + h.c. \\ &= \bar{\Psi}_L M \Psi^c_R + \bar{\Psi}^c_R M \Psi_L \end{aligned} \tag{4.4.14}$$

where, in the last step, the following was used

$$M = \begin{pmatrix} m_L & m_D \\ m_D & m_R \end{pmatrix} \qquad \Psi_L = \begin{pmatrix} \psi_L \\ \psi^c_L \end{pmatrix} = \begin{pmatrix} \psi_L \\ (\psi_R)^c \end{pmatrix} \tag{4.4.15}$$

implying

$$(\Psi_L)^c = \begin{pmatrix} (\psi_L)^c \\ \psi_R \end{pmatrix} = \begin{pmatrix} \psi^c_R \\ \psi_R \end{pmatrix} = \Psi^c_R. \tag{4.4.16}$$

In the case of CP conservation the elements of the mass matrix M are real. Coming back to neutrinos, in the known neutrino interactions only ψ_L and ψ^c_R are present (active neutrinos) and not the fields ψ_R and ψ^c_L (sterile neutrinos), it is quite common to distinguish between both types in the notation: $\psi_L = \nu_L$, $\psi^c_R = \nu^c_R$, $\psi_R = N_R$, $\psi^c_L = N^c_L$. With this notation, eq. 4.4.14 becomes:

$$\begin{aligned} 2\mathcal{L} &= m_D(\bar{\nu}_L N_R + \bar{N}^c_L\nu^c_R) + m_L\bar{\nu}_L\nu^c_R + m_R\bar{N}^c_L N_R + h.c. \\ &= (\bar{\nu}_L, \bar{N}^c_L)\begin{pmatrix} m_L & m_D \\ m_D & m_R \end{pmatrix}\begin{pmatrix} \nu^c_R \\ N_R \end{pmatrix} + h.c. \end{aligned} \tag{4.4.17}$$

The mass eigenstates are obtained by diagonalizing M

$$\psi_{1L} = \cos(\theta)\psi_L - \sin(\theta)\psi^c_L \qquad \psi^c_{1R} = \cos(\theta)\psi^c_R - \sin(\theta)\psi_R \tag{4.4.18}$$

$$\psi_{2L} = \sin(\theta)\psi_L + \cos(\theta)\psi^c_L \qquad \psi^c_{2R} = \sin(\theta)\psi^c_R + \cos(\theta)\psi_R \tag{4.4.19}$$

while the mixing angle θ is given by

$$\tan(2\theta) = \frac{2m_D}{m_R - m_L}. \tag{4.4.20}$$

The corresponding mass eigenvalues are:

$$\tilde{m}_{1,2} = \frac{1}{2}\left[(m_L + m_R) \pm \sqrt{(m_L - m_R)^2 + 4m^2_D}\right] \tag{4.4.21}$$

To get positive masses, we use:

$$\tilde{m}_k = \epsilon_k m_k \quad \text{with} \quad m_k = |\tilde{m}_k| \quad \text{and} \quad \epsilon_k = \pm 1 \quad (k = 1, 2) \tag{4.4.22}$$

To get a similar expression as eq. 4.4.12, two independent Majorana fields with masses m_1 and m_2 (with $m_k \geq 0$) are introduced via $\phi_k = \psi_{kL} + \epsilon_k\psi^c_{kR}$ or, explicitly

$$\phi_1 = \psi_{1L} + \epsilon_1\psi^c_{1R} = \cos(\theta)(\psi_L + \epsilon_1\psi^c_R) - \sin(\theta)(\psi^c_L + \epsilon_1\psi_R) \tag{4.4.23}$$

$$\phi_2 = \psi_{2L} + \epsilon_2\psi^c_{2R} = \sin(\theta)(\psi_L + \epsilon_2\psi^c_R) + \cos(\theta)(\psi^c_L + \epsilon_2\psi_R) \tag{4.4.24}$$

and, as required for Majorana fields,

$$\phi_k^c = (\psi_{kL})^c + \epsilon_k \psi_{kL} = \epsilon_k(\epsilon_k \psi_{kR}^c + \psi_{kL}) = \epsilon_k \phi_k. \tag{4.4.25}$$

ϵ_k is the CP eigenvalue of the Majorana neutrino ϕ_k. So we finally get the analogous expression to eq. 4.4.12:

$$2\mathcal{L} = m_1 \bar{\phi}_1 \phi_1 + m_2 \bar{\phi}_2 \phi_2 \tag{4.4.26}$$

From this general discussion one can take some interesting special aspects:

(1) $m_L = m_R = 0$ ($\theta = 45^o$): Resulting in $m_{1,2} = m_D$ and $\epsilon_{1,2} = \mp 1$. As Majorana eigenstates, two degenerated states emerge:

$$\phi_1 = \frac{1}{\sqrt{2}}(\psi_L - \psi_R^c - \psi_L^c + \psi_R) = \frac{1}{\sqrt{2}}(\psi - \psi^c) \tag{4.4.27}$$

$$\phi_2 = \frac{1}{\sqrt{2}}(\psi_L + \psi_R^c + \psi_L^c + \psi_R) = \frac{1}{\sqrt{2}}(\psi + \psi^c) \tag{4.4.28}$$

These can be used to construct a Dirac field ψ:

$$\frac{1}{\sqrt{2}}(\phi_1 + \phi_2) = \psi_L + \psi_R = \psi \tag{4.4.29}$$

The corresponding mass term eq. 4.4.26 is (because $\bar{\phi}_1 \phi_2 + \bar{\phi}_2 \phi_1 = 0$):

$$\mathcal{L} = \frac{1}{2} m_D (\bar{\phi}_1 + \bar{\phi}_2)(\phi_1 + \phi_2) = m_D \bar{\psi} \psi \tag{4.4.30}$$

We are left with a pure Dirac field. As a result, a Dirac field can be seen, using eq. 4.4.29, to be composed of two degenerated Majorana fields, i.e. a Dirac ν can be seen as a pair of degenerated Majorana ν. The Dirac case is, therefore, a special solution of the more general Majorana case.

(2) $m_D \gg m_L, m_R$ ($\theta \approx 45^o$): In this case the states $\phi_{1,2}$ are, almost generated with $m_{1,2} \approx m_D$ and such an object is called a pseudo-Dirac neutrino.

(3) $m_D = 0$ ($\theta = 0$): In this case $m_{1,2} = m_{L,R}$ and $\epsilon_{1,2} = 1$. So $\phi_1 = \psi_L + \psi_R^c$ and $\phi_2 = \psi_R + \psi_L^c$. This is the pure Majorana case.

(4) $m_R \gg m_D, m_L = 0$ ($\theta = (m_D/m_R) \ll 1$): One obtains two mass eigenvalues:

$$m_\nu = m_1 = \frac{m_D^2}{m_R} \quad m_N = m_2 = m_R \left(1 + \frac{m_D^2}{m_R^2}\right) \approx m_R \tag{4.4.31}$$

and

$$\epsilon_{1,2} = \mp 1. \tag{4.4.32}$$

The corresponding Majorana fields are:

$$\phi_1 \approx \psi_L - \psi_R^c \quad \phi_2 \approx \psi_L^c + \psi_R \tag{4.4.33}$$

It is interesting that with the largest Dirac mass eigenvalue of the order of the electroweak scale, $m_D \sim 200$ GeV, the right handed scale $m_R \sim 10^{15}$ GeV which is close to the typical GUT scales, one obtains the mass of the heaviest of the light neutrinos $m_\nu \sim (10^{-2} - 10^{-1})$ eV, which is just of the right order of magnitude for the neutrino oscillation. The last scenario is especially popular within the seesaw model of neutrino mass generation and will be discussed now.

4.5 See-saw mechanism

Although the Standard Model has been marvelously successful for the last couple of decades, in 1998 the breakthrough regarding the neutrino flavour oscillations became a discovery. Indeed, the direct implication was that neutrinos could *not* be massless. Then if neutrinos have mass we know they may be either *Dirac* or *Majorana* particles. But the corresponding mass terms are not possible in the Standard Model because:

- Right-handed neutrinos are absent so that a *Dirac mass* is not possible
- Lepton number is exactly conserved so that a *Majorana mass* is not possible

Hence, any attempt to generate non-zero neutrino masses has to violate one of the above two assumptions and is by that way demolishing the dream of the Standard Model as a final theory. So, how can we extend the Standard Model so as to accommodate non-zero neutrino masses? We have mainly three theoretical level:

- To extend the scalar content (the mass could come from another VEV)
- To extend the fermion content (coupling with heavy particles could generate mass)
- To enlarge the gauge group (i.e. add new symmetries)

The natural mass scale in the Standard Model is the electroweak scale which is of order $v \simeq 246$ GeV. The smallness of, e.g., the electron mass $m_e \simeq 0.511$ MeV is not explained; however, it is easily accommodated in the Standard Model through the proper choice of the corresponding Yukawa coupling, $f_e \simeq 3 \cdot 10^{-6}$. At the same time, similar explanation of the smallness of the electron neutrino mass, $m_{\nu_e} \leq 5$ eV, would require the Yukawa coupling $f_{\nu_e} \leq 3 \cdot 10^{-11}$. Does this pose any problem? If we are willing to accept a very small Yukawa coupling of the electron, why should not we accept small neutrino Yukawa couplings as well? After all, 10^{-11} may be as good (or as bad) as 10^{-6}. The problem is that, except for neutrinos, the masses of all the fermions in each of the three generations are within 1-2 orders of magnitude of each other. The inclusion of neutrinos leads to huge disparities of the fermion masses within each generation. Therefore, if a future more complete theory explains why there is a large mass hierarchy between generations, it would still remain to be explained why neutrinos are so light compared to the other fermions of the same generation.

The see-saw mechanism provides a very simple and attractive explanation of the smallness of neutrino mass. It generates a small non-zero mass with the existence of a very large unknown scale Λ generated by higher dimensional operators. The operator needed in the see-saw mechanism, and the lowest dimensional operator beyond the Standard Model, is the dimension 5 operator,

$$\mathcal{O}_5 = \frac{1}{M}(\phi\tau_2\psi)^T C(\phi\tau_2\psi) \tag{4.5.1}$$

where M is the cutoff scale of the effective field theory. In the minimal standard electroweak model there exists three types of see-saw models, leading to this effective operator at tree-level, using only renormalizable interactions. The Standard Model lepton doublet $\psi = (\nu_L, l_L)^T$ and the Higgs doublet $\phi = (\phi^+, \phi^0)^T$ are used in all three models, and interact in the following ways.

4.5.1 The type I see-saw mechanism

The most suggestive completion of the minimal Standard Model is the introduction of ν_R (per family of fermion), a gauge singlet chiral fermion. This is a right handed neutrino, whose existence is appealing from the structural quark-lepton symmetry. A new renormalizable Yukawa coupling (written here for one generation case only) then follows:

$$\mathcal{L} = y_D \bar{\ell}_L \sigma_2 \Phi^* \nu_R + \frac{M_R}{2} \nu_R^T C \nu_R + h.c. \tag{4.5.2}$$

In type I, if we use same condition, we will get eigenvalues for the neutrinos from eq. 4.4.32. This is the original see-saw formula to accommodate small neutrino masses.

4.5.2 The type II see-saw mechanism

Instead of ν_R, a $Y = 2$ triplet Higgs $\Delta_L \equiv \mathbf{\Delta}_L \cdot \boldsymbol{\sigma}$ can play the same role. From the new Yukawas

$$\mathcal{L}(\Delta) = y_\Delta^{ij} \ell_i^T C \sigma_2 \Delta_L \ell_j + h.c. \tag{4.5.3}$$

where $i, j = 1, ..., N$ counts the generations, neutrinos get a mass when Δ_L gets a VEV

$$M_\nu = y_\Delta \langle \Delta \rangle. \tag{4.5.4}$$

The VEV $\langle \Delta \rangle$ results from the cubic scalar interaction

$$V = \mu \Phi^T \sigma_2 \Delta_L^* \Phi + M_\Delta^2 \mathrm{Tr}[\Delta_L^\dagger \Delta_L] + .. \tag{4.5.5}$$

with

$$\langle \Delta \rangle \simeq \frac{\mu v^2}{M_\Delta^2} \tag{4.5.6}$$

where one expects μ of order M_Δ. If $M_\Delta >> v$, neutrinos are naturally light. Notice that equations 4.5.4 and 4.5.6 reproduce again eq. 4.4.32 as it must be: For large scales of new physics, neutrino mass must come from $d = 5$ operator.

4.5.3 The type III see-saw mechanism

The Yukawa interaction in eq. 4.5.2 for new singlet fermions carries on straightforwardly to SU(2) triplets too, written now in the Majorana notation (where for simplicity the generation index is suppressed and also an index counting the number of triplet - recall that at least two are needed in order to provide two massive light neutrinos):

$$\mathcal{L}(\Sigma) = y_\Sigma \ell^T C_2 \boldsymbol{\sigma} \cdot \mathbf{\Sigma} \Phi + M_\Sigma \mathbf{\Sigma} C \mathbf{\Sigma} \tag{4.5.7}$$

In exactly the same manner as before in type I, one gets a type III see-saw for $M_\Sigma >> v$:

$$M_\nu = -y_\Sigma^T \frac{1}{M_\Sigma} y_\Sigma v^2 \tag{4.5.8}$$

Again, as in the type I case, one would need at least two triplets to account for the solar and atmospheric neutrino oscillations (or triplet and a singlet). And, as before, eq. 4.5.8 simply reproduces eq. 4.4.32 for large M_Σ. This is some of the see-saw mechanisms in the literature and there also exists other ways in generating non-zero neutrino masses. For more information, look at [[30], [31], [32]].

5

Neutrino oscillations

In the case of a non-vanishing rest mass of the neutrino, the weak and mass eigenstates are not necessarily identical. This allows for the phenomenon of neutrino oscillations, a kind of flavour oscillation which is already known in other particle systems. It can be described by pure quantum mechanics. They are observable as long as the neutrino wave packets from a coherent superposition of states. Such oscillations among the different neutrino flavours do not conserve individual lepton numbers, only total lepton number. We start with the most general case first, before turning to the more common two- and three-flavour scenarios.

5.1 General formalism

Let us assume that there is an arbitrary number of n orthonormal eigenstates. The n flavour eigenstates $|\nu_\alpha\rangle$ with $\langle\nu_\beta|\nu_\alpha\rangle = \delta_{\alpha\beta}$ are connected to the n mass eigenstates $|\nu_i\rangle$ with $\langle\nu_i|\nu_j\rangle = \delta_{ij}$ via a unitary mixing matrix U

$$|\nu_\alpha\rangle = \sum_i U_{\alpha i}|\nu_i\rangle \qquad |\nu_i\rangle = \sum_\alpha (U^\dagger)_{i\alpha}|\nu_\alpha\rangle = \sum_\alpha U^*_{\alpha i}|\nu_\alpha\rangle \tag{5.1.1}$$

with the relations

$$U^\dagger U = 1 \qquad \sum_i U_{\alpha i}U^*_{\beta i} = \delta_{\alpha\beta} \qquad \sum_\alpha U_{\alpha i}U^*_{\alpha j} = \delta_{ij}. \tag{5.1.2}$$

In the case of antineutrinos, i.e. $U_{\alpha i}$ has to be replaced by $U^*_{\alpha i}$:

$$|\bar\nu_\alpha\rangle = \sum_i U^*_{\alpha i}|\bar\nu_i\rangle \tag{5.1.3}$$

In general, a unitary $n \times n$ matrix depends on $n(n-1)/2$ angles and $n(n+1)/2$ phases. In the Dirac case, $2n-1$ phases can be removed by a proper rephasing of the left-handed fields, leaving $n(n+1)/2 - (2n-1) = (n-1)(n-2)/2$ physical phases. Thus, in the Dirac case CP non-conservation is only possible in the case $n \geq 3$ generations. In the Majorana case there is less freedom to rephase the fields since the Majorana mass terms are of the form $\nu_L\nu_L + h.c.$ rather than the form $\bar\nu_R\nu_L + h.c.$ and so the phases of neutrino fields cannot be absorbed. Therefore, in the Majorana case only n phases can be removed, leaving $n(n+1)/2 - n = n(n-1)/2$ physical phases. Out of these, $(n-1)(n-2)/2$ are the usual Dirac-type phases while the remaining $n-1$ are specific for the Majorana case, so called Majorana phases.

The mass eigenstates $|\nu_i\rangle$ are stationary states and show a time dependence according to

$$|\nu_i(t)\rangle = e^{-iE_it}|\nu_i\rangle \tag{5.1.4}$$

assuming neutrinos with momentum p emitted by a source positioned at $x = 0$ ($t = 0$)

$$|\nu_i(0)\rangle = |\nu_i\rangle \tag{5.1.5}$$

and being relativistic

$$E_i = \sqrt{m_i^2 + p_i^2} \simeq p_i + \frac{m_i^2}{2p_i} \simeq E + \frac{m_i^2}{2E} \tag{5.1.6}$$

for $p >> m_i$ and $E \approx p$ as neutrino energy. The flavour neutrino is a coherent superposition of neutrino states with definite mass. Neutrinos are produced and detected as flavour states. Therefore, neutrinos with flavour $|\nu_\alpha\rangle$ emitted by a source at $t = 0$ develop with time into a mass eigenstate as follows:

$$|\nu_\alpha(t)\rangle = \sum_i U_{\alpha i} e^{-iE_i t} |\nu_i\rangle = \sum_{i,\beta} U_{\alpha i} U^*_{\beta i} e^{-iE_i t} |\nu_\beta\rangle \tag{5.1.7}$$

Different neutrino masses imply that the phase factor in eq. 5.1.7 is different. This means that the flavour content of the final states differs from the initial one. At macroscopic distances this effect can be large in spite of small differences in neutrino masses. The time-dependent transition amplitude for a flavour conversion $\nu_\alpha \to \nu_\beta$ is given by:

$$A(\alpha \to \beta)(t) = \langle \nu_\beta | \nu_\alpha(t) \rangle = \sum_i U^*_{\beta i} U_{\alpha i} e^{-iE_i t} \tag{5.1.8}$$

Using eq. 5.1.6 this can be written as

$$A(\alpha \to \beta)(t) = \langle \nu_\beta | \nu_\alpha(t) \rangle = \sum_i U^*_{\beta i} U_{\alpha i} \exp\left(-i \frac{m_i^2}{2} \frac{L}{E}\right) = A(\alpha \to \beta)(L) \tag{5.1.9}$$

with $L = x = ct$ being the distance between source and detector. In an analogous way, the amplitude for antineutrino transitions is obtained:

$$A(\bar{\alpha} \to \bar{\beta})(t) = \sum_i U_{\beta i} U^*_{\alpha i} e^{-iE_i t} \tag{5.1.10}$$

The transition probability P can be obtained from the transition amplitude [33]

$$\begin{aligned} P(\alpha \to \beta)(t) &= |A(\alpha \to \beta)|^2 = \sum_i \sum_j U_{\alpha i} U^*_{\alpha j} U^*_{\beta i} U_{\beta j} e^{-i(E_i - E_j)t} \\ &= \delta_{\alpha\beta} - 4 \sum_{i>j=1}^{3} \mathrm{Re}(U_{\alpha i} U^*_{\beta i} U^*_{\alpha j} U_{\beta j}) \sin^2\left(\frac{\Delta m^2_{ij} L}{4E}\right) \\ &+ 4 \sum_{i>j=1}^{3} \mathrm{Im}(U_{\alpha i} U^*_{\beta i} U^*_{\alpha j} U_{\beta j}) \sin\left(\frac{\Delta m^2_{ij} L}{4E}\right) \cos\left(\frac{\Delta m^2_{ij} L}{4E}\right) \end{aligned} \tag{5.1.11}$$

with

$$\Delta m^2_{ij} = m_i^2 - m_j^2. \tag{5.1.12}$$

If you want the probability for antineutrinos, you have to change the plus sign to a minus sign in front of the third term in eq. 5.1.11. Using CP invariance ($U_{\alpha i}$ real), this can be simplified to:

$$P(\alpha \to \beta)(t) = \delta_{\alpha\beta} - 4 \sum_{j>i} U_{\alpha i} U_{\alpha j} U_{\beta i} U_{\beta j} \sin^2\left(\frac{\Delta m^2_{ij}}{4} \frac{L}{E}\right) \tag{5.1.13}$$

Evidently, the probability of finding the original flavour is given by:

$$P(\alpha \to \alpha) = 1 - \sum_{\alpha \neq \beta} P(\alpha \to \beta) \tag{5.1.14}$$

As can be seen from eq. 5.1.11 there will be oscillatory behavior as long as one of the involving neutrino mass eigenstates are different from zero and if there is a mixing (non-diagonal terms in U) among the flavours. In addition, the observation of oscillations allow no absolute mass measurement, oscillations are only sensitive to Δm^2. Last but not least, neutrino masses should not be exactly degenerated. Another important feature is the dependence of the oscillation probability on L/E. Majorana phases are unobservable.

5.2 CP and T violation in neutrino oscillations

Comparison of eq. 5.1.8 with eq. 5.1.10 yields a relation between neutrinos and antineutrinos

$$P(\bar{\alpha} \to \bar{\beta})(t) = P(\alpha \to \beta)(t) \neq P(\beta \to \alpha)(t) \tag{5.2.1}$$

if CPT is conserved. This relation is a direct consequence of the CPT theorem. CP violation manifests itself if the oscillation probabilities of $\nu_\alpha \to \nu_\beta$ is different from its CP conjugate process $\bar{\nu}_\alpha \to \bar{\nu}_\beta$. So an observable would be:

$$\Delta P^{CP}_{\alpha\beta} = P(\nu_\alpha \to \nu_\beta) - P(\bar{\nu}_\alpha \to \bar{\nu}_\beta) \neq 0 \quad \alpha \neq \beta \tag{5.2.2}$$

Similarly, T violation can be tested if the probabilities of $\nu_\alpha \to \nu_\beta$ are different from the T conjugate process $\nu_\beta \to \nu_\alpha$. If CPT conservation holds, violation of T is equivalent to that of CP. From CPT invariance one finds $\Delta P_{\alpha\beta} = -\Delta P_{\beta\alpha}$. Using U_{PMNS} (see eq. 5.4.1) it can be shown explicitly that in vacuum $\Delta P^{CP}_{\alpha\beta}$ and $\Delta P^{T}_{\alpha\beta}$ are equal:

$$\begin{aligned}\Delta P^{CP}_{\alpha\beta} = \Delta P^{T}_{\alpha\beta} =& 4 s_{12} c_{12} s_{13} c^2_{13} c_{23} s_{23} \sin(\delta) \\ &\times \left[\sin\left(\frac{\Delta m^2_{21} L}{2E}\right) + \sin\left(\frac{\Delta m^2_{32} L}{2E}\right) + \sin\left(\frac{\Delta m^2_{13} L}{2E}\right) \right]\end{aligned} \tag{5.2.3}$$

Again for antineutrinos, you have to do the transformation $\delta \to -\delta$. This expression has several interesting features. Note that for CP or T violation effects to be present, all the angles must be non-zero and, therefore, three-flavour mixing is essential. Second, it vanishes in the limit $\delta = 0$ or $\delta = \pi$. Third, since the mass differences satisfy the relation (if we don't care about sterile neutrinos) $\Delta m^2_{21} + \Delta m^2_{32} + \Delta m^2_{13} = 0$, the CP-odd asymmetry vanishes if even one of Δm^2_{ij} is zero. To be a bit more specific we now consider the case of two flavour oscillations.

5.3 Oscillations with two flavours

In this case the relation between the neutrino states is described by one mixing angle θ and one mass difference $\Delta m^2 = m^2_2 - m^2_1$. The unitary transformation in eq. 5.1.1 is analogous to the Cabibbo matrix given by (taking ν_e and ν_μ):

$$\begin{pmatrix} \nu_e \\ \nu_\mu \end{pmatrix} = \begin{pmatrix} \cos(\theta) & \sin(\theta) \\ -\sin(\theta) & \cos(\theta) \end{pmatrix} \begin{pmatrix} \nu_1 \\ \nu_2 \end{pmatrix} \tag{5.3.1}$$

Using the formula from the previous section, the corresponding transítion probability is:

$$\begin{aligned} P(\nu_e \to \nu_\mu) = P(\nu_\mu \to \nu_e) = P(\bar{\nu}_e \to \bar{\nu}_\mu) = P(\bar{\nu}_\mu \to \bar{\nu}_e) \\ = \sin^2(2\theta) \sin^2\left(\frac{\Delta m^2 L}{4E}\right) = 1 - P(\nu_e \to \nu_e) \end{aligned} \tag{5.3.2}$$

This formula explicitly shows that oscillations only occur if both θ and Δm^2 are non-vanishing. That is the reason why neutrinos need mass. The phase factor can be rewritten as

$$\frac{\Delta m^2 c^3 L}{4\hbar E} = \frac{\text{GeV fm}}{4\hbar c} \times \frac{\Delta m^2}{\text{eV}^2} \frac{L/\text{km}}{E/\text{GeV}} \approx 1.267 \times \frac{\Delta m^2}{\text{eV}^2} \frac{L/\text{km}}{E/\text{GeV}} \tag{5.3.3}$$

where in the last step some practical units were used. The oscillatory term can be expressed as:

$$\sin^2\left(\frac{\Delta m_{ij}^2 L}{4E}\right) = \sin^2\left(\pi \frac{L}{L_0}\right) \quad \text{with} \quad L_0 = 4\pi\hbar c \frac{E}{\Delta m^2} = 2.48 \frac{E/\text{GeV}}{\Delta m^2/\text{eV}^2} \tag{5.3.4}$$

The oscillation length L_0 describes the period of one full oscillation cycle. Increasing the energy the oscillations becomes more damped whereas increasing Δm^2 more rapid oscillations occurs. The mixing angle $\sin^2(2\theta)$ determines the amplitude of the oscillation while Δm^2 influences the oscillation length.

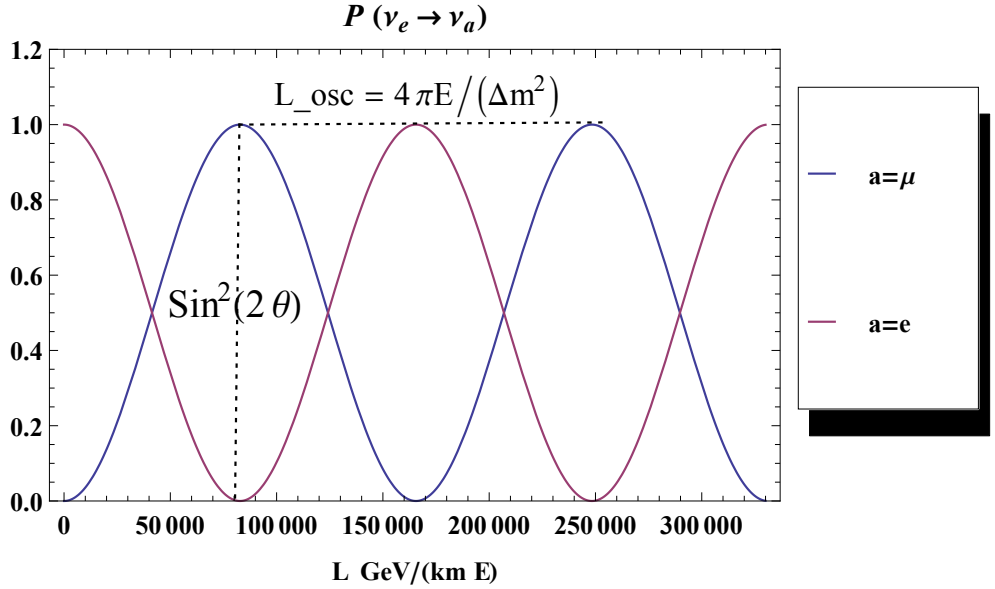

Figure 5.3.1: *Probability P that a neutrino of flavour e oscillates into a neutrino of flavour $a = e, \mu$ as a function of baseline L over energy E for the two flavour case. Oscillation parameters:* $\sin^2(2\theta) = 1, \Delta m^2 = 7.59 \cdot 10^{-5}\, eV^2$

5.4 The case for three flavours

A probably more realistic scenario to consider is that of three known neutrino flavours. The mixing matrix U_{PMNS} can be parameterized by the following

$$U_{\text{PMNS}}^{\text{Dirac}} = \begin{pmatrix} c_{12}c_{13} & s_{12}c_{13} & s_{13}e^{-i\delta} \\ -s_{12}c_{23} - c_{12}s_{23}s_{13}e^{i\delta} & c_{12}c_{23} - s_{12}s_{23}s_{13}e^{i\delta} & s_{23}c_{13} \\ s_{12}s_{23} - c_{12}s_{23}s_{13}e^{i\delta} & -c_{12}s_{23} - s_{12}c_{23}s_{13}e^{i\delta} & c_{23}c_{13} \end{pmatrix} \tag{5.4.1}$$

where $s_{ij} = \sin(\theta_{ij})$, $c_{ij} = \cos(\theta_{ij})$, (i, j = 1, 2, 3). In the Majorana case, the requirement of particle and antiparticle to be identical, restricts the freedom to redefine the fundamental fields. For three flavours two additional phases have to be introduced resulting in

a mixing matrix of the form:

$$U_{\text{PMNS}}^{\text{Majorana}} = U_{\text{PMNS}}^{\text{Dirac}} \text{diag}(1, e^{i\alpha}, e^{i\beta}) \tag{5.4.2}$$

Note that now more Δm^2 quantities are involved both in magnitude and sign: Although in two flavour oscillation in vacuum the sign does not enter, in three flavour oscillation, which includes both matter effects (will be discussed later) and CP violation, the signs of the Δm^2 quantities enter and can, in principle, be measured. In the absence of any matter effects, the probability is given by

$$\begin{aligned} P(\nu_\alpha \to \nu_\beta) =& \delta_{\alpha\beta} - 4 \sum_{i>j=1}^{3} \text{Re}(K_{\alpha\beta,ij}) \sin^2\left(\frac{\Delta m_{ij}^2 L}{4E}\right) \\ &+ 4 \sum_{i>j=1}^{3} \text{Im}(K_{\alpha\beta,ij}) \sin\left(\frac{\Delta m_{ij}^2 L}{4E}\right) \cos\left(\frac{\Delta m_{ij}^2 L}{4E}\right) \end{aligned} \tag{5.4.3}$$

where

$$K_{\alpha\beta,ij} = U_{\alpha i} U_{\beta i}^* U_{\alpha j}^* U_{\beta j}. \tag{5.4.4}$$

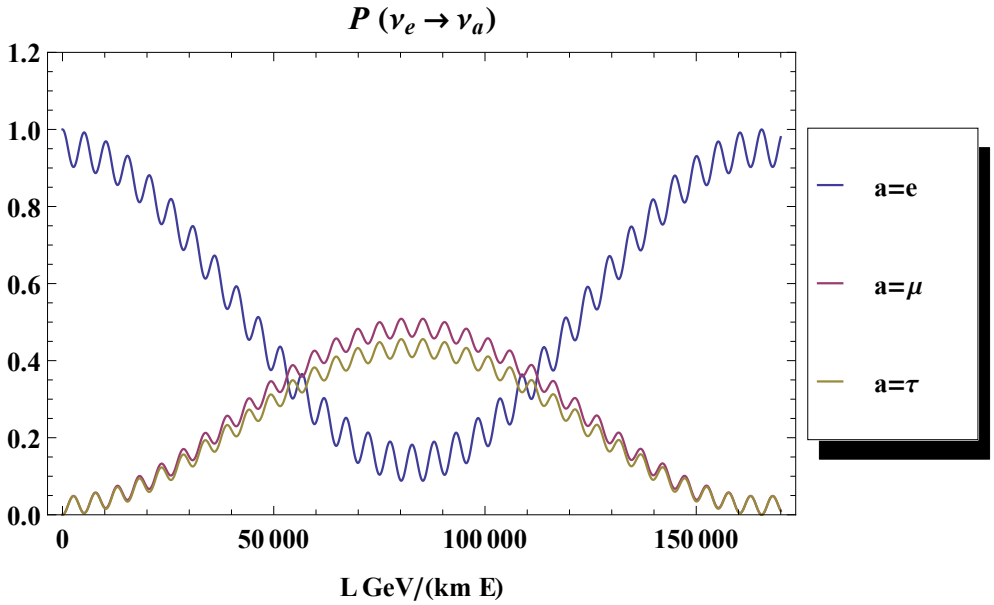

Figure 5.4.1: *Probability P that a neutrino of flavour e oscillates into a neutrino of flavour $a = e, \mu, \tau$ as a function of baseline L over energy E for the three flavour case. Oscillation parameters:* $\sin^2(\theta_{12}) = 0.3127$, $\sin^2(\theta_{13}) = 0.0245$, $\sin^2(\theta_{23}) = 0.5$, $\Delta m_{21}^2 = 7.59 \cdot 10^{-5}\, eV^2$, $\Delta m_{32}^2 = 2.43 \cdot 10^{-3}\, eV^2$ *and* $\delta = 0$

As you can see in figure 5.4.1 there are two oscillations, a fast and a slow one. These oscillations depends on the mass differences, which can be seen from eq. 5.3.4. From this equation we can determine that the fast oscillation comes from Δm_{32}^2 and the slow oscillation comes from Δm_{21}^2. Unlike in the two flavour case, transition probabilities in general do not have a simple form. There are, however, several practically important limiting cases in which one can obtain very simple approximate expressions for the oscillation probabilities in terms of the two flavour ones. Assume first that the neutrino mass difference have a hierarchy:

$$|\Delta m_{21}^2| << |\Delta m_{31}^2| \simeq |\Delta m_{32}^2| \tag{5.4.5}$$

This means that either $m_1 << m_2 << m_3$ (direct hierarchy) or $m_3 << m_1 \approx m_2$ (inverted mass hierarchy). These cases are of practical interest since the solar neutrino data indicate that one needs a small mass difference $\Delta m^2_{21} \sim 10^{-5}\,\mathrm{eV}^2$ for the solution of the solar neutrino problem through matter-enhanced neutrino oscillations whereas the explanation for the atmospheric neutrino experiments through the neutrino oscillations requires $\Delta m^2_{23} \sim 10^{-3}\,\mathrm{eV}^2$, much larger than Δm^2_{21}. Consider first the oscillations over the baselines L for which:

$$\frac{\Delta m^2_{21} L}{2E} << 1 \tag{5.4.6}$$

This case is relevant for atmospheric, reactor and accelerator neutrino experiments. It follows from this assumption that the oscillations due to the small mass difference Δm^2_{21} are effectively frozen in this case, and one can consider the limit $\Delta m^2_{21} \to 0$. The probability of $\nu_\alpha \to \nu_\beta$ oscillations then takes a very simple form:

$$P(\nu_\alpha \to \nu_\beta) = 4|U_{\alpha 3}|^2 |U_{\beta 3}|^2 \sin^2\left(\frac{\Delta m^2_{13} L}{4E}\right) \tag{5.4.7}$$

It resembles the two flavour oscillation probability. The probabilities of oscillations between ν_e, ν_μ and ν_τ are

$$P(\nu_e \to \nu_\mu) = 4|U_{e3}|^2 |U_{\mu 3}|^2 \sin^2\left(\frac{\Delta m^2_{31} L}{4E}\right) = s^2_{23} \sin^2(2\theta_{13}) \sin^2\left(\frac{\Delta m^2_{31} L}{4E}\right) \tag{5.4.8}$$

$$P(\nu_e \to \nu_\tau) = 4|U_{e3}|^2 |U_{\tau 3}|^2 \sin^2\left(\frac{\Delta m^2_{31} L}{4E}\right) = c^2_{23} \sin^2(2\theta_{13}) \sin^2\left(\frac{\Delta m^2_{31} L}{4E}\right) \tag{5.4.9}$$

$$P(\nu_\mu \to \nu_\tau) = 4|U_{\mu 3}|^2 |U_{\tau 3}|^2 \sin^2\left(\frac{\Delta m^2_{31} L}{4E}\right) = c^4_{13} \sin^2(2\theta_{23}) \sin^2\left(\frac{\Delta m^2_{31} L}{4E}\right) \tag{5.4.10}$$

with $P(\nu_\beta \to \nu_\alpha) = P(\nu_\alpha \to \nu_\beta)$. They depend only on the elements of the third column of the lepton mixing matrix and one mass difference. The survival probability for electron neutrinos takes a particularly simple form

$$P(\nu_e \to \nu_e) = 1 - \sin^2(2\theta_{13}) \sin^2\left(\frac{\Delta m^2_{31} L}{4E}\right) \tag{5.4.11}$$

i.e. it coincides with the ν_e survival probability in the two flavour case with mass difference $\Delta m^2 = \Delta m^2_{31}$ and mixing angle $\theta = \theta_{13}$. Consider now another limiting case, which is relevant for the solar neutrino oscillations and also for very long baseline reactor experiments. We shall be again assuming the hierarchy eq. 5.4.5 and in addition

$$\frac{\Delta m^2_{31} L}{2E} \simeq \frac{\Delta m^2_{32} L}{2E} >> 1 \tag{5.4.12}$$

whereas the condition eq. 5.4.6 is no longer necessary. In this case the oscillations due to the mass differences Δm^2_{31} and Δm^2_{32} are very fast and lead to an averaged effect; the ν_e survival probability is:

$$P(\nu_e \to \nu_e) \simeq c^4_{13} \left[1 - \sin^2(2\theta_{12}) \sin^2\left(\frac{\Delta m^2_{21} L}{4E}\right)\right] + s^4_{13} \tag{5.4.13}$$

Finally, consider the limit $U_{e3} = 0$ (the results will be also approximately valid for $|U_{e3}| << 1$). In this case one obtains

$$P(\nu_e \to \nu_\mu) = c^2_{23} \sin^2(2\theta_{12}) \sin^2(\Delta_{21}) \tag{5.4.14}$$

$$P(\nu_e \to \nu_\tau) = s^2_{23} \sin^2(2\theta_{12}) \sin^2(\Delta_{21}) \tag{5.4.15}$$

$$P(\nu_\mu \to \nu_\tau) = \sin^2(\theta_{23})(-s^2_{12}c^2_{12} \sin^2(\Delta_{21}) + s^2_{12} \sin^2(\Delta_{31}) + c^2_{12} \sin^2(\Delta_{32})) \tag{5.4.16}$$

where $\Delta_{ij} = \Delta m^2_{ij} L/(4E)$ and no assumption about the hierarchy of the mass differences has been made. Notice that the limiting cases are not mutually excluding, i.e. have some overlap with each other. In general, when considering the propagation of solar neutrinos in the Sun or in the Earth, one should take into account matter effects on neutrino oscillations. The same is true for the terrestrial atmospheric and long baseline accelerator neutrino oscillation experiments in which the neutrino trajectories or their significant portions go through the matter of the Earth. Matter effects on $\nu_\mu \leftrightarrow \nu_\tau$ oscillations are relatively small (they vanish in the two flavour approximation), but they may be quite appreciable for $\nu_e \leftrightarrow \nu_\mu$ and $\nu_e \leftrightarrow \nu_\tau$ oscillations.

5.5 Experimental consideration

The search for neutrino oscillations can be performed in two different ways - an appearance or disappearance mode. In the latter case one explores whether less than the expected number of neutrinos of a produced flavour arrive at a detector or whether the spectral shape changes if observed at various distances from a source. This method is not able to determine the new neutrino flavour. An appearance experiment searches for possible new flavours, which do not exist in the original beam or produce an enhancement of an existing neutrino flavour. The identification of the various flavours relies on the detection of the corresponding charged lepton produced in the charged current interactions

$$\nu_\ell + N \to \ell^- + X \qquad \text{with} \quad \ell \equiv e, \mu, \tau \tag{5.5.1}$$

where X denotes the hadronic final state. Several neutrino sources can be used to search for oscillations. The most important are:

- nuclear power plants ($\bar{\nu}_e$)
- accelerators (ν_e, ν_μ, $\bar{\nu}_e$, $\bar{\nu}_\mu$)
- the atmosphere (ν_e, ν_μ, $\bar{\nu}_e$, $\bar{\nu}_\mu$)
- the Sun (ν_e)

Which part of the $\Delta m^2 - \sin^2(2\theta)$ parameter space is explored depends on the ratio L/E. The relation

$$\Delta m^2 \propto E/L \tag{5.5.2}$$

shows that the various mentioned sources sometimes cannot probe each other, i.e. high-energy accelerators ($E \sim 1 - 100$ GeV, $L \sim 1$ km) are not able to check the solar neutrino data ($E \sim 1$ MeV, $L \sim 10^8$ km). The equation above also defines the minimal Δm^2 which can be explored. Three cases have to be considered with respect to a possible observation of oscillation:

- $L/E \ll \frac{4}{\Delta m^2}$, i.e. $L \ll L_0$. Here, the experiment is too close to the source and the oscillations have no time to develop.

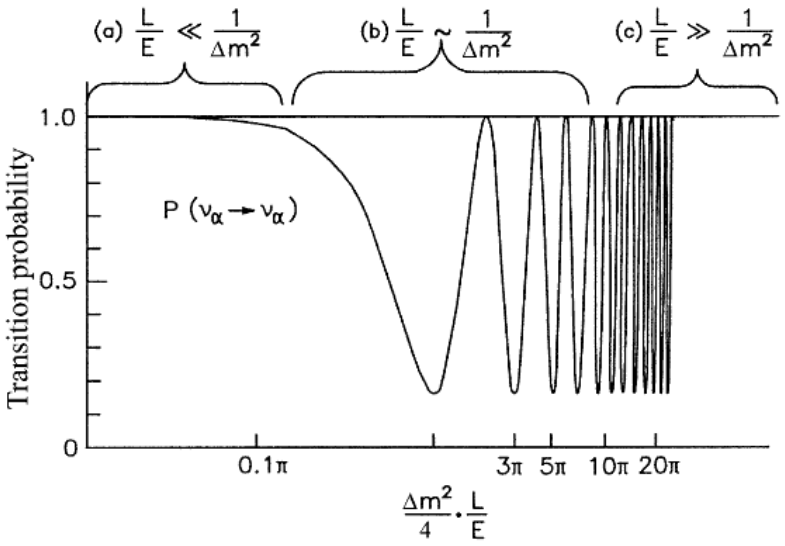

Figure 5.5.1: *Logarithmic plot of the oscillation probability $P(\nu_\alpha \to \nu_\alpha)$ as a function of L/E for $\sin^2(2\theta) = 0.83$. The brackets denote three possible cases: (a) no oscillations ($L/E \ll 1/\Delta m^2$); (b) oscillation $L/E \sim 1/\Delta m^2$; and (c) average oscillation for $L/E \gg 1/\Delta m^2$.*

- $L/E \sim \frac{4}{\Delta m^2}$, i.e. $L \sim L_0$. This is a necessary condition to observe oscillations and it is the most sensitive region
- $L/E \gg \frac{4}{\Delta m^2}$, i.e. $L \gg L_0$. Several oscillations have happened between the source and the detector. Normally, experiments do then measure L/E not precisely enough to resolve the oscillation pattern but measure only an average transition probability.

Two points which influence the experimental sensitivity and the observation of oscillations have to be considered. First of all, L is not often not well defined. This is the case when dealing with an extended source (Sun, atmosphere, decay tunnels). Alternatively, E might not be known exactly. This might be the case if the neutrino source has an energy spectrum N(E) and E will not be measured in a detector. Last but not least, for some experiments there is no chance to vary L and/or E because it is fixed (e.g. in the case of the Sun); therefore, the explorable Δm^2 region is constrained by Nature.

5.6 Neutrino mass hierarchy, θ_{23} octant and matter effects

The mixing angles θ_{ij} and the magnitudes of the mass differences Δm^2_{ij} are well measured by several neutrino experiments, using neutrinos produced in the Sun, in the atmosphere, in reactors or with accelerators [[34], [35], [36], [37]]. One remaining question is the order of the neutrino masses. We differentiate between normal neutrino mass hierarchy (NH), $m_1 < m_2 < m_3$, and inverted neutrino mass hierarchy (IH), $m_3 < m_1 < m_2$ (see figure 5.6.1). The problem of the correct mass hierarchy cannot be solved by studying only neutrino oscillations in vacuum because these oscillations do not depend on the sign of Δm^2_{23}. The situation changes if we take into account that neutrinos can interact with nucleons and electrons if they propagate through matter on their way to the detector. These matter effects can enhance three flavour transition and depend on the sign of Δm^2_{32}. This is also how the sign of Δm_{21} was measured. Knowing the mass hierarchy will help alot in the determination of the octant of the mixing angle θ_{23} since there will be

one less parameter you have to vary in the fit (will be discussed later). However, the θ_{23} octant can be resolved through matter effects even without the knowledge of the neutrino mass hierarchy.

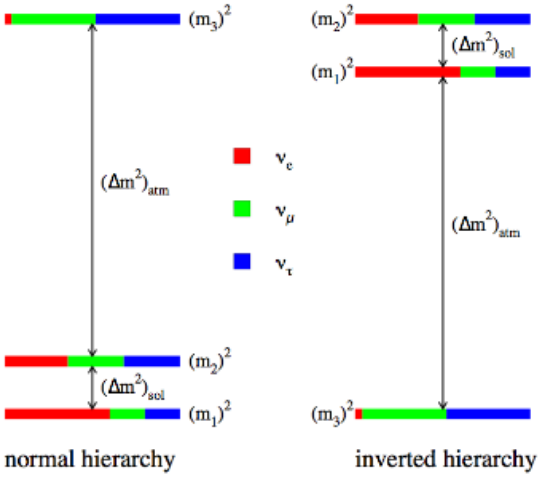

Figure 5.6.1: *Pictorial representation of the possible neutrino mass hierarchies. Note* Δm^2_{atm} *is equivalent to* Δm^2_{32} *and* Δm^2_{sol} is equivalent to Δm^2_{21}.

5.6.1 Neutrino oscillation in matter

Neutrino oscillations in matter may differ from the oscillations in vacuum in a very significant way. The most striking manifestation of the matter effects on neutrino oscillations is the resonance enhancement of the oscillation probability - the Mikheyev-Smirnov-Wolfenstein (MSW) effect. In vacuum, the oscillation probability cannot exceed $\sin^2(2\theta_0)$, and for small mixing angles it is always small. Matter can enhance neutrino mixing, and the probabilities of neutrino oscillations in matter can be large (close to unity) even if the mixing angle in vacuum is very small. Matter enhanced neutrino oscillations of solar and atmospheric neutrinos inside the Earth can be quite important.

How does the matter affect neutrino propagation? Neutrinos can be absorbed by the matter constituents, or scattered off them, changing their momentum and energy. However, the probabilities of these processes, being proportional to the square of the Fermi constant G_F, are typically very small. Neutrinos can also experience forward scattering, an elastic scattering in which their momentum is not changed. This process is coherent, and it creates mean potentials V_α for neutrinos which are proportional to the number densities of the scatters. These potentials are of the first order in G_F, but one could still expect them to be too small and of no practical interest. This expectation, however, would be wrong. To assess the importance of matter effects on neutrino oscillations, one has to compute the matter-induced potentials of neutrinos V_α with the characteristic neutrino kinetic energy differences $\Delta m^2/2E$. Although the potentials V_α are typically very small, so are $\Delta m^2/2E$; if V_α are comparable to or larger than $\Delta m^2/2E$, matter can strongly affect neutrino oscillations.

5.6.2 Evolution equation

We shall now consider neutrino oscillations in matter in some detail. Neutrinos of all three flavours - ν_e, ν_μ, ν_τ - interact with electrons, protons and neutrons of matter through neutral current (NC) interaction mediated by Z^0 bosons. Electron neutrinos in addition

have charged current (CC) interactions with the electrons of the medium, which are mediated by the $W^{\pm}$ exchange. Let us consider the CC interactions. At low neutrino energies, they are described by the effective Hamiltonian [38]

$$H_{CC} = \frac{G_F}{\sqrt{2}}[\bar{e}\gamma_\mu(1-\gamma_5)\nu_e][\bar{\nu}_e\gamma^\mu(1-\gamma_5)e] = \frac{G_F}{\sqrt{2}}[\bar{e}\gamma_\mu(1-\gamma_5)e][\bar{\nu}_e\gamma^\mu(1-\gamma_5)\nu_e] \quad (5.6.1)$$

where we have used the Fierz transformation. In order to obtain the coherent forward scattering contribution to the energy of ν_e in matter (i.e. the matter-induced potential for ν_e) we fix the variables corresponding to ν_e and integrate over all the variables that correspond to the electron:

$$H_{\text{eff}}(\nu_e) = \langle H_{CC}\rangle_{\text{electron}} \equiv \bar{\nu}_e V_e \nu_e \quad (5.6.2)$$

Furthermore, we have

$$\langle\bar{e}\gamma_0 e\rangle = \langle e^\dagger e\rangle = N_e \quad \langle\bar{e}\vec{\gamma}e\rangle = \langle\vec{v}_e\rangle \quad \langle\bar{e}\gamma_0\gamma_5 e\rangle = \langle\frac{\vec{\sigma}_e\vec{p}_e}{E_e}\rangle \quad \langle\bar{e}\vec{\gamma}\gamma_5 e\rangle = \langle\vec{\sigma}_e\rangle \quad (5.6.3)$$

where N_e is the electron number density. For unpolarized medium of zero total momentum only the first term survives, and we obtain:

$$(V_e)_{CC} \equiv V_{CC} = \sqrt{2}G_F N_e \quad (5.6.4)$$

Analogously, one can find the NC contributions V_{NC} to the matter-induced neutrino potentials. Since NC interaction are flavour independent, these contributions are the same for neutrinos of all three flavours. In an electrically neutral medium, the number densities of protons and electrons coincide, and the corresponding contributions to V_{NC} cancel. The direct calculation of the contribution due to the NC scattering of neutrinos off neutrons gives $(V_\alpha)_{NC} = -G_F N_n/\sqrt{2}$, where N_n is the neutron number density. Together with eq. 5.6.4 this gives:

$$V_e = \sqrt{2}G_F\left(N_e - \frac{N_n}{2}\right) \qquad V_\mu = V_\tau = \sqrt{2}G_F\left(-\frac{N_n}{2}\right) \quad (5.6.5)$$

For antineutrinos, one has to replace $V_\alpha \to -V_\alpha$. Let us now consider the evolution of a system of oscillating neutrinos in matter. In vacuum, the evolution is most easily followed in the mass eigenstates basis. In matter it is more convenient to do that in the flavour basis because the effective potentials of neutrinos are diagonal in this basis. Consider the two flavour case. As usual, we write $\nu_{f_l} = U\nu_m$ where ν_{f_ℓ} and ν_m are two-component vectors of neutrino fields in the flavour and mass eigenstate bases and the matrix U is given by the mixing matrix in two flavour case in vacuum. In the absence of matter, the evolution equation in the mass eigenstate basis is $i(d/dt)|\nu_m\rangle = H_m|\nu_m\rangle$, where $H_m = \text{diag}(E_1, E_2)$. This gives the evolution equation in the flavour basis: $i(d/dt)|\nu_{f_l}\rangle = H_{f_l}|\nu_{f_l}\rangle = UH_mU^\dagger|\nu_{f_l}\rangle$. For relativistic neutrinos $E_i \simeq p + m_i^2/2E_i$, and we thus obtain:

$$i\frac{d}{dt}\begin{pmatrix}\nu_e\\ \nu_\mu\end{pmatrix} = \begin{pmatrix}(p + \frac{m_1^2+m_2^2}{4E}) - \frac{\Delta m^2}{4E}\cos(2\theta_0) & \frac{\Delta m^2}{4E}\sin(2\theta_0)\\ \frac{\Delta m^2}{4E}\sin(2\theta_0) & (p + \frac{m_1^2+m_2^2}{4E}) + \frac{\Delta m^2}{4E}\cos(2\theta_0)\end{pmatrix}\begin{pmatrix}\nu_e\\ \nu_\mu\end{pmatrix} \quad (5.6.6)$$

Here ν_e and ν_μ stand for time dependent amplitudes of finding the electron and muon neutrino respectively. The expressions in the brackets in the diagonal elements of the effective Hamiltonian in eq. 5.6.6 coincide. They can only modify the common phase of the neutrino states and therefore have no effect on neutrino oscillations which depend on

the phase differences. For this reason one can omit these terms. The evolution equation describing neutrino oscillations in vacuum in flavour basis then takes the form:

$$i\frac{d}{dt}\begin{pmatrix}\nu_e\\ \nu_\mu\end{pmatrix} = \begin{pmatrix}-\frac{\Delta m^2}{4E}\cos(2\theta_0) & \frac{\Delta m^2}{4E}\sin(2\theta_0)\\ \frac{\Delta m^2}{4E}\sin(2\theta_0) & \frac{\Delta m^2}{4E}\cos(2\theta_0)\end{pmatrix}\begin{pmatrix}\nu_e\\ \nu_\mu\end{pmatrix} \tag{5.6.7}$$

We now proceed to derive the neutrino evolution equation in matter. To do that, one has to add the matter-induced potentials V_e and V_μ to the diagonal elements of the effective Hamiltonian H_{f_l} in eq. 5.6.7. Notice that V_e and V_μ contain a common term due to NC interactions. As we already know, such common terms in the diagonal elements are of no consequence for neutrino oscillations; we can therefore omit the NC matter-induced potentials. This gives [39]:

$$i\frac{d}{dt}\begin{pmatrix}\nu_e\\ \nu_\mu\end{pmatrix} = \begin{pmatrix}-\frac{\Delta m^2}{4E}\cos(2\theta_0)+\sqrt{2}G_F N_e & \frac{\Delta m^2}{4E}\sin(2\theta_0)\\ \frac{\Delta m^2}{4E}\sin(2\theta_0) & \frac{\Delta m^2}{4E}\cos(2\theta_0)\end{pmatrix}\begin{pmatrix}\nu_e\\ \nu_\mu\end{pmatrix} \tag{5.6.8}$$

This is the evolution equation which describes $\nu_e \leftrightarrow \nu_\mu$ oscillations in matter. The equation for $\nu_e \leftrightarrow \nu_\tau$ oscillations has the same form. In the two flavour approximation, $\nu_\mu \leftrightarrow \nu_\tau$ oscillations are not modified in matter since $V_\mu = V_\tau$; however, in the full three flavour framework matter does influence the $\nu_\mu \leftrightarrow \nu_\tau$ oscillations because of the mixing with ν_e.

5.6.3 Constant density case

Let us now consider the evolution equation 5.6.8. In general, the electron number density N_e depends on the coordinate along the neutrino trajectory or, in our description in eq. 5.6.8, on time t. We shall consider a simple case of constant matter density and chemical composition, i.e. N_e = constant. Diagonalization of the effective Hamiltonian gives the following neutrino eigenstates in matter

$$\nu_A = \nu_e\cos(\theta_m) + \nu_\mu\sin(\theta_m) \tag{5.6.9}$$

$$\nu_B = -\nu_e\sin(\theta_m) + \nu_\mu\cos(\theta_m) \tag{5.6.10}$$

where the mixing angle θ_m is given by

$$\sin^2(2\theta_m) = \frac{\sin^2(2\theta_0)}{\left(\cos(2\theta_0) \mp \frac{2\sqrt{2}G_F N_e E}{\Delta m^2}\right)^2 + \sin^2(2\theta_0)} \tag{5.6.11}$$

where the minus sign is valid for neutrinos and the plus sign for antineutrinos. It is different from the vacuum mixing angle θ_0 and therefore the matter eigenstates ν_A and ν_B do not coincide with mass eigenstates ν_1 and ν_2. The difference of neutrino eigenmass in matter is

$$m^2_{1m,2m} = \frac{1}{2}\left[(\Sigma + A) \mp \sqrt{(A - \Delta m^2\cos(\theta_0))^2 + (\Delta m^2)^2\sin^2(2\theta_0)}\right] \tag{5.6.12}$$

where $\Sigma = m_2^2 + m_1^2$ and $A = 2\sqrt{2}G_F E N_e$. For $A \to 0$, it follows that $m^2_{1m,2m} \to m^2_{1,2}$ and $\theta \to \theta_0$. Using the relation

$$\Delta m^2_m = m^2_{2m} - m^2_{1m} = \Delta m^2\sqrt{\left(\frac{A}{\Delta m^2} - \cos(2\theta_0)\right)^2 + \sin^2(2\theta_0)} \tag{5.6.13}$$

the oscillation probabilities in matter can be written analogously to those of the vacuum

$$P_m(\nu_e \to \nu_\mu) = \sin^2(2\theta_m)\sin^2\left(\frac{\Delta m_m^2 L}{4E}\right) \tag{5.6.14}$$

$$P_m(\nu_e \to \nu_e) = 1 - P_m(\nu_e \to \nu_\mu) \tag{5.6.15}$$

with a corresponding oscillation length in matter

$$L_m = \frac{4\pi E}{\Delta m_m^2} = \frac{L_0}{\sqrt{\left(\frac{A}{\Delta m^2} - \cos(2\theta_0)\right)^2 + \sin^2(2\theta_0)}} = \frac{\sin(2\theta_m)}{\sin(2\theta_0)} L_0. \tag{5.6.16}$$

Note already that eq. 5.6.11 allows the possibility of maximal mixing in matter, $\sin(2\theta_m) \simeq 1$, even for small $\sin(\theta_0)$ because of the resonance type form. It is called the MSW resonance condition. For the resonance enhancement of neutrino oscillations in matter to be possible, the rhs. of

$$A = \Delta m^2 \cos(2\theta_0) \tag{5.6.17}$$

must be positive

$$\Delta m^2 \cos(2\theta_0) = (m_2^2 - m_1^2)(\cos^2(\theta_0) - \sin^2(\theta_0)) > 0 \tag{5.6.18}$$

i.e. if ν_2 is heavier than ν_1, one needs $\cos^2(\theta_0) > \sin^2(\theta_0)$, and vice versa. It follows from eq. 5.3.1 that the condition eq. 5.6.18 is equivalent to the requirement that of the two mass eigenstates ν_1 and ν_2, the lower-mass one have a larger ν_e component. If one chooses the convention $\cos(2\theta_0) > 0$ then eq. 5.6.18 reduces to $\Delta m^2 \equiv \Delta_{21}^2 > 0$. The resonance condition for antineutrinos is then $\Delta m^2 < 0$. Therefore, for a given sign of Δm^2, either neutrinos or antineutrinos (but not both - see figure 5.6.2) can experience the resonantly enhanced oscillations in matter. For a more information about adiabatic approximation and a more realistic three flavour oscillations in matter, look at [40] and [41]

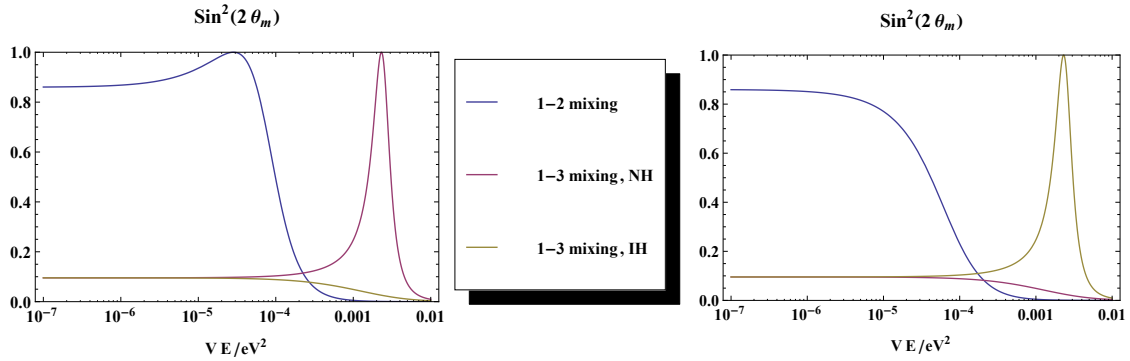

Figure 5.6.2: *Mixing angle in matter in two flavour approximation for different vacuum oscillation parameters as a function of the matter-induced neutrino potential* $V = \sqrt{2}\,G_F N_e$ *and the neutrino energy, left for neutrinos and right for antineutrinos.*

6

Atmospheric neutrinos

In recent years the study of atmospheric neutrinos has become one of the most important fields in neutrino physics. Atmospheric neutrinos are produced in meson and muon decays, created by interactions of cosmic rays within the atmosphere. The study of these neutrinos revealed evidence for neutrino oscillations. With energies in the GeV range and baselines from about 10 km to as long as the Earth diameter ($L \approx 10^4$ km), mass differences in the order of $\Delta m^2 \geq 10^{-4}\text{eV}^2$ or equivalent values in the L/E ratio from $10-10^5$ km GeV^{-1} are probed. Most measurements are based on relative quantities because absolute neutrino flux calculations are still affected by large uncertainties. The obtained results depend basically on four factors: The primary cosmic-ray flux and its modulations, the production cross-sections of secondaries in atmospheric interactions, the neutrino interaction cross-section in the detector and the detector acceptance and efficiency. We want to discuss the first few steps later in a little more detail. More quantitatively the observed number of events is given by

$$\frac{dN_\ell(\theta, p_\ell)}{d\Omega_\theta dp_\ell} = t_{\text{obs}} \sum_{\pm} \int N_t \, \frac{d\phi^{\pm}_{\nu_\ell}(E_\nu, \theta)}{d\Omega_\theta dE_\nu} \frac{d\sigma^{\pm}(E_\nu, p_\ell)}{dp_\ell} F(q^2) dE_\nu \tag{6.0.1}$$

where ℓ stands for $e^{\pm}$ or $\mu^{\pm}$, p_ℓ the lepton momentum, E_ν the neutrino energy, θ the zenith angle, t_{obs} the observation time, N_t the number of target particles, $\phi^{\pm}_{\nu_\ell}(E_\nu, \theta)$ the neutrino flux and $\sigma(E_\nu, p_\ell)$ the cross-section. $F(q^2)$ takes into account the nuclear effects such as the Fermi momenta of target nucleons, Pauli blocking of recoil nucleons etc. The summation ($\pm$) is done for ν_ℓ and $\bar{\nu}_\ell$, since current observations do not distinguish the lepton charge (except ICAL@INO).

6.1 Cosmic rays

The primary cosmic rays hitting the atmosphere consist of about 98 % hadrons and 2 % electrons. The hadronic component itself is dominated by protons ($\approx 87\%$) mixed with α-particles ($\approx 11\%$) and heavier nuclei ($\approx 2\%$). Because the neutrino flux depends on the number of nucleons rather than on the number of nuclei, a significant fraction of the flux is produced by He and CNO (+ heavier nuclei). The differential energy spectrum follows a power law of the form

$$N(E)dE \propto E^{-\gamma} dE \tag{6.1.1}$$

with $\gamma \simeq 2.7$ for $E < 10^{15}$ eV. From this point the spectrum steepens (the 'knee') to $\gamma \simeq 3$. At about 10^{18} eV the sepctrum flattens again (the 'ankle') and datasets for the ultra-high energy part of cosmic rays well above are still limited by statistics. The part of the comic-ray spectrum dominantly responsible for the current atmospheric neutrino investigations is the energy range below 1 TeV.

The intensity of primary nucleons in that energy range can be approximated by [43]

$$I_N(E) \sim 1.8 E^{-2.7} \quad \text{nucleons cm}^{-2}\ \text{s}^{-1}\ \text{sr}^{-1}\ \text{GeV}^{-1} \tag{6.1.2}$$

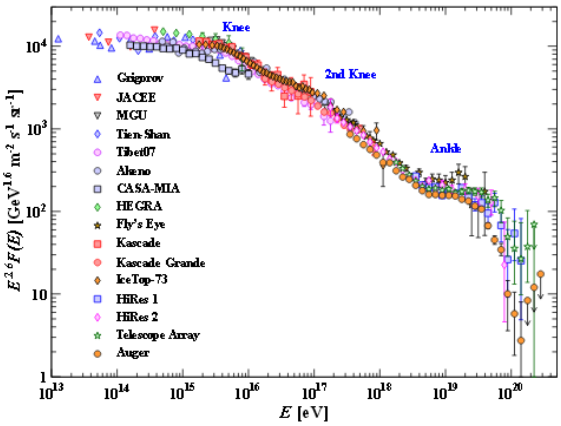

Figure 6.1.1: *The all-particle spectrum as a function of E (energy-per-nucleus) from air shower measurements* [42]

where E is the energy per nucleon. In the low energy range several effects can occur. First of all, there is the modulation of the primary cosmic-ray spectrum with solar activity. The solar wind prohibits low energy galactic cosmic rays from reaching the earth. This effect is most prominent for energies below 10 GeV. Such particles have, in contrast, a rather small effect on atmospheric neutrino fluxes, because the geomagnetic field prevents these low energy particles from entering the atmosphere anyway. The geomagnetic field bends the trajectories of cosmic rays and determine the minimum rigidity called the cutoff rigidity for particles to arrive at the earth. The dynamics of any high energy particle in a magnetic field configuration B depends on the rigidity R by

$$R = \frac{pc}{ze} = r_L \times B \tag{6.1.3}$$

with p as the relativistic 3-momentum, z as the electric charge and r_L as the gyroradius. Particles with different masses and charge but identical R show the same dynamics in a magnetic field. The cutoff rigidity depends on the position at the Earth surface and the arrival direction of the cosmic ray. The geomagnetic field, therefore, produces two prominent effects: The latitude (the cosmic-ray flux is larger near the geomagnetic poles) and the east-west (the cosmic-ray flux is larger for east-going particles) effect. The last one is an azimuthal effect not depending on any physics and can be used to check the shower simulations. Such a measurement was performed by Super-Kamiokande (SK) with a statistics of 45 kt $\times$ yr and cuts on the lepton momentum ($400 < p_l < 3000$ MeV/c and zenith angle $|\cos(\theta)| < 0.5$) to gain sensitivity, an east-west effect is clearly visible shown in figure 6.1.2

6.2 Interactions within the atmosphere

The atmospheric neutrinos stem from the decay of secondaries produced in interactions of primary cosmic rays with the atmosphere. The dominant part is the decay chain [45]:

$$\pi^+ \to \mu^+\nu_\mu \quad \mu^+ \to e^+\nu_e\bar{\nu}_\mu \tag{6.2.1}$$

$$\pi^- \to \mu^-\bar{\nu}_\mu \quad \mu^- \to e^-\bar{\nu}_e\nu_\mu \tag{6.2.2}$$

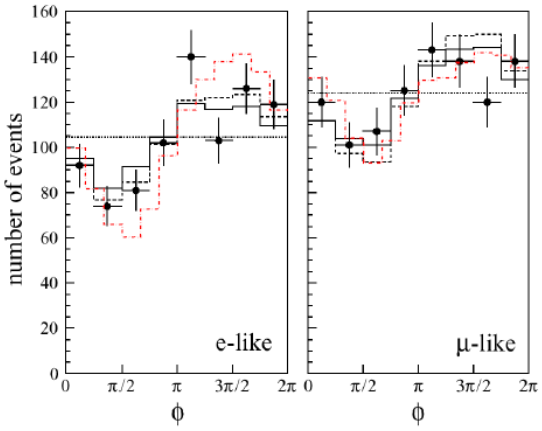

Figure 6.1.2: *East-west effect observed by neutrino. Data points are from SK experiment, and solid and dashed lines are prediction by using the one-dimensional calculation of Honda et al. and Bartol group respectively. Dash-dot are predictions by Lipari taking into account the muon bending normalized by the average value* [44]

Depending on the investigated neutrino energy additional contributions come from kaon decay, especially the modes:

$$K^{\pm} \rightarrow \mu^{\pm}\nu_{\mu}(\bar{\nu}_{\mu}) \tag{6.2.3}$$

$$K_L \rightarrow \pi^{\pm}e^{\pm}\nu_e(\bar{\nu}_e) \tag{6.2.4}$$

The latter is the dominant source for ν_e above $E_\nu \approx 1$ GeV. In the low energy range ($E_\nu \approx 1$ GeV) there is the previously mentioned contribution from muon decay. However, for larger energies the Lorentz boost for muons is high enough in a way that they reach the Earth surface. For example, most muons are produced in the atmosphere at about 15 km. This length corresponds to the decay length of a 2.4 GeV muon, which is shortened to 8.7 km by energy loss (a vertical muon loses about 2 GeV in the atmosphere by ionization according to the Bethe-Bloch formula [46]). Therefore, at E_ν larger than several GeV this component can be neglected. At higher energies the contribution of kaons becomes more and more important. The general consensus of all these decays is that the ratio of fluxes

$$R = \frac{\nu_e + \bar{\nu}_e}{\nu_\mu + \bar{\nu}_\mu} \tag{6.2.5}$$

can be predicted with an accuracy of about 5 % which is about 1/2 for sub-GeV and becomes smaller for ($E_\nu \sim 1$ GeV) since the muons reach the Earth. Therefore, the only component of electron neutrinos in the multi-GeV energy range is eq. 6.2.4. Also at really high energies, the pion and kaon would rather interact with the atmosphere then decay into the various processes given above. From this fact, the atmospheric neutrino flux is more steeply in the high energy range compared to neutrino flux coming from charm decay.

However, in the absolute flux predictions there is some disagreement on the level of 20-30 % in the spectra and overall normalization of the neutrino flux. Recently two new experimental approaches have arrived which might help to improve the situation considerably. First of all, there are measurements of muons in the atmosphere. Strongly connected with neutrino production from meson decay is the production of muons. Assume the two-body decays $M \rightarrow m_1 + m_2$. The magnitude of the momenta of secondaries

in the rest frame of M are given by:

$$p_1^* = p_2^* = p^* = \frac{M^4 - 2M^2(m_1^2 + m_2^2) + (m_1^2 - m_2^2)^2}{2M} \tag{6.2.6}$$

In the laboratory frame the energy of the decay product is

$$E_i = \gamma E_i^* + \beta\gamma p^* \cos(\theta^*) \tag{6.2.7}$$

where β and γ are the velocity and Lorentz factor of the parent in the laboratory system. Therefore, the limits on the laboratory energy of the secondary i are:

$$\gamma(E_i^* - \beta p^*) \leq E_i \leq \gamma(E_i^* + \beta p^*) \tag{6.2.8}$$

In the absence of polarization there is, in addition,

$$\frac{dn}{d\Omega^*} = \frac{dn}{2\pi d\cos(\theta^*)} \propto \frac{dn}{dE_i} = \text{constant} \tag{6.2.9}$$

meaning that, in such cases, a flat distribution for a product of a two-body decay between the limits of eq. 6.2.8 results. For example, for process eq. 6.2.3 this results in

$$\frac{dn}{dE_\nu} = \frac{dn}{dE_\mu} = \frac{0.635}{1 - (m_\mu^2/m_K^2)p_K} \tag{6.2.10}$$

with p_K as the laboratory momentum of the kaon and the factor 0.635 stems from the branching ratio of decay eq. 6.2.8. Often we deal with decays of relativistic particles, resulting in $\beta \to 1$, which would imply for decays $M \to \mu\nu$ kinematic limits on the laboratory energies of the secondaries of

$$E\frac{m_\mu^2}{m_M^2} \leq E_\mu \leq E \tag{6.2.11}$$

and

$$0 \leq E_\nu \leq \left(1 - \frac{m_\mu^2}{m_M^2}\right) E \tag{6.2.12}$$

with E as the laboratory energy of the decay meson. Average values are:

$$\langle E_\mu\rangle/E_\pi = 0.79 \quad \text{and} \quad \langle E_\nu\rangle/E_\pi = 0.21 \quad \text{for } \pi \to \mu\nu \tag{6.2.13}$$

$$\langle E_\mu\rangle/E_K = 0.52 \quad \text{and} \quad \langle E_\nu\rangle/E_K = 0.48 \quad \text{for } K \to \mu\nu \tag{6.2.14}$$

It is a consequence of the kinematics that if one of the decay products has a mass close to the parent meson, it will carry most of the energy. Since low energy muons are absorbed in the atmosphere and decay with a high probability, only high altitude measurements allow a precise measurement of muons that are most strictly associated with sub-GeV neutrino events. A compilation of various atmospheric neutrino flux calculations are shown in figure 6.2.1. As can be seen it consists basically of ν_μ and ν_e neutrinos and its antineutrinos. At very high energies ($E_\nu \gg$ TeV) neutrinos from charm production become an additional source. A possible atmospheric ν_τ flux is orders of magnitude less than the ν_μ flux. As can be seen from the atmospheric neutrino flux at first order, the energy spectrum reflects the primary cosmic ray spectrum in the energy range from 10 to 100 GeV. At higher energies, it steepens asymptotically to $E^{-\gamma-1}$. The harder spectrum

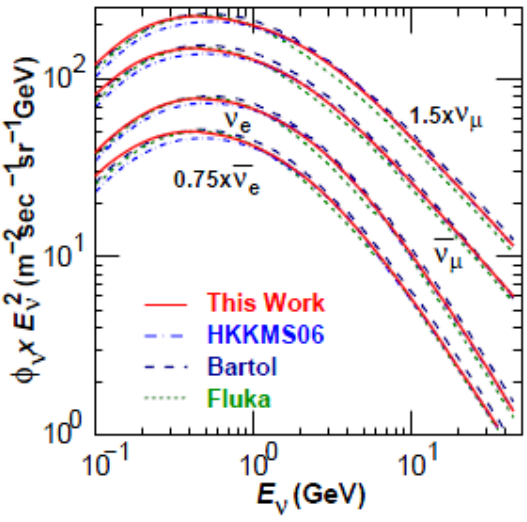

Figure 6.2.1: *Comparison of atmospheric neutrino fluxes calculated for Kamioka averaged over all directions* [47]

is a consequence of the decay probability being proportional to E^{-1}, while the hadronic interaction length stays constant.

Another important feature for the PINGU detector is the ratio of positive to negative muons in the atmosphere. The measured value of ~ 1.25 is nearly independent of energy. It reflects the excess of protons over neutrons in the incident cosmic rays. But if this were all, the charge ratio would go to zero at high energy because of multiplicity per collision of produced pions (the parents of the muons) becomes very large so that one extra charge becomes negligible. But this is not the whole story. Because of the steepness of the cosmic ray energy spectrum, muons of a given energy come from relatively fast secondaries, i.e. they reflect the projectile fragmentation region. Since the fragmentation region of the proton reflects the momentum distribution of its quark, and since it has two u-quarks of charge +2/3 each and only one d-quark (charge -1/3), positive pions are favored in the fragmentation region. This causes an excess of positive over negative muons at all energies [[48], [49]].

The zenith distribution for atmospheric neutrinos can be seen in figure 6.2.2. Neutrinos enter the detector from both sides because the cross-section of neutrinos are so small that they can pass the Earth's interior without being absorbed as it is the case for the atmospheric muons. The zenith distribution is not flat; more neutrinos enter the detector from near the horizon. For small values of $\cos(\theta)$, the average difference in height needed for the decay of a pion or kaon is small. With increasing $|\cos(\theta)|$ values, this difference in height increases for muons, which results in a smaller number of electron neutrinos. Therefore, the ratio of meson to electron neutrinos increases in these ranges [[44], [47]].

6.3 Neutrino cross-section

Neutrinos can interact with the nucleons in a medium over the exchange of charged $W^{\pm}$-bosons in charged-current interactions (CC), and neutral Z^0-bosons in neutral-current interactions (NC). For neutrinos detection, the most important process at neutrino energies $E_\nu > 10$ GeV is deep inelastic scattering, where the initial nucleon N is destroyed

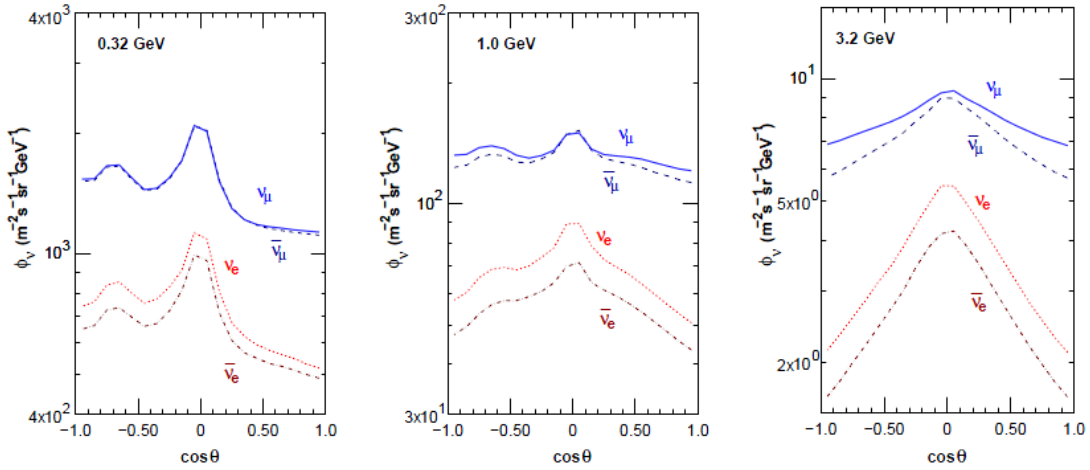

Figure 6.2.2: *The zenith angle dependence of atmospheric neutrino flux averaged over all azimuthal angle calculated for Kamioka. Here θ is the arrival direction of the neutrino, with $\cos(\theta) = 1$ for vertically downward going neutrinos, and $\cos(\theta) = -1$ for vertically upward going neutrinos* [47].

and a hadronic cascade X is produced:

$$\nu_\ell + N \to \ell + X \quad \text{(CC)} \tag{6.3.1}$$

$$\nu_\ell + N \to \nu_\ell + X \quad \text{(NC)} \tag{6.3.2}$$

This hadronic cascade is produced in both interaction types, CC and NC. A lepton ℓ corresponding to the initial neutrino flavour is only produced in CC interactions. Thus, the initial neutrino can be observed indirectly by detecting the secondary particles produced in these weak interactions. With the information from the CC interactions, NC interactions are even less known, which make them very difficult to predict. This can be seen in [50].

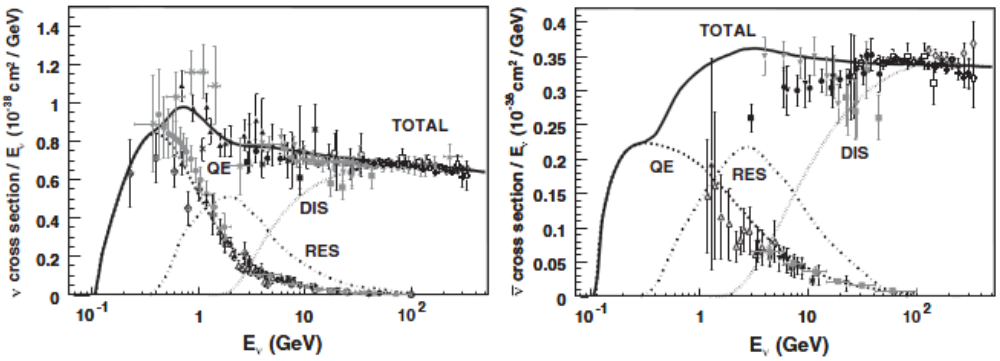

Figure 6.3.1: *(Anti-)Neutrino CC cross sections divided by the neutrino energy for different processes: Quasi-elastic scattering (QE), resonance production (RES) and deep inelastic scattering (DIS)* [50]

For energies below 10 GeV (which are relevant for PINGU), cross-sections of futher processes like quasi-elastic scattering (QE scattering - nucleon remains intact) and resonance

production (nucleon is excited to a resonance state) start to dominate. For energies above 10 GeV, the total neutrino cross-section increases almost with energy. Because of helicity arguments, the cross-section of antineutrinos is a factor of about two lower than neutrinos [50].

The charged leptons, produced in CC interactions, lose energy while travelling through the medium due to various processes. In the GeV regime, electrons dominantly lose energy by bremsstrahlung, $-dE/dx = E_0/X_0$ with radiation length X_0, and muons by ionization, described by the Bethe-Bloch equation [46]. Taus decay almost instantly (lifetime of $\sim 10^{-13}$ s) into hadrons in $\sim 85\%$ of the cases and induce further hadronic cascades.

6.4 Experimental consideration

Atmospheric neutrinos have the potential to resolve the octant of the atmospheric angle θ_{23} via matter enhanced oscillation within the Earth. Resonant oscillation occurs either for neutrinos in the case of the normal hierarchy, or antineutrinos for the inverted hierarchy. Determination of the octant requires measurement of the energy and direction of Earth-crossing atmospheric neutrinos with energies in the range 2 to 10 GeV. Massive detectors ($\geq$ Mton) are required to obtain sufficient signal statistics within a few years of operation. Existing proposals use either water Cherenkov (PINGU, ORCA, HyperK), liquid Argon TPC (LBNE, LBNO), or magnetized iron calorimeter (INO) detectors. Primary concerns are detector properties such as total mass, energy resolution and angular resolution.

6.5 The Earth's matter density profile

The Earth's matter density profile is given by the *Preliminary Reference Earth Model* (PREM) [51], shown in figure 6.5.1. It is based on measurements with seismic waves. The inner Earth consists of three main density domains in each of which the change in density is relatively slow: The mantle domain, the outer and inner core domain. The Earth's core consists mostly of iron mixed with light elements; its exact composition is not well known. At the transition of outer core to mantle, the density decreases dramatically by a factor of almost two, which has a significant impact on the oscillation probability of neutrinos.

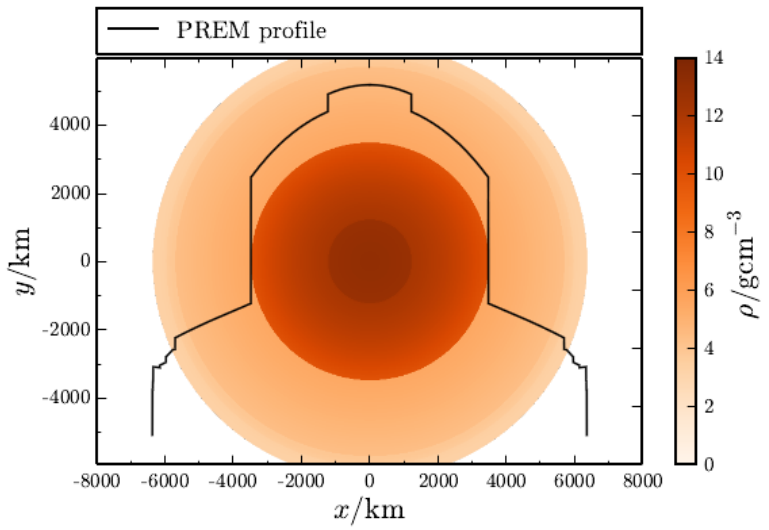

Figure 6.5.1: *Matter density (color-coded) according to the Preliminary Reference Earth Model (PREM). The solid line represents the density profile.*

6.6 Atmospheric neutrino oscillations

The oscillation probability of neutrinos depends on the neutrino energy and on the baseline. For atmospheric neutrinos traversing the inner Earth, the baseline is a function of the neutrino zenith angle. Thus, neutrino oscillation in the Earth and the effect of matter can be described completely by contours of equal oscillation probability in the plane of neutrino energy versus cosine of the neutrino zenith angle as shown in figure 6.6.1 for various transition respectively.
The oscillation pattern for electron neutrinos shows several distinct features:

1. Electron neutrinos with $\cos(\theta) \leq 0.84$ travel only through the mantle domain and exhibit a MSW resonance with the main peak between 5 to 7 GeV.

2. The oscillation pattern of core-crossing electron neutrino trajectories ($\cos(\theta) > 0.84$) show three resonance ridges at $E_\nu > 3$ GeV due to parametric enhancement.

3. Below 3 GeV, the core-crossing electron neutrinos exhibit an additional MSW resonance with the main peak between 2.5 to 2.7 GeV.

4. For $E_\nu < 5$ GeV and $\cos(\theta) < 0.84$, the oscillation probability shows a regular pattern as it is expected for vacuum oscillations.

Matter effects in the Earth are driven by θ_{13}; higher values lead to more distinctive effects, and only occur because of θ_{13} being non-zero. In figure 6.6.1, the effects of the 1-2 mixing are not shown because these effects are only important for energies smaller than about 0.2 GeV, below the expected energy threshold of the PINGU detector.

The oscillations of atmospheric muon neutrinos are also affected by matter due to their mixing with electron neutrinos. As one can see in the bottom plot of figure 6.6.1, the regular oscillation pattern for vacuum oscillations is distorted in the energy region below $\sim$ 10 GeV. In this energy region, matter effects have the strongest effect on the oscillation probability of electron neutrinos.

Oscillation of neutrinos are enhanced by matter in the case of normal neutrino mass hierarchy while antineutrinos are not. The opposite is true in the case of inverted neutrino mass hierarchy. Taking this into account, atmospheric muon neutrinos traveling through the Earth facilitate to probe the neutrino mass hierarchy and are the subject of the study on atmospheric neutrino oscillation with the PINGU detector [52].

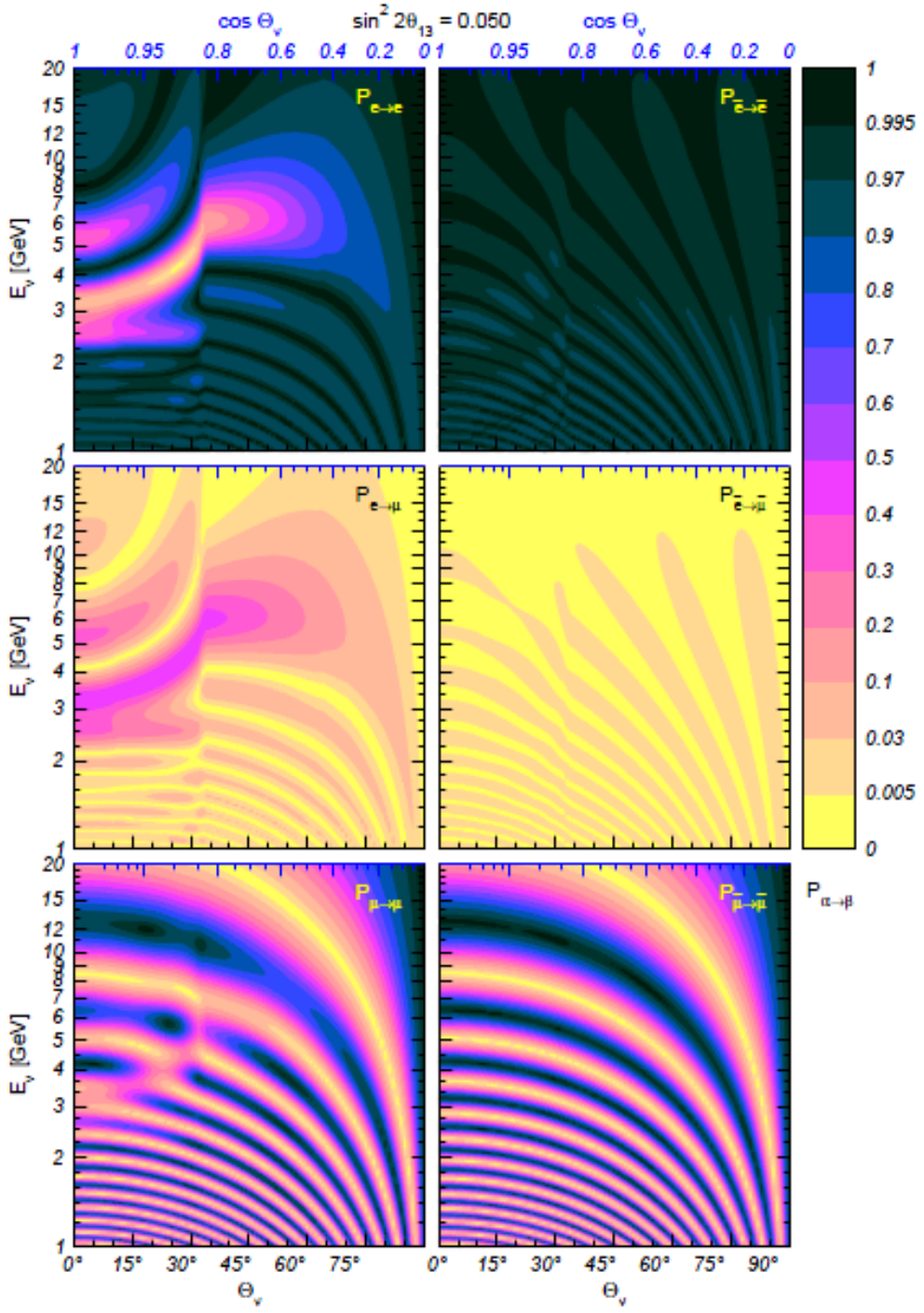

Figure 6.6.1: *Neutrino energy versus cosine of the neutrino zenith angle, color-coded is the probability of neutrinos in the Earth* [52]. *The left panel being neutrinos and right panel being antineutrinos. Top being electron neutrino survival, middle muon neutrino to electron neutrino and bottom being muon neutrino survival.*

7

Sensitivity of PINGU to the octant of θ_{23}

All the tools and knowledge needed for the computations are described in the previous chapters. In the beginning of this chapter, the introduction of the numerical analysis is descripted and later the sensitivity to the octant of mixing angle θ_{23} is shown for various resolution functions for energy and zenith angle. The main idea for the simulations are taken from this article [53]. More information can be found in these additional articles [54] and [55]. The intention of this thesis is to go beyond this simulation by considering new systematic uncertainties, neutrino fluxes and other input.

7.1 Earth matter effects in oscillation probabilities

Atmospheric (anti)neutrinos are produced in both ν_μ and ν_e ($\bar{\nu}_\mu$ and $\bar{\nu}_e$) flavours. The neutrinos, on their way of production in the atmosphere to the detector, undergo flavour oscillations. On arrival at the detector, they produce the corresponding charged leptons through charged current interactions on nucleons. Since the oscillated atmospheric neutrino "beam" is a combination of all three flavours, they produce electrons, muons, as well as tau leptons (and their antiparticle) in the detector. Since the oscillated muon type neutrinos arriving at the detector are a combination of the survived ν_μ and the flavour oscillated ν_μ coming from ν_e produced in the atmosphere, the oscillation probability channels relevant for atmospheric muon neutrinos are the survival probability $P_{\mu\mu}$ and transition probability $P_{e\mu}$ (we neglect the tau contribution).

The quantity describing the neutrino mass hierarchy is:

$$\Delta m^2_{\text{eff}} = \Delta m^2_{31} - (\cos^2(\theta_{12}) - \cos(\delta_{CP})\sin(\theta_{13})\sin(2\theta_{12})\tan(\theta_{23}))\Delta m^2_{21} \tag{7.1.1}$$

The reason as follows: We can see the role of θ_{13}-driven Earth matter effects by the equation 5.6.11 and the neutrino mass hierarchy is determined by these effects. For $\theta_{13} = 0$, in the limit $\Delta m^2_{21} = 0$, the oscillation probabilities becomes $P_{e\mu} = 0$ and $P_{\mu\mu}$ is the same for both hierarchies. However, for non-zero $\theta_{13} \neq 0$ we get a difference in $P_{e\mu}$ and $P_{\mu\mu}$ between $\Delta m^2_{31} > 0$ and $\Delta m^2_{31} < 0$ due the earth matter effects. All would be perfect, if it were not for the assumption $\Delta m^2_{21} = 0$. For $\Delta m_{21} \neq 0$, it turns out that the survival probability $P_{\mu\mu}$ becomes different for $\Delta m^2_{31} > 0$ and $\Delta m^2_{31} < 0$, even for $\theta_{13} = 0$. This aspect has been discussed in detail [[56], [57]]. To alleviate this issue we use the definition 7.1.1 as a quantity for the neutrino mass hierarchy and define $\Delta m^2_{\text{eff}} > 0$ ($\Delta m^2_{\text{eff}} < 0$) as normal hierarchy (inverted hierarchy) [53]. The impact of the definition of the neutrino mass hierarchy (whatever to use Δm^2_{31} or Δm^2_{eff}) as a measure of the neutrino mass hierarchy (the sign of these quantities) seems to have no difference in determining the neutrino mass hierarchy, only the oscillation probabilities [55].

Even though the Δm^2_{eff} depends on δ_{CP}, which is unknown, it will only influence the value of the effective mass splitting, not the sign of it. This can be used to make a good measurement of $\cos(\delta_{CP})$ [57] and atmospheric neutrino can give the first hint of CP violation [58].

7.2 Description of numerical analysis

Since the PINGU detector measures charged leptons of the associated neutrino eq. 6.3.1, the number of ν_μ-like events expected in PINGU after T years of running the experiment is

$$\begin{aligned}(N_\mu)_{ij} = 2\pi N_T T \int_{(\cos(\Theta))_i}^{(\cos(\Theta))_{i+1}} d\cos(\Theta) \int_{E_j}^{E_{j+1}} dE \epsilon \rho_{\text{ice}} V_{\text{eff}}(E) \times \\ \left[\left(\frac{d^2\phi_{\nu_\mu}}{d\cos(\Theta')dE'} P_{\mu\mu} + \frac{d^2\phi_{\nu_e}}{d\cos(\Theta')dE'} P_{e\mu} \right) \sigma_{CC}(E) \right. \\ \left. + \left(\frac{d^2\phi_{\bar{\nu}_\mu}}{d\cos(\Theta')dE'} P_{\bar{\mu}\bar{\mu}} + \frac{d^2\phi_{\bar{\nu}_e}}{d\cos(\Theta')dE'} P_{\bar{e}\bar{\mu}} \right) \bar{\sigma}_{CC}(E) \right]\end{aligned} \tag{7.2.1}$$

where N_T are the number of targets in the detector, T is the exposure time, ϵ is the detector efficiency, $\rho_{\text{ice}} V_{\text{eff}}$ is the effective mass of the detector, V_{eff} is the effective volume, $d^2\phi_\alpha/dE'd\cos(\Theta')$ is the neutrino flux of flavour α at the South Pole [59], $\sigma_{CC}(E)$ is the neutrino cross-section given by GENIE. Since the detector is not magnitized, it will not be able to distinguish between particle and antiparticle. For this reason, the number of events from neutrinos and antineutrinos are added together.

$R(E, E')$ and $R(\Theta, \Theta')$ are the energy and angle resolution functions of the detector respectively, and $P_{\mu\mu}$ and $P_{e\mu}$ are the muon neutrino survival probability and electron neutrino to muon neutrino conversion probabilities respectively. The resolution functions relate the true energy E' and true zenith angle Θ' with the reconstructed energy E and reconstructed zenith angle Θ of the neutrino. We assume Gaussian functional form for the resolution functions with widths:

$$\sigma_E = a + bE'_{\text{GeV}} \qquad \sigma_\Theta = c \cdot \sqrt{\frac{1\text{GeV}}{E'_{\text{GeV}}}} \tag{7.2.2}$$

Since the final resolution widths for PINGU is still being estimated from detailed simulations, two sets of values for the energy resolution width σ_E corresponding to $a = 0, b = 0.2$ and $a = 2, b = 0$, and two sets of values for the angle resolution width σ_Θ corresponding to $c = 1$ ($\simeq 60$) and $c = 0.5$ ($\simeq 30$), where c is in radians (degrees), will be assumed. These values for the resolution functions agree with that in the literature [[15], [19], [60], [61], [62]]. The effective mass of the detector is read from [63] for the curve labelled "Triggered Effective Volume, R=100m". The probabilities $P_{\mu\mu}$ and $P_{e\mu}$ are calculated numerically solving the propagation equation of the neutrinos through the atmosphere and inside the Earth, and using the PREM profile for the Earth matter density. For simplicity $\epsilon = 1$, since any flat ϵ can be easily adjusted against the exposure taken at the detector. The index i runs over the number of $\cos(\Theta)$ bins in the data while j runs over the number of energy bins. We will take $\cos(\Theta)$ to run from -1 to 0 while the energy runs from 1 GeV to 20 GeV. The data is generated for the oscillation parameters given in table 7.2.1 for either the normal or inverted hierarchy and for a given value of $\sin^2(\theta_{23})$. The simulated $\chi^2 is fitted with the wrong octant solution of \sin^2(\theta_{23})$ for the theoretical event rates, allowing the test variables $|\Delta m^2_{\text{eff}}|$, $\sin^2(\theta_{13})$, $\sin^2(\theta_{23})$ as well as the neutrino mass hierarchy to vary in the fit. The statistical fit is performed using a χ^2 function defined as

$$\chi^2 = \min_{\xi_j} \sum_{ij} \left[\frac{(N^{\text{th}}_{ij} - N^{\text{ex}}_{ij})^2}{N^{\text{ex}}_{ij}} \right] + \sum_{s=1}^{k} \xi_s^2 \tag{7.2.3}$$

$$N^{\text{th}}_{ij} = N_{ij} \left(1 + \sum_{s=1}^{k} \pi^s_{ij} \xi_s \right) + \mathcal{O}(\xi_s^2) \tag{7.2.4}$$

where N_{ij}^{ex} is the observed number of muon events in the $i^{th}\cos(\Theta)$ and j^{th} energy bin and N_{ij}^{th} is the corresponding theoretically predicted event spectrum for the wrong octant solution of θ_{23}. The π_{ij}^{s} is the ij^{th} systematic uncertainty in the $i^{th}\cos(\Theta)$ and j^{th} energy bin and ξ_s is the pull variable corresponding to the uncertainty π_{ij}^{s}. Five systematic uncertainties are included in the analysis. They are, a flux normalization error of 20 %, a cross-section uncertainty of 10 %, a 5 % uncertainty on the zenith angle dependence of the fluxes, a 5 % energy dependent "tilt factor" of the fluxes and a 5 % additional overall uncertainty [[60], [64]]. The parameters $|\Delta m^2_{\text{eff}}|$ and $\sin^2(2\theta_{13})$ are varied in the fit obeying the contours (see figures 7.5.1 and 7.5.2) in the 3σ range given in table 7.2.1. For $\sin^2(\theta_{23})$(test), we vary it freely in the range $[0.4 - 0.6]$ around the wrong octant for any given $\sin^2(\theta_{23})$(true). The values in the table comes from [65]. Finally, the χ^2 is computed for both the test hierarchies and the minimum χ^2 is chosen.

Parameter	True value used in data	3σ range used in fit
Δm^2_{21}	7.6×10^{-5} eV^2	$[7.1 - 8.2] \times 10^{-5}$ eV^2
$\sin^2(\theta_{12})$	0.323	[0.278 - 0.375]
$\lvert\Delta m^2_{\text{eff}}\rvert$	2.4×10^{-3} eV^2	$[2.1 - 2.6] \times 10^{-3}$ eV^2
δ_{CP}	0	$[0 - 2\pi]$
$\sin^2(2\theta_{13})$	0.093	[0.071 - 0.115]

Table 7.2.1: *Benchmark true values of oscillation parameters set in the simulations, unless otherwise stated. The range over which they are allowed to vary in the 3σ contours.* $\sin^2(\theta_{23})$*(true) is varied in the range* $[0.4 - 0.6]$ *around the wrong octant* $\sin^2(\theta_{23})$ *for any given* $\sin^2(\theta_{23})$*(true). In the simulations,* Δm^2_{21}, $\sin^2(\theta_{12})$ *and* δ_{CP} *are fixed at their true value.*

7.3 Neutrino flux

The fluxes of neutrinos reaching the Earth from the atmosphere are vital to this project. Taking the data (ic79) of the neutrino fluxes released by the IceCube collaboration [[66], [67]], it is superimposed to the low energy region by a χ^2 fit; however only the neutrino fluxes. The antineutrino fluxes have been made by taking the neutrino fluxes and reducing it by $\sim$ 30 % since there are an overproduction of positive charged pions over negative charged pions. This gives the reason to reducing the antineutrino fluxes and that phenomenon is described in a previous chapter. The fluxes are shown in figure 7.3.1 with the best chi square fit plus one sigma band. The colors are given as such: Muon neutrino (red), muon antineutrino (light green), electron neutrino (dark green) and electron antineutrino (pink). Also shown in the plot are simulations of the neutrino fluxes from [59] where the colors are given the flavour of neutrinos: Muon neutrino (dark blue), muon antineutrino (cyan), electron neutrino (purple) and electron antineutrino (orange). The data points and simulations do not lay on top on each other since the 'knee' in the primordial spectrum is neglected in article [59]. The atmospheric fluxes used in various

IceCube simulations originate from a Honda model, but have an extenstion which takes the 'knee' into account [[68], [69]].

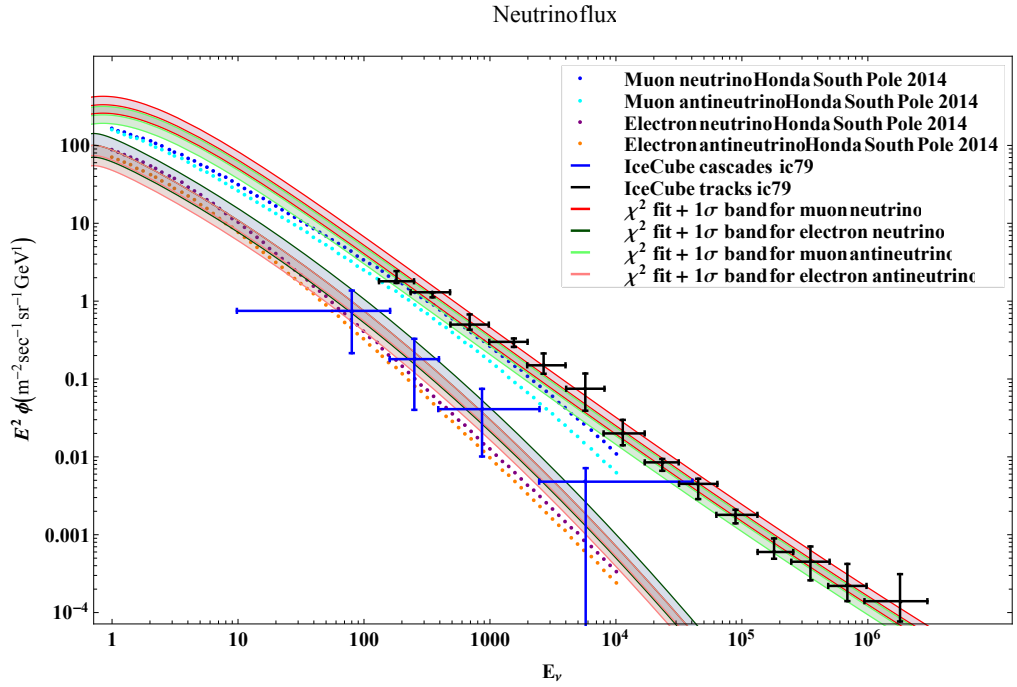

Figure 7.3.1: *Power-law fit to the Icecube data of the flux of neutrinos. Also shown is simulations of flux from* [59].

7.4 GENIE cross-section

GENIE (Generates Events for Neutrino Interaction Experiments) is a universal object-oriented neutrino Monte Carlo generator supported and developed by an international collaboration of scientists whose expertise covers a very broad range of neutrino physics aspects, both phenomenological and experimental. GENIE is currently being used by T2K, NOvA, MINERvA, MicroBooNE, ArgoNEUT, LAGUNA-LBNO, LBNE, INO, IceCUBE, NESSiE and others. To give a familiar picture of the cross-section plus the uncertainty, it is plotted in figure 7.4.1. The cross-section in figure 7.4.1 has similar shape as the cross-section in figure 6.3.1 in the previous chapter. However, more low-energy points are needed so that the theoretical predicted cross-section is the same as the experimental evidence. For more technical information, look at [[70], [71], [72]].

7.5 Contour plots from global data

The measurement of the reactor angle θ_{13} had influence on the other mixing parameters. The solar angle θ_{12} did not change much, however the atmospheric angle θ_{23} changed substantially. The figures 7.5.1 and 7.5.2 gives the allowed contours for some of the mixing parameters [73]. There are several plots in each figure; top is for normal hierarchy whereas the bottom is for inverted hierarchy. The three sets of columns add more data in the global fit; left: LBL accelerator + solar + KamLAND, middle: + SBL reactor data

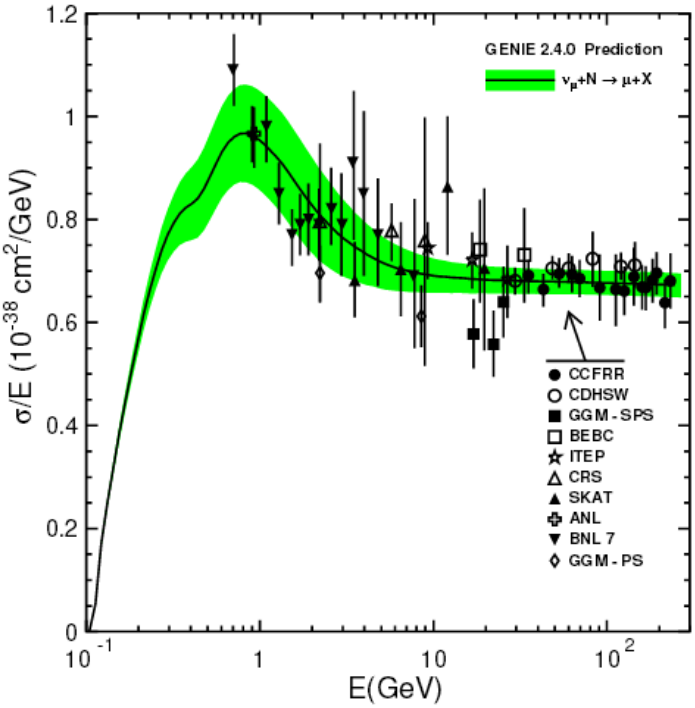

Figure 7.4.1: *GENIE generated cross-section for the charged ν_μ interaction.*

and right: + SK atmospheric data. The colors of the contours are different significance: Pink (1σ), blue (2σ) and black (3σ).

The first figures show the contour of the $(\sin^2(\theta_{23}), \Delta m^2)$-plane whereas the other figures show the $(\sin^2(\theta_{23}), \sin^2(\theta_{13}))$-plane. From these plots there is a slightly preference for non-maximal mixing ($\theta_{23} \neq 45°$). However, it gets diluted since T2K data prefer maximal mixing whereas MINOS and atmospheric data prefer non-maximal mixing. Moreover, the indications about the octant appears to be unstable in different combinations of data [73]. These plots are illustrative and gives information about their behavior as the parameters are varied. However, the parameters shown in the figures and the ones used in the analysis are completely different. In the analysis is used $\sin^2(2\theta_{13})$ and Δm^2_{eff} whereas in the figures are shown $\sin^2(\theta_{13})$ and $\Delta m^2 = m^2_3 - (m^2_1 + m^2_2)/2 = \Delta m^2_{31} - \Delta m^2_{21}/2$. However, by folding the mixing parameters correctly, then the mixing parameters used in the analysis also obeys their own contours. There are only a minimal difference between the contours shown in article [73] and the contours for the mixing parameters $\sin^2(\theta_{23})$(test), $\sin^2(2\theta_{13})$ and Δm^2_{eff}.

7.6 Event rates

The event rates were calculated by eq. 7.2.1 and the fine-binned distribution of events with $\Delta(\cos(\theta)) = 0.025°$ and $\Delta E_\nu = 0.5$ GeV are shown in figure 7.6.1. The number of events decreases with E_ν and the pattern of events follows the oscillatory picture due to the main $\nu_\mu \to \nu_\mu$ mode of the oscillations with a clear distortion in the resonance region. In the high event density bins the number of events reach ~ 120, and the total number of events are about $\mathcal{O}(70.000)$.

The neutrino fluxes for each neutrino flavour are built into the Monte Carlo generator and the events are calculated as follows. Every ν_μ event has a characterized true energy

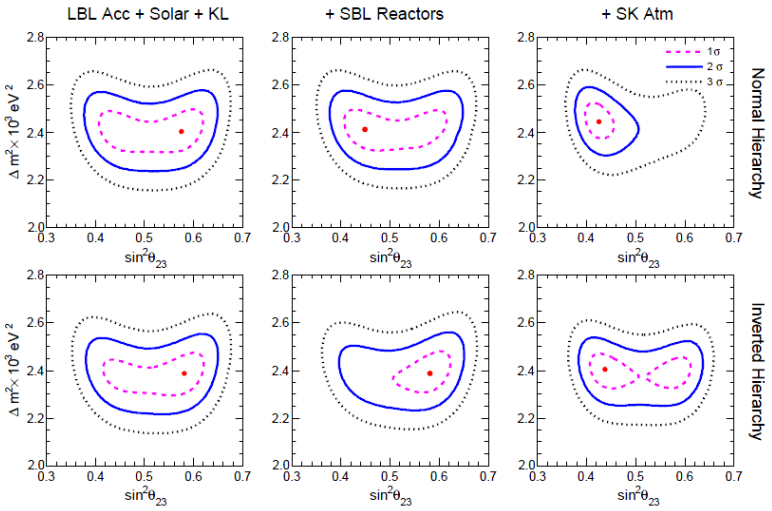

Figure 7.5.1: *Results from global in the plane charted by* $(\sin^2(\theta_{23}), \Delta m^2)$*, where all other parameters are being marginalized away. From left to right, regions allowed at 1,2 and* 3σ *refer to increasingly rich datasets: LBL accelerator + solar + KamLAND data (left panels), plus SBL reactor data (middle panels), plus SK atmospheric data (right panels). Best fits are marked by dots. The three upper (lower) panels refer to normal (inverted) hierarchy* [73].

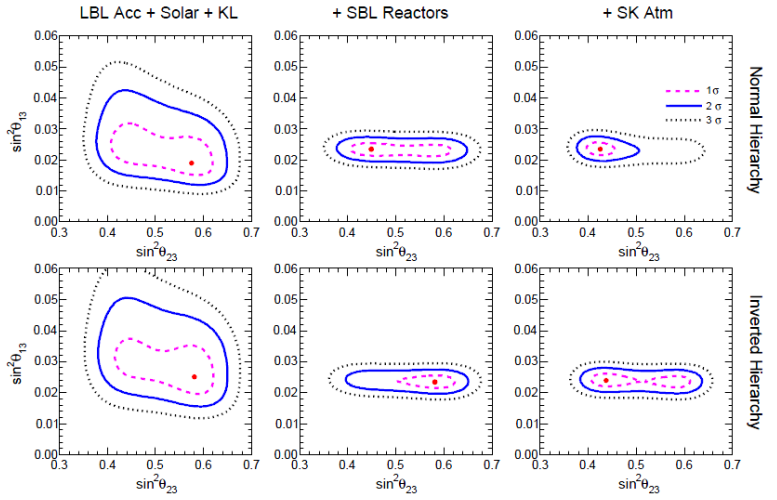

Figure 7.5.2: *As in figure 7.5.1, but in the plane* $(\sin^2(\theta_{23}), \sin^2(\theta_{13}))$ [73].

and true zenith angle given by the event generator. For this neutrino energy and neutrino zenith angle, the probabilities $P_{\mu\mu}$ and $P_{e\mu}$ are calculated numerically for any given set of oscillation parameters. A random number R between zero and one is generated. If $R < P_{e\mu}$, it is classified as a ν_e event, whereas if $R > (P_{e\mu} + P_{\mu\mu})$, then it is classified as a ν_τ event. However, if it happens $P_{e\mu} < R < (P_{e\mu} + P_{\mu\mu})$, then it means that this event is an atmospheric ν_μ which has survived as a ν_μ and is hence selected as muon neutrino event. Only the muon neutrino events are relevant for us, while the others are discarded. Since we do this for a statistically large event sample, we get a ν_μ "survived" event spectrum that follows the survival probability. One could also get muon neutrino events in the detector from oscillations of atmospheric ν_es to ν_μs. To find these events, they are generated using the atmospheric ν_e fluxes but ν_μ charged current interactions

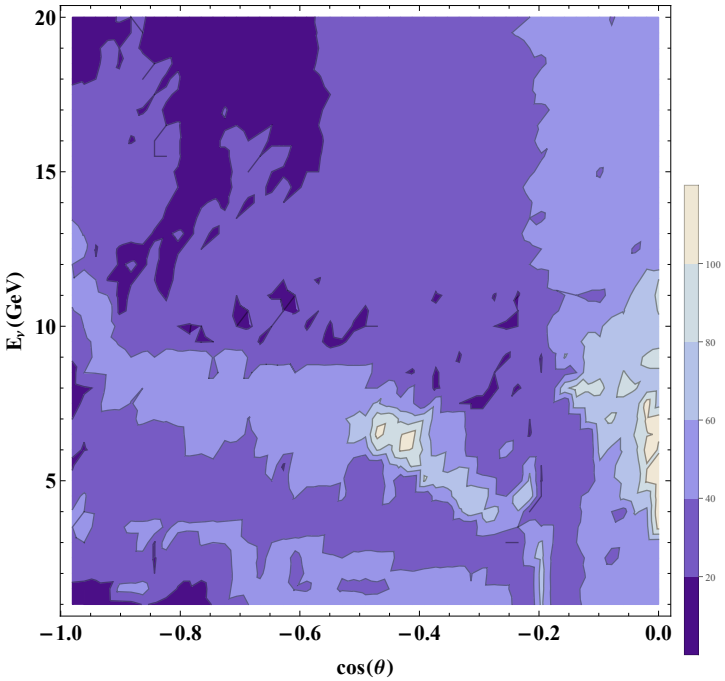

Figure 7.6.1: *The fine-binned distribution of the number of ν_μ-like events in the $(E_\nu, \cos(\theta))$ plane that can be collected by the PINGU detector during 1 year; NH is assumed.*

in the detector, with the oscillation probability part of the code switched off. In order to get the oscillated muon neutrino event from this sample, another random number S is generated to classify these events. That is, if $S < P_{e\mu}$, then the event is taken as an "oscillated" ν_μ event, which is the only part relevant for us. The net number of muon neutrino events are obtained by adding the "survived" and the "oscillated" ν_μ events.

7.7 Sensitivity to the octant of the atmospheric angle θ_{23}

Ever since the MINOS experiment have released their results of the atmospheric angle of $\sin^2(2\theta_{23}) > 0.90$ at 90 % confidence limit [74] (more recent results of $\sin^2(\theta_{23}) = [0.35 - 0.65]$ (90 % C.L.) for NH and $\sin^2(\theta_{23}) = [0.34 - 0.67]$ (90 % C.L.) for IH [[34], [75], [13]]), the scientific community have speculated if the atmospheric angle is maximal or not. The global fit of neutrino oscillation data prefers non-maximal, however this is diluted by the data samples from T2K which prefers maximal. This gives the scientific community an opportunity to measure the atmospheric angle accurately since the current precision of the mixing angle θ_{23} is not good enough to solve this issue (see figure 4 in [76]). The present and future neutrino experiments have entered the precision era.

However, there is a problem, namely a degeneracy if the atmospheric angle is non-maximal (i.e. $\theta_{23} \neq \frac{\pi}{4}$). This can be seen from this formula:

$$\sin^2(\theta_{23}) = 1 - \frac{1}{2}\left[1 \pm \sqrt{1 - \sin^2(2\theta_{23})}\right] \tag{7.7.1}$$

As seen from eq. 7.7.1, if $\sin^2(2\theta_{23}) = 1$, then $\sin^2(\theta_{23}) = 0.5$. This problem enters in the transition probabilities since it depends mostly on $\sin^2(2\theta_{23})$-terms which do not have any sensitivity to the octant. However, the addition of sub-dominant terms in the oscillation probabilities gives sensitivity to the octant since these terms contains $\sin(\theta_{23})$.

This breaks the degeneracy and gives sensitivity to the octant of the atmospheric angle θ_{23}, so it is distinguable between θ_{23} being in the first octant (i.e. $\theta_{23} < \frac{\pi}{4}$) or the second octant (i.e. $\theta_{23} > \frac{\pi}{4}$).

An idea for a possible way to distinguish between lower or higher octant is given in [77] where they look at the transition probabilities [78] written as a series expansion of $\sin(\theta_{13})$ and $\alpha = \frac{|\Delta m^2_{21}|}{|\Delta m^2_{31}|}$ to $\mathcal{O}(\alpha)$ for constant matter potential. A way to distinguish between these two solutions are reparameterizing the atmospheric mixing angle as $\theta_{23} = \frac{\pi}{4} + \epsilon$. Then the probabilities have sensitivity to the sign of ϵ and can possibly be able to determine the value of ϵ. However, there is a δ_{CP} degeneracy in the formulas which makes the determination of the sign of ϵ more difficult. This idea was also for constant matter potential which simplifies the calculation. By considering varying matter, it becomes even more difficult.

With the event rates calculated, a χ^2 fit is performed by using eq. 7.2.3 where the pull variables ξ_i are minimized. The difference $\Delta\chi^2 = \chi^2(NH) - \chi^2(IH)$ is plotted on the y-axis since the neutrino mass hierarchy is still unknown. In the simulations, the number of years running the experiment is three where the result of our analysis to the octant of θ_{23} is shown in fig. 7.7.1.

The figures shows the impact of a variety of things on the octant sensitivity at PINGU. Let us start by looking at the impact of the resolution functions on the octant sensitivity. For top left panel, if the normal hierarchy was true and the test hierarchy was kept fixed as normal, the wrong θ_{23} octant could be ruled out more than 3σ C.L. if $\sin^2(\theta_{23})(\text{true}) < 0.427$ and $\sin^2(\theta_{23})(\text{true}) > 0.59$ for $\sigma_E = 0.2E'_{\text{GeV}}$ and $\sigma_\Theta = 0.5\sqrt{1\text{GeV}/E'_{\text{GeV}}}$. To show the impact of the resolution functions on the octant sensitivity, the simulations were repeated for different combinations of σ_E and σ_Θ. Keeping $\sigma_\Theta = 0.5\sqrt{1\text{GeV}/E'_{\text{GeV}}}$ and changing σ_E from $0.2E'_{\text{GeV}}$ to 2GeV reduces the statistical significance of the octant measurement and a 3σ sensitivity is expected for $\sin^2(\theta_{23})(\text{true}) < 0.418$ and $\sin^2(\theta_{23})(\text{true}) > 0.6$. The impact of worsening the zenith angle resolution have even a shaper effect on the sensitivity. This can be seen by keeping $\sigma_E = 0.2E'_{\text{GeV}}$ and changing $\sigma_\Theta = 0.5\sqrt{1\text{GeV}/E'_{\text{GeV}}}$ to $\sigma_\Theta = 1.0\sqrt{1\text{GeV}/E'_{\text{GeV}}}$, this reduces the statistical significance of the octant measurement significantly and now there is only 2σ sensitivity for $\sin^2(\theta_{23})(\text{true}) < 0.417$ and $\sin^2(\theta_{23})(\text{true}) > 0.586$. For the case where both energy resolution and angle resolution are worsened to $\sigma_E = 2\text{GeV}$ and $\sigma_\Theta = 1.0\sqrt{1\text{GeV}/E'_{\text{GeV}}}$, the wrong octant can be ruled out only at 2σ for $\sin^2(\theta_{23})(\text{true}) < 0.403$ and $\sin^2(\theta_{23})(\text{true}) > 0.6$.

The top right panel shows the sensitivity of PINGU to the octant of θ_{23} if the inverted hierarchy was true and the test hierarchy was kept fixed at inverted hierarchy. For inverted hierarchy the sensitivity falls significantly, and even for $\sin^2(\theta_{23})(\text{true}) = 0.4$, the wrong octant lies just below the 2σ C.L. As can be seen from the figures, there is a difference between if the true hierarchy is normal or inverted. The reasoning for this difference can be found in [53] where the final argumentation gives:

$$\chi^2(IH) < \frac{\chi^2(NH)}{4} \tag{7.7.2}$$

This rough comparison between the expected octant sensitivity between normal and inverted mass hierarchy cases are seen to agree rather well with the results.

Another striking result from the plots are the difference between figures in the top and bottom panel. For the true inverted hierarchy case there is no difference in keeping the test hierarchy fixed or letting it vary in the fit. It has no impact on the octant sensitivity of the experiment. However, for true normal hierarchy there is a significant reduction in the $\Delta\chi^2$ for low values of $\sin^2(\theta_{23})(\text{true})$. In particular for $\sin^2(\theta_{23})(\text{true}) = 0.4$, the

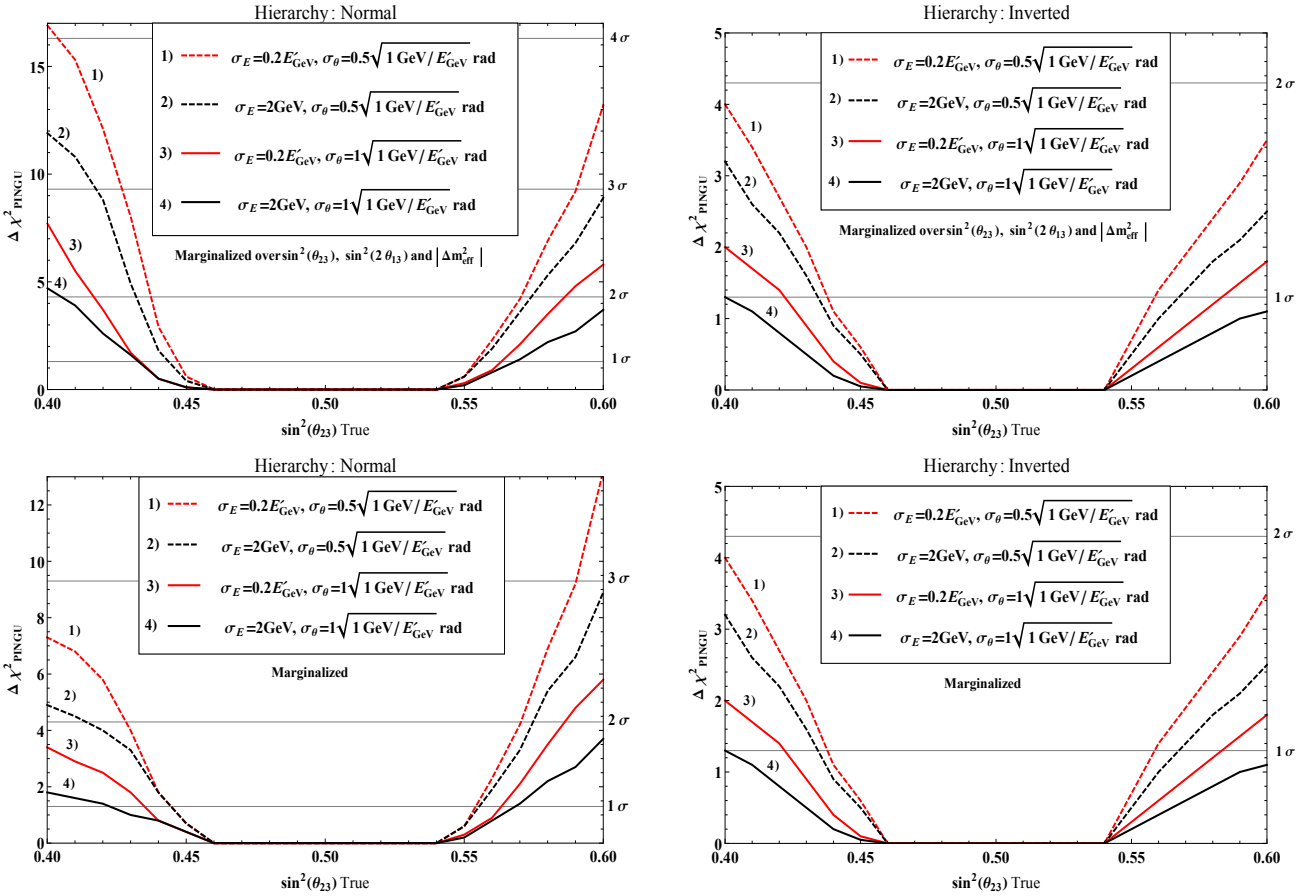

Figure 7.7.1: *$\Delta\chi^2$ for the wrong octant obtained from the PINGU data with 3 years statistics, as a function of $\sin^2(\theta_{23})$(true). The left panel is for normal hierarchy taken as true while the right panel is for inverted hierarchy taken as true. In the top panels, the χ^2 is varied over the oscillation parameters, $\sin^2(\theta_{23})$, $\sin^2(2\theta_{13})$ and $|\Delta m^2_{eff}|$ as described in the text, but the mass hierarchy is held fixed to the assumed true case in the fit. In the bottom panels, the χ^2 is varied over the oscillation parameters, $\sin^2(\theta_{23})$, $\sin^2(2\theta_{13})$ and $|\Delta m^2_{\rm eff}|$ as weel as the mass hierarchy, keeping mass hierarchy free in the fit. The four lines are for the four possible combinations for the choices of the energy and angle resolution of PINGU. See appendix for larger verions.*

statistical significance of the octant determination from 3 years of PINGU data, comes down from $\Delta\chi^2 = 16.9$ to $\Delta\chi^2 = 7.3$ for the optimal resolution case of $\sigma_E = 0.2E'_{\rm GeV}$ and $\sigma_\Theta = 0.5\sqrt{1{\rm GeV}/E'_{\rm GeV}}$. For the other choices of the combination of σ_E and σ_Θ we also see a similar trend, wherein the data with true normal hierarchy is fitted with the wrong test inverted hierarchy, reducing thereby the octant sensitivity from PINGU. However, for $\sin^2(\theta_{23})$(true) > 0.44 the variation over hierarchy does not have any impact what-so-ever on the octant sensitivity of PINGU, even for the case of true normal hierarchy.

With the 3 years of data, there is a region around $\sin^2(\theta_{23})$(true) ~ 0.5 where the octant sensitivity disappears. This disappearence comes from the variation of the oscillation parameters in the fit. If they were fixed, then the sensitivity to the octant would display a parabola with only one point being zero, namely in $\sin^2(\theta_{23})$(true) $= 0.5$. However, this "valley" can become visible by including more data from PINGU and/or include data from other experiments which can further constrain the other oscillation parameters.

7.8 Systematic uncertainties

In this section, the systematic uncertainties and their influence on the $\Delta\chi^2$ are examined. As mentioned before, there are 5 systematic uncertainties. They are a flux normalization error of 20 %, a cross-section uncertainty of 10 %, a 5 % uncertainty on the zenith angle dependence of the fluxes, a 5 % energy dependent "tilt factor" of the fluxes and a 5 % additional overall uncertainty.

In order to study the impact of these systematic uncertainties on the octant, the sensitivity is shown with and without systematic uncertainties in figure 7.8.1. Systematic uncertainties are the combined effect of theoretical and experimental uncertainties and reduces the sensitivity of the analysis.

Three of the five systematic uncertainties, namely flux normalization, cross-section and overall uncertainty has minimal impact on the final result. The reason can be understood from the fact that the atmospheric neutrinos comes from all zenith angles and over a wide range of energies. The flux normalization uncertainty is the same for all bins, while the Earth matter effects are important only in certain zenith angle bins and range of energies. Therefore, the effect of the flux normalization uncertainty get cancelled between different bins. On the other hand, the "tilt factor" could be used to modify the energy spectrum of the neutrinos and the zenith angle uncertainty allows changes to the zenith angle distribution. Therefore, these errors do not cancel between the different bins and can dilute the significance of the data. In particular, the effects of the zenith angle and energy dependent systematic errors on the atmospheric neutrino fluxes have a major impact on lowering the $\Delta\chi^2$ for the octant sensitivity.

The impact of the systematic uncertainties are shown in figure 7.8.1. For each plot there is a specific energy resolution given in the upper right corner of the plot. There the angular resolution is also given, though with a constant c. For each line there is a specific constant c shown in the plot legend. As can be seen, the dashed lines have $c = 0.5$ rad while the solid lines have $c = 1.0$ rad. The red color means there is no systematic uncertainties in the fit whereas the black has all five systematic uncertainties included in the fit. The other colors in the plot have one specific systematic uncertainty switch off: Overall systematic (dark blue), cross-section (cyan), flux normalization (grey), energy dependent "tilt factor" (purple) and zenith dependence (green). As can be seen in the figures, the systematic uncertainties that have the most impact on the χ^2 are the energy and zenith dependent systematic uncertainties while the other uncertainties as mentioned before have minimal impact as mentioned before. On the right side of the plots are shown the significance level. Again the plots with normal hierarchy have higher significance than the plots with inverted hierarchy.

7.9 Another relevant systematic uncertainty

In addition to the systematic uncertainties in the reconstruction of the incident neutrino and energy, we wish to highlight the particle identification (PID) uncertainty as another limiting factor for octant sensitivity. The five systematic uncertainties were original from the article [53], whereas the sixth systematic uncertainty, a PID uncertainty is included in this section. This is done by introducing a regularization function to the event rate eq. 7.2.1, reducing the effective mass of the detector. This uncertainty scales as a function of energy, so that only a certain amount of the energy will get deposited into the detector. The charged current ν_μ will only deposit 30 % of its true energy at 3 GeV into the detector, 70 % at 8 GeV and 90 % at 13 GeV. At 15 GeV, it will be a 100 % up to 20 GeV. There will be a correlation between the PID uncertainty and those concerning the energy and

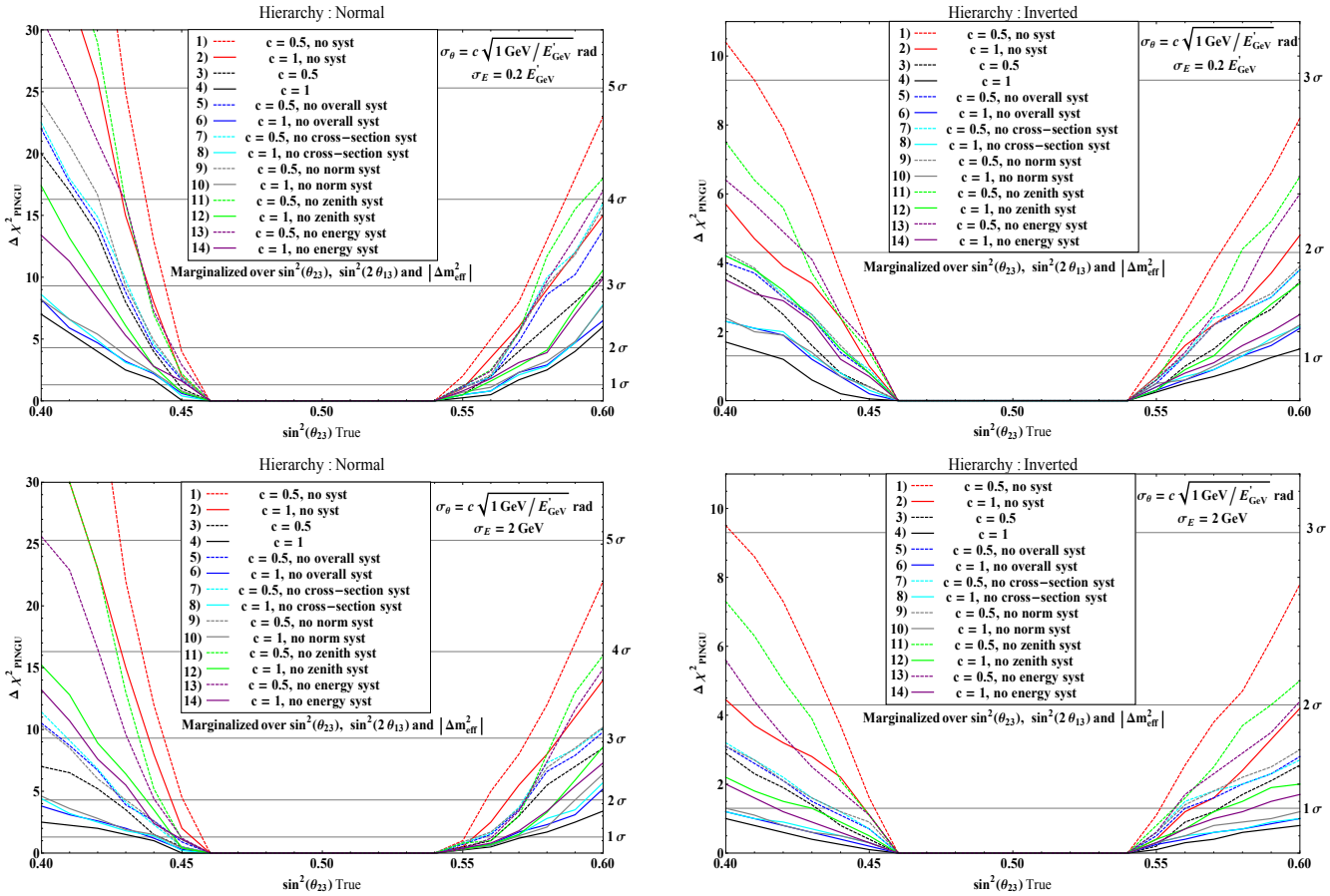

Figure 7.8.1: *Impact of systematic uncertainties on the $\Delta\chi^2$ for the wrong octant obtained from the PINGU data with 3 years statistics, as a function of $\sin^2(\theta_{23})$(true). The solid lines show the $\Delta\chi^2$ with $\sigma_\Theta = 1.0\sqrt{1\,GeV/E'_{GeV}}$, while the dashed lines are obtained with $\sigma_\Theta = 0.5\sqrt{1\,GeV/E'_{GeV}}$. The energy resolution is given in the plot. We show the results for all combinations of σ_E and σ_Θ. The left panel is for normal hierarchy while the right panel is for inverted hierarchy. The test hierarchy is kept fixed at the true value for all cases. See appendix for larger versions.*

angular dependence of the atmospheric neutrino flux.

The influence of this systematic uncertainty is shown in figure 7.9.1 which shows the old fit with only five systematic uncertainties and the new fit with six systematic uncertainties. As can be seen from the figure 7.9.1, this uncertainty have some impact on the octant sensitivity since the low-energy of the ν_μ gets poorly determined. The parametric enhancement and the MSW effect gives a higher signal to the octant which happens in the region below 10 GeV, so if the energy of the neutrinos are more poorly determined by the PID uncertainty, the signal is reduced. This is the reason why the PID uncertainty has a bigger influence on the octant sensitivity than the flux normalization uncertainty. With the reduction of the sensitivity to the octant, a longer time is needed for making the same confidence level with this sixth systematic included than if it was without this systematic uncertainty. From figure 7.9.1 in top left corner, you can see that with the resolution function $\sigma_E = 0.2E'_{\mathrm{GeV}}$ and $\sigma_\theta = 0.5\sqrt{1\mathrm{GeV}/E'_{\mathrm{GeV}}}$ the reduction from 3σ to below 3σ for $\sin^2(\theta_{23})(\mathrm{true}) > 0.428$ and $\sin^2(\theta_{23})(\mathrm{true}) < 0.590$ whereas for the other combinations of resolution functions, the sensitivity also gets worse. In the top right corner of figure 7.9.1, the old fit with resolution functions $\sigma_E = 0.2E'_{\mathrm{GeV}}$ and

$\sigma_\theta = 0.5\sqrt{1\text{GeV}/E'_{\text{GeV}}}$ is already below 2σ and the inclusion of the sixth systematic uncertainty with the same resolution functions gives a 1.4σ C.L for $\sin^2(\theta_{23}(\text{true}) < 0.423$ and $\sin^2(\theta_{23})(\text{true}) > 0.586$. The other combinations of resolution functions gives a C.L. below 2σ and even below 1σ for some combinations of resolution functions, with or without this sixth systematic uncertainty.

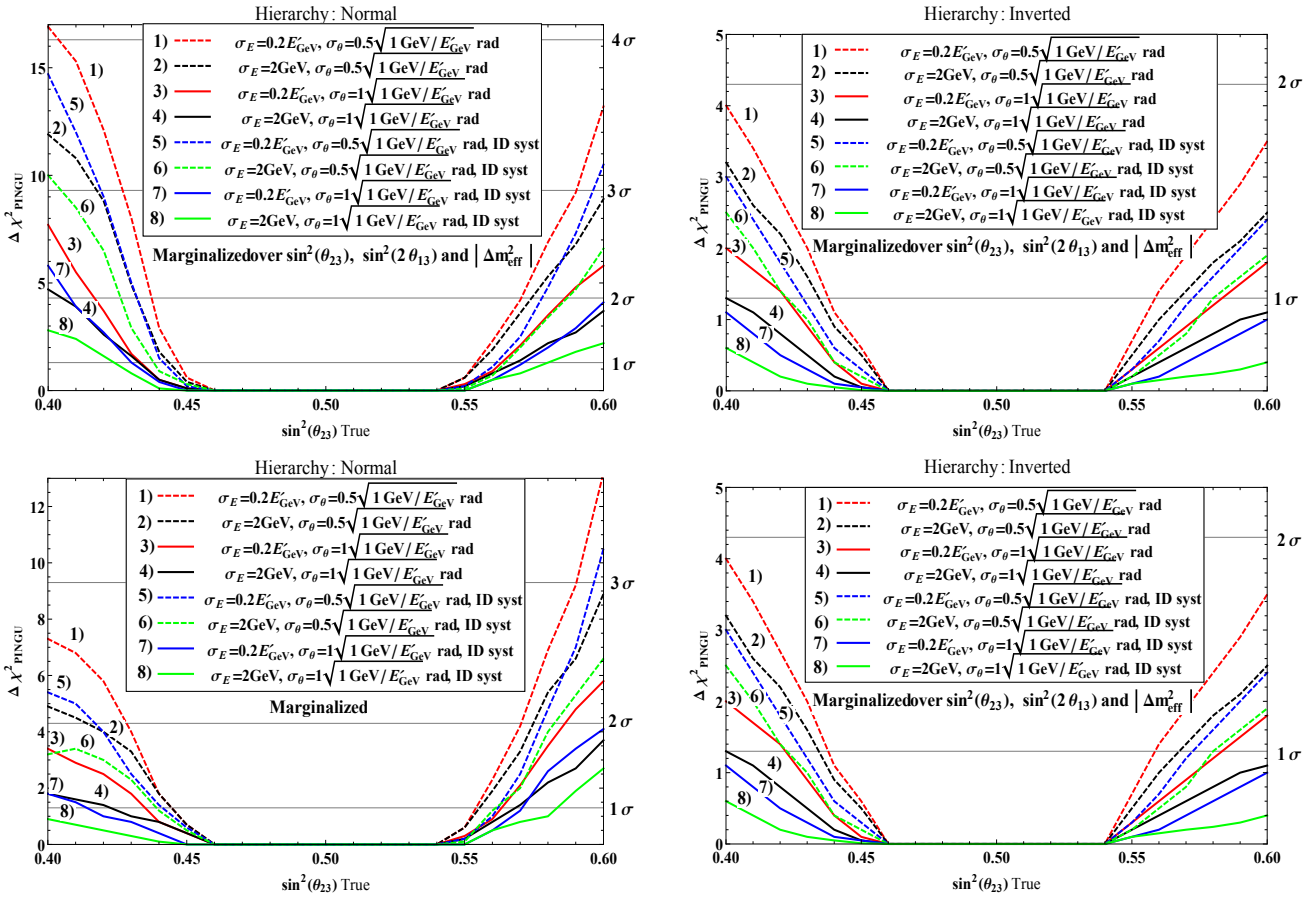

Figure 7.9.1: *Same as 7.7.1, but also fits with the sixth systematic uncertainty in particle identification. See appendix for larger versions.*

With the results in the various plots from different subsections, a comparison between the simulations from the IceCube-PINGU Collaboration in [15] and this thesis's results are presented. In chapter 6 of [15] is an analysis of the sensitivity to non-maximal θ_{23} mixing. The main result is given in figure 21 and 22 which show the contour plot of $\sin^2(\theta_{23})$ vs. Δm^2_{atm} for both hierarchies and both octants. They show the separation is achievable in 5 years between the current global best fit and maximal θ_{23} mixing for some combination of the true θ_{23} octant and the true mass hierarchy. The octant sensitivity is highly dependent on the true mass hierarchy and true θ_{23} octant. This can be seen in the two plots of figure 21 and 22 in [15]. If the true oscillation parameter of θ_{23} lies in the first octant and the true hierarchy is normal, PINGU may exclude the entire second octant more than 5σ. If the oscillation parameter lies in the second octant, then PINGU may exclude the first octant after five years by 3σ for normal hierarchy, or by 1σ for an inverted hierarchy.

However, there are differences between the results in [15] and the plots in this thesis. Their simulations is realized in 5 years of data whereas the projected time in this thesis is 3 years of data. This means they have accumulated more data which gives more significance

to the octant. This difference can easily be fixed by a scaling factor to the event rates. However, if $\Delta\chi^2 \approx 0$, then the scaling would not help and insight of the octant sensitivity around $\sin^2(\theta_{23}) = 0.5$ would be lost. However, if the simulations are for 5 years of data, the sensitivity would rise in the outer edges of this "valley". A second and more crucial thing is that the resolution functions in [15] are fixed by a constant, i.e. $\sigma_E = 2.5$ GeV and $\sigma_\theta = 8.5°$ whereas in reality they depend on the energy. In a comparison, the σ_E is not that important since the energy resolution function could be fixed by a constant. However, by fixing the σ_θ to a constant increases the signal since there is a cross-over where the constant σ_θ performs better than one which depends on the energy. This cross-over happens near 10 GeV (for $c = 0.5$ rad) which is a crucial energy since the most sensitivity to the octant is in the low-energy region from 1 to 10 GeV. If the constant in front of the square root in the angular resolution function is one, then the performance is even worse compared to a constant σ_θ.

8

Impact of different flavour symmetries on the analysis

In the previous chapter the analysis was done from global fit data and without the knowledge of which flavour symmetry is correct. However, in this chapter there is given a introduction to flavour models and a comparison between different flavour symmetries. By implementing various flavour symmetries, you will get different sensitivities to the octant of the atmospheric angle. With this in hand, you can constrain flavour models as the family symmetry. First is given a introduction to group theory which is an essential part of flavour models and gives the allow terms in the Lagrangian and output of oscillation parameters. Thereafter will be shown some examples of flavour symmetries used in models. These models are not correct any more since the prediction of mixing angles are not in the allow range from neutrino data. However, it is suppose to show the idea behind flavour models in the use of various flavour symmetries to explain the current neutrino oscillation parameters.

8.1 Group theory

Non-Abelian (as well Abelian) discrete symmetries appear to play an important role in understanding the physics of flavour. These are described by group theory and this is a brief introduction to the main mathematical concepts of finite group theory. A group G is a set consisting of elements $\{g_i\}$ together with a rule for multiplication. They satisfy the following properties [79]:

- Closure under multiplication: If g_1 and g_2 are in G, so is $g_1 \cdot g_2$.
- Associativity: For any three elements g_1, g_2, $g_3 \in G$, $g_1 \cdot (g_2 \cdot g_3) = (g_1 \cdot g_2) \cdot g_3$.
- Identity: There exists an element $e \in G$ such that $e \cdot g = g$ for every $g \in G$.
- Inverse: For every $g \in G$ there exists an inverse, $g^{-1} \in G$, such that $g \cdot g^{-1} = g^{-1} \cdot g = e$.

The most basic way of defining a group is given in terms of the multiplication table, where the result of each product of two elements is listed. In the case of the smallest non-Abelian finite group, the permutation group S_3, we have: The six elements are classified into the identity element e, elements b_i whose square is e and finally elements a_i for which the square does not yield e but, as can be seen easily, the cube does. It is generally true for any finite group that there exists some exponent n for each element g such that $g^n = e$. The smallest exponent for which this holds is called the order of the element g. This is not to be confused with the order of a group G which simply means the number of elements contained in G.

S_3	e	a_1	a_2	b_1	b_2	b_3
e	e	a_1	a_2	b_1	b_2	b_3
a_1	a_1	a_2	e	b_2	b_3	b_1
a_2	a_2	e	a_1	b_3	b_1	b_2
b_1	b_1	b_3	b_2	e	a_2	a_1
b_2	b_2	b_1	b_3	a_1	e	a_2
b_3	b_3	b_2	b_1	a_2	a_1	e

Table 8.1.1: *Multiplication table of the permutation group S_3*

8.1.1 Group presentation

Clearly, the definition of a finite group in terms of its multiplication table becomes cumbersome very quickly with increasing order of G. It is therefore necessary to find a more compact way of defining G. Noticing that all six elements of S_3 can be obtained by multiplying only a subset of all elements, we arrive at the notion of generators of a group. Denoting $a_1 = a$ and $b_1 = b$, we obtain $a_2 = a^2$ as well as $b_2 = ab$ and $b_3 = ba$. In other words, a and b generate the group S_3. Being the group of permutations on three objects which is isomorphic to the group of symmetry transformations of an equilateral triangle, a corresponds to a 120^o rotation and b to a reflection. This observation leads to the definition of S_3 using the so-called presentation

$$\langle a, b | a^3 = b^2 = e, bab^{-1} = a^{-1} \rangle \tag{8.1.1}$$

where the generators have to respect the rules listed on the right. Depending the these presentation rules, a group can be defined uniquely in a compact way. Unfortunately, such an abstract definition of a group is not very useful for physical applications as it does not show the possible irreducible representations of the group. We therefore quickly continue our journey through the fields of finite group theory towards the important notion of character tables.

8.1.2 Character table

In order to understand the meaning of a character table, is it mandatory to introduce the idea of conjugacy classes and irreducible representations. Conjugacy classes are subsets of elements of G which are obtained from collecting all these elements related to a given element g_i by conjugation gg_ig^{-1}, for all $g \in G$. The union of all possible conjugacy classes is nothing but the set of all elements of G. In the case of S_3 we find three different classes:

$$1C^1(1) = \{g1g^{-1} | g \in S_3\} = \{1\} \tag{8.1.2}$$

$$2C^3(a) = \{gag^{-1} | g \in S_3\} = \{a, a^2\} \tag{8.1.3}$$

$$3C^2(b) = \{gbg^{-1} | g \in S_3\} = \{b, ab, ba\} \tag{8.1.4}$$

Here we have used the notation $N_iC^{n_i}(g_i)$, where g_i is an element of the class, N_i gives the number of different elements contained in that class, and n_i denotes the order of these elements, which is identical for all gg_ig^{-1} with $g \in G$.

The other ingredient for constructing a character table is the set of possible irreducible representations of the group G. In general non-Abelian groups can be realized in terms

of $r \times r$ matrices, where the positive intergers r depend on the group. Then, the abstract generators of a group are promoted to matrices which satisfies the presentation rules. Such matrix representations are called reducible if there exists a basis in which the $r \times r$ matrices of all generators of G can be brought into the same block diagonal form. If this is not possible, the representation is called irreducible. Clearly, the trivial singlet representation $\underline{1}$, where all generators of G are identically 1, satisfies any presentation rule and is thus an irreducible representation of all groups. In the case of S_3, the irreducible representations compatible with the presentation rules of eq. 8.1.1 take the form:

$$\underline{1} : a = 1, \quad b = 1 \tag{8.1.5}$$

$$\underline{1}' : a = 1, \quad b = -1 \tag{8.1.6}$$

$$\underline{2} : a = \begin{pmatrix} e^{2\pi i/3} & 0 \\ 0 & e^{-2\pi i/3} \end{pmatrix}, \quad b = \begin{pmatrix} 0 & 1 \\ 1 & 0 \end{pmatrix} \tag{8.1.7}$$

The fact that S_3 has three irreducible representations and also three conjugacy classes is not a coincidence. It is generally true that the number of irreducible representations of a finite group is equal to the number of its conjugacy classes. Moreover, summing up the squares of the dimensions of all irreducible representations always yields the order of the group G. For example, in S_3 we get $1^1 + 1^2 + 2^2 = 6$. These two facts can be used to work out all irreducible representations of a given group G.

In the case of irreducible representations $\underline{r}$ with $r > 1$, the explicit matrix form of the generators depends on the basis. In order to obtain a basis independent quantity, one defines the character $\chi_{g_i}^{[\underline{r}]}$ of the matrix representation of a group element g_i to be its trace. Since the elements of a conjugacy class are all related by gg_ig^{-1} with $g \in G$, it is meaningful to speak of the character $\chi_i^{[\underline{r}]}$ of the elements of a conjugacy class i. Therefore one can define the character table where the rows list the irreducible representations and the columns show the conjugacy classes. Using eq. 8.1.5-8.1.7, we find the following character table of S_3.

S_3	$1C^1(1)$	$2C^3(a)$	$3C^2(b)$
$\chi_i^{[\underline{1}]}$	1	1	1
$\chi_i^{[\underline{1}']}$	1	1	-1
$\chi_i^{[\underline{2}]}$	2	-1	0

Table 8.1.2: *Character table of the permutation group S_3*

Defining a group in terms of its character table is much more suitable for physical applications than the previous definitions. First, it immediately lists all possible irreducible representations which might be used in constructing particle physics models. Secondly, it is also straightforward to extract the Kronecker products of a finite group G from its character table.

8.1.3 Kronecker products and Chebsch-Gordan coefficients

Multiplying arbitrary irreducible representations $\underline{r}$ and $\underline{s}$

$$\underline{r} \otimes \underline{s} = \sum_{\underline{t}} d(\underline{r}, \underline{s}, \underline{t})\underline{t} \tag{8.1.8}$$

one can calculate the multiplicity $d(\underline{r},\underline{s},\underline{t})$ with which the irreducible representation $\underline{t}$ occurs in the product by

$$d(\underline{r},\underline{s},\underline{t}) = \frac{1}{N}\sum_i N_i \chi_i^{[r]} \chi_i^{[s]} \chi_i^{[t]*} \tag{8.1.9}$$

where the sum is over all classes. N denotes the order of the group G and the asterisk indicates complex conjugation. With this, we obtain the following non-trivial Kronecker products from the S_3 character table:

$$\underline{1}' \otimes \underline{1}' = \underline{1} \tag{8.1.10}$$

$$\underline{1}' \otimes \underline{2} = \underline{2} \tag{8.1.11}$$

$$\underline{2} \otimes \underline{2} = \underline{1} + \underline{1}' + \underline{2} \tag{8.1.12}$$

The Kronecker products are necessarily independent of the basis of the irreducible representations $\underline{r}$ with $r > 1$. When formulating and spelling out the details of a model, particular bases have to be chosen by hand. With the bases fixed, it is possible to work out the basis dependent Clebsh-Gordan coefficients of a group. Denoting the components of the two multiplet of a product by α_i and β_j, the resulting representation with components γ_k are obtained from

$$\gamma_k = \sum_{i,j} c_{ij}^k \alpha_i \beta_j \tag{8.1.13}$$

where c_{ij}^k are the Clebsch-Gordan coefficients. These are determined by the required transformation properties of the components γ_k under the group generators. In the case of S_3 using the basis equations 8.1.5-8.1.7, one gets

$$\underline{1}' \otimes \underline{1}' \to \underline{1} \quad \alpha\beta \tag{8.1.14}$$

$$\underline{1}' \otimes \underline{2} \to \underline{2} \quad \alpha \begin{pmatrix} \beta_1 \\ -\beta_2 \end{pmatrix} \tag{8.1.15}$$

$$\underline{2} \otimes \underline{2} \to \underline{1} \quad \alpha_1\beta_2 + \alpha_2\beta_1 \tag{8.1.16}$$

$$\underline{2} \otimes \underline{2} \to \underline{1}' \quad \alpha_1\beta_2 - \alpha_2\beta_1 \tag{8.1.17}$$

$$\underline{2} \otimes \underline{2} \to \underline{2} \quad \begin{pmatrix} \alpha_2\beta_2 \\ \alpha_1\beta_1 \end{pmatrix} \tag{8.1.18}$$

where α_i refers to the first factor of the Kronecker product and β_j to the second. We conclude our discussion of the most important concepts in finite group theory by pointing out that - due to the choice of convenient bases - a representation which is real (that is for which there exists a basis where all generators are explicitly real) may have complex generators. This is for instance the case for the doublet of S_3 in the basis of equations 8.1.5-8.1.7.

8.1.4 Finite groups with triplet representations

For applications in flavour physics, we are interested in finite groups with triplet representations. They can be found among subgroups of SU(3) and fall into four classes [79]:

- Groups of the type $(Z_n \times Z_m) \rtimes S_3$
- Groups of the type $(Z_n \times Z_m) \rtimes Z_3$
- The simples groups A_5 and $PSL_2(7)$ plus a few more "exceptional" groups
- The double covers of the tetrahedral (A_4), octahedral (S_4) and icosahedral (A_5) groups

The latter are subgroups of SU(2), whose triplet representations are identical to the triplets of the respective rotation groups. Many of the physically useful symmetries are special cases within these general classes.

For instance, S_4, the natural symmetry of tribimaximal mixing in direct models is isomorphic to $\Delta(6n^2) = (Z_n \times Z_n) \rtimes S_3$ with $n = 2$. The presentation rules of $\Delta(6n^2)$ can be given in terms of four generators, a, b, c, d:

$$a^3 = b^2 = (ab)^2 = c^n = d^n = 1, \qquad cd = dc \tag{8.1.19}$$

$$aca^{-1} = c^{-1}d^{-1}, \qquad ada^{-1} = c, \qquad bcb^{-1} = d^{-1}, \qquad bdb^{-1} = c^{-1} \tag{8.1.20}$$

The dimensions of all irreducible representations can only take values 1, 2, 3 or 6. A faithful triplet representation is found, e.g. in the following set of matrices

$$a = \begin{pmatrix} 0 & 1 & 0 \\ 0 & 0 & 1 \\ 1 & 0 & 0 \end{pmatrix}, \quad b = -\begin{pmatrix} 0 & 0 & 1 \\ 0 & 1 & 0 \\ 1 & 0 & 0 \end{pmatrix}, \quad c = \begin{pmatrix} \eta & 0 & 0 \\ 0 & \eta^{-1} & 0 \\ 0 & 0 & 1 \end{pmatrix}, \quad d = \begin{pmatrix} 1 & 0 & 0 \\ 0 & \eta & 0 \\ 0 & 0 & \eta^{-1} \end{pmatrix} \tag{8.1.21}$$

where $\eta = e^{2\pi i/3}$. With $n = 2$ this triplet representation is explicitly real, and therefore does not correspond to the basis in which the S_4 order three generator T is diagonal and complex. To make connection to the S_4 triplet generators S, U and T we have to perform the basis transformation

$$S = wdw^{-1}, \qquad U = w(aba^{-1})w^{-1}, \qquad T = waw^{-1} \tag{8.1.22}$$

where

$$w = \frac{1}{\sqrt{3}} \begin{pmatrix} 1 & 1 & 1 \\ 1 & \omega & \omega^2 \\ 1 & \omega^2 & \omega \end{pmatrix} \tag{8.1.23}$$

with $\omega = e^{2\pi i/3}$ and $\omega^2 = e^{-2\pi i/3}$. This shows how the tribimaximal Klein symmetry $Z_2 \times Z_2$ of the neutrino mass matrix in the diagonal charged lepton basis, generated by

$$S = \frac{1}{3} \begin{pmatrix} -1 & 2 & 2 \\ 2 & -1 & 2 \\ 2 & 2 & -1 \end{pmatrix}, \qquad U = -\begin{pmatrix} 1 & 0 & 0 \\ 0 & 0 & 1 \\ 0 & 1 & 0 \end{pmatrix} \tag{8.1.24}$$

is inherited from $\Delta(24) = (Z_2 \times Z_2) \rtimes S_3$: One Z_2 factor (namely S) originates from the first factor, $Z_2 \times Z_2$, and the other (namely U) is derived for the second, S_3.

Another series of groups can be obtained from the presentation of eq. 8.1.20 by simply dropping the generator b, and consequently all conditions involving b. This results in the group $\Delta(3n^2) = (Z_n \times Z_n) \rtimes Z_3$ which only allow for irreducible representations of dimensions 1 and 3. The case with $n = 2$ generates the tetrahedral group A_4 which will be discussed later. With the formal introduction to group theory it will be shown where the mixing matrix enters in the field of neutrino oscillation.

8.2 Flavour symmetries

The experimental efforts of the last decade have shown that neutrinos do mix, and the mixing angles have been determined to a great degree of accuracy. The question is whether the elements of the mixing matrix U_{PMNS}, and ultimately the elements of the lepton mass matrices, are simply random numbers or whether they point to some deeper structure or symmetry. It is natural to imagine that there is a family (flavour) symmetry that links the three lepton families. The weak interaction terms involving W and lepton fields are given by:

$$\mathcal{L}_{W\ell\nu} = \frac{g}{\sqrt{2}} W_\mu^+ (U_{\nu L}^\dagger U_{\ell L})_{i\alpha} \bar{\nu}_L'^i \gamma^\mu \ell_L'^\alpha + h.c. \tag{8.2.1}$$

The lepton mixing matrix U_{PMNS} depends on mixing in both the charged lepton and neutrino sectors given as:

$$U_{PMNS} = U_{\ell L}^\dagger U_{\nu L} \tag{8.2.2}$$

The unitary matrices $U_{\ell L}$ and $U_{\nu L}$ diagonalize the charged lepton and neutrino mass matrices respectively, i.e.

$$U_{\ell L}^\dagger M_\ell U_{\ell R} = m_\alpha \delta_{kj} \tag{8.2.3}$$

$$U_{\nu L}^\dagger M_\nu U_{\nu R} = m_k \delta_{kj} \tag{8.2.4}$$

where m_α ($\alpha = e, \mu, \tau$) and m_k ($k = 1, 2, 3$) are the charged lepton and neutrino masses respectively. The SM symmetries do not constrain the form of the mass matrices; the matrix M_l can be any 3×3 matrix. The addition of a family symmetry, G_{family}, extends the SM symmetries to

$$G = SU(3)_C \times SU(2)_L \times U(1)_Y \times G_{\text{family}} \tag{8.2.5}$$

which constrains the mass matrices further, requiring that the Lagrangian remain invariant under the following transformations of the three generations of left-handed lepton doublets, right-handed charged lepton singlets and neutrinos:

$$L_L \to X_L L_L \qquad \ell_R \to X_R \ell_R \qquad \nu \to X_\nu \nu \tag{8.2.6}$$

The unitary matrices X_ν, X_L and X_R will belong to a representation of some symmetry group (G_{family}), thus constraining the form of the mass matrices by:

$$M_\nu = X_\nu^\dagger M_\nu X_\nu \tag{8.2.7}$$

$$M_\ell = X_L^\dagger M_\ell X_R \tag{8.2.8}$$

The models in the literature look to find an underlying symmetry that can explain the pattern of neutrino mixing [[80], [81]]. Hereafter are given examples of flavour symmetries used to predict specific mixing matrices. These are not correct any more due to the discovery of the non-zero θ_{13}. However, they are only to give the idea behind the use of flavour symmetries to explain neutrino oscillation and they give a good zero order approximation of the mixing matrix. Thereafter, you could extend the model by implementing various effects which can accommodate the current mixing matrix.

8.2.1 A μ-τ symmetric mass matrix

A class of models proposes a mass matrix that is invariant under exchange of the μ and τ elements. In the basis where the charged lepton mass matrix is diagonal, the neutrino mass matrix, M_ν, is diagonalized by the unitary mixing matrix U, i.e.:

$$U^T M_\nu U = m_k \delta_{kj} \tag{8.2.9}$$

The neutrino masses are given by m_k for $k = 1, 2, 3$. Now, if M_ν is μ-τ symmetric then

$$M_\nu = M^{(\mu\tau)} \equiv \begin{pmatrix} x & y & y \\ y & z & w \\ y & w & z \end{pmatrix} \tag{8.2.10}$$

and atmospheric mixing is maximal ($|U_{\mu 3}| = |U_{\tau 3}|$). This symmetry can be represented by the matrix

$$T = \begin{pmatrix} 1 & 0 & 0 \\ 0 & 0 & 1 \\ 0 & 1 & 0 \end{pmatrix} \tag{8.2.11}$$

so that $TM_\nu T = M_\nu$, which is a $\mathbb{Z}_2$ symmetry. Diagonalizing the mass matrix in eq. 8.2.10 gives the mixing matrix:

$$U = \begin{pmatrix} \cos(\theta_{12}) & \sin(\theta_{12}) & 0 \\ -\frac{\sin(\theta_{12})}{\sqrt{2}} & \frac{\cos(\theta_{12})}{\sqrt{2}} & \frac{1}{\sqrt{2}} \\ -\frac{\sin(\theta_{12})}{\sqrt{2}} & \frac{\cos(\theta_{12})}{\sqrt{2}} & -\frac{1}{\sqrt{2}} \end{pmatrix} \tag{8.2.12}$$

If the solar mixing angle is set to $\sin^2(\theta_{12}) = \frac{1}{3}$, a somewhat ad-hoc estimate, the matrix eq. 8.2.12 becomes the tribimaximal (TBM) matrix:

$$U_{TBM} = \begin{pmatrix} \frac{2}{\sqrt{6}} & \frac{1}{\sqrt{3}} & 0 \\ -\frac{1}{\sqrt{6}} & \frac{1}{\sqrt{3}} & \frac{1}{\sqrt{2}} \\ -\frac{1}{\sqrt{6}} & \frac{1}{\sqrt{3}} & -\frac{1}{\sqrt{2}} \end{pmatrix} \tag{8.2.13}$$

8.2.2 C_3 and $S_2 \times S_2$ symmetry

This model was first introduced by [82], who proposed a simple model based on two discrete symmetries. Their initial idea is the mass matrices are shown to be related to the symmetry groups C_3 and S_3 and their class operators. In order to reproduce TBM, one can start with mass matrices of the form [82]

$$M_\ell = \begin{pmatrix} a & b & b^* \\ b^* & a & b \\ b & b^* & a \end{pmatrix} \qquad M_\nu = \begin{pmatrix} x & 0 & y \\ 0 & z & 0 \\ y & 0 & x \end{pmatrix} \tag{8.2.14}$$

where a, b, b^* are related to the charged lepton masses, and x, y, z are related to three independent neutrino masses. The matrix M_ℓ is of circulant form, and can be generated by a C_3 symmetry (a cyclic permutation of three objects), whereas the matrix M_ν is generated by an $S_2 \times S_2$ symmetry. For an Abelian symmetry, a mass matrix that is invariant under the regular representation of the group is a linear combination of the representation matrices themselves [83]. In the case of C_3, the regular representation is given by

$$\left\{ \begin{pmatrix} 1 & 0 & 0 \\ 0 & 1 & 0 \\ 0 & 0 & 1 \end{pmatrix}, \begin{pmatrix} 0 & 1 & 0 \\ 0 & 0 & 1 \\ 1 & 0 & 0 \end{pmatrix}, \begin{pmatrix} 0 & 0 & 1 \\ 1 & 0 & 0 \\ 0 & 1 & 0 \end{pmatrix} \right\} \tag{8.2.15}$$

and it is obvious that the matrix M_ℓ in eq. 8.2.14 is a linear combination of the matrices in eq. 8.2.15. The mass matrices M_ℓ and M_ν in eq. 8.2.14 are diagonalized by

$$U_{\ell L} = U_{\ell R} = \frac{1}{\sqrt{3}} \begin{pmatrix} 1 & 1 & 1 \\ 1 & \omega & \omega^2 \\ 1 & \omega^2 & \omega \end{pmatrix} \quad \text{and} \quad U_{\nu L} = U_{\nu R} = \frac{1}{\sqrt{2}} \begin{pmatrix} 1 & 0 & -1 \\ 0 & \sqrt{2} & 0 \\ 1 & 0 & 1 \end{pmatrix} \tag{8.2.16}$$

respectively, where $\omega \equiv e^{2\pi i/3}$ and $\omega^2 \equiv e^{-2\pi i/3}$. Combining these two matrices using eq. 8.2.2 gives TBM eq. 8.2.13. In the case of the C_3 Abelian symmetry, the columns of the diagonalization matrix $U_{\ell L} = U_{\ell R}$ correspond to the one-dimensional representations of the group:

$$\{1, 1, 1\}, \{1, \omega, \omega^2\}, \{1, \omega^2, \omega\} \tag{8.2.17}$$

In the case of the $S_2 \times S_2$ symmetry, the representation to generate the neutrino mass matrix M_ν is not the regular representation, but rather:

$$\left\{ \begin{pmatrix} 1 & 0 & 0 \\ 0 & 1 & 0 \\ 0 & 0 & 1 \end{pmatrix}, \begin{pmatrix} 0 & 1 & 0 \\ 0 & 0 & 1 \\ 1 & 0 & 0 \end{pmatrix}, \begin{pmatrix} 0 & 0 & 1 \\ 1 & 0 & 0 \\ 0 & 1 & 0 \end{pmatrix} \right\} \tag{8.2.18}$$

The mixing matrix U_ν is in this case not clearly related to the representation of the symmetry $S_2 \times S_2$, but the mass matrix M_ν in eq. 8.2.14 is a linear combination of the matrices in eq. 8.2.18.

However, the problem with this model is that it is not compatible with the $SU(2)_L$ symmetry of the SM, with its left-handed lepton doublets. According to eq. 8.2.15 and eq. 8.2.18, the left-handed neutrinos transform in a different way to the left-handed charged leptons, breaking the $SU(2)_L$ symmetry. In the general case, "discrete unbroken generation symmetries (Abelian and non-Abelian) with the $SU(2)_L$ constraint...cannot generate tri-bimaximal mixing" [83], so that Higgs scalars with non-zero VEVs must be introduced into the framework of neutrino mass models.

8.2.3 Tetrahedral symmetry A_4

Assuming TBM, the neutrino mass matrix can be written as

$$M_\nu = U_{TBM} m_k \delta_{kj} U_{TBM}^T \tag{8.2.19}$$

which, combined with eq. 8.2.13 gives

$$M_\nu = \left[\frac{m_3}{2} \begin{pmatrix} 0 & 0 & 0 \\ 0 & 1 & -1 \\ 0 & -1 & 1 \end{pmatrix} + \frac{m_2}{3} \begin{pmatrix} 1 & 1 & 1 \\ 1 & 1 & 1 \\ 1 & 1 & 1 \end{pmatrix} + \frac{m_1}{6} \begin{pmatrix} 4 & -2 & -2 \\ -2 & 1 & 1 \\ -2 & 1 & 1 \end{pmatrix} \right]. \tag{8.2.20}$$

The eigenvalues of M_ν are m_1, m_2, m_3 with eigenvectors $(-2, 1, 1)/\sqrt{6}$, $(1, 1, 1)/\sqrt{3}$ and $(0, 1, -1)/\sqrt{2}$, respectively, and the simplicity of these column vectors motivates an underlying non-Abelian family symmetry. There have been many attempts in the literature to construct models of neutrino mass and mixing based on the non-Abelian group A_4, the tetrahedral group (as well as other flavour symmetries). The natural 3-dimensional representation (denoted by $\underline{3}$) makes A_4 a good candidate for describing the symmetry of the three families observed in Nature. In constructing a model, different types of particles are assigned to the irreducible representations of A_4, which are $\underline{1}$, $\underline{1}'$, $\underline{1}''$ and $\underline{3}$. The group multiplication rules and product composition rules dictate the form of the resulting Lagrangian, which in turn gives the structure of the neutrino and charged lepton mass matrices (see appendix).

Case study: The Altarelli-Feruglio A_4 model

In the original Altarelli-Feruglio model [[84], [85]], lepton doublets are assigned to the $\underline{3}$ representation, and right-handed lepton singlets to the $\underline{1}, \underline{1}'$ and $\underline{1}''$ representations. There are two SM Higgs doublets, which are invariant under A_4, along with two real triplets ϕ and ϕ', and a real singlet ξ, all three of which are gauge singlets. Using the A_4 multiplication rules, the Lagrangian of the Yukawa interactions in the lepton sector can be written as

$$\mathcal{L}_{\text{Yukawa}} = y_e e^c(\phi\ell) + y_\mu \mu^c(\phi\ell)'' + y_\tau \tau^c(\phi\ell)' + x_a \xi(\ell\ell) + x_d(\phi'\ell\ell) + h.c. + ... \quad (8.2.21)$$

where $(\underline{33})$ transforms as $\underline{1}$, $(\underline{33})'$ transforms as $\underline{1}'$, and $(\underline{33})''$ as $\underline{1}''$, and y_a, x_a and x_d are coupling constants. The notation in this Lagrangian is simplified (for instance $y_e e^c(\phi\ell)$ stands for $y_e e^c(\phi\ell)h_d/\Lambda$, $x_a\xi(\ell\ell)$ stands for $x_a\xi(\ell h_u \ell h_u)/\Lambda^2$ and so on). The dots stand for higher dimensional operators - in this model these are suppressed by additional powers of the cut-off Λ, as long as the VEVs are sufficiently smaller than Λ. For the model to work, the scalar fields must develop VEVs along the directions:

$$\langle\phi\rangle = (v, v, v) \quad \langle\phi'\rangle = (v', 0, 0) \quad \langle\xi\rangle = u \quad (8.2.22)$$

This vacuum alignment is crucial part of A_4 models: The realization of these specific alignments break the A_4 symmetry in the correct way, so that TBM is achieved. In general, corrections to the VEV alignment can come from higher order operators or the tree-level exchange of heavy fermions. Assuming the VEV alignment, the mass matrices M_l and M_ν for charged leptons and neutrino are

$$M_\ell = v_d \frac{v}{\Lambda} \begin{pmatrix} y_e & y_e & y_e \\ y_\mu & y_\mu\omega^2 & y_\mu\omega \\ y_\tau & y_\tau\omega & y_\tau\omega^2 \end{pmatrix} \quad (8.2.23)$$

$$M_\nu = \frac{v_u^2}{\Lambda} \begin{pmatrix} a & 0 & 0 \\ 0 & a & d \\ 0 & d & a \end{pmatrix} \quad (8.2.24)$$

where

$$a = x_a \frac{u}{\Lambda} \quad d = x_d \frac{v'}{\Lambda}. \quad (8.2.25)$$

The matrix diagonalizing the charged lepton mass matrix is

$$V_\ell = \frac{1}{\sqrt{3}} \begin{pmatrix} 1 & 1 & 1 \\ 1 & \omega^2 & \omega \\ 1 & \omega & \omega^2 \end{pmatrix} \quad (8.2.26)$$

which is the same as the matrix in eq. 8.2.16 (with a phase change). This similarity comes from the fact that C_3 is a subgroup of A_4. The charged fermion masses are:

$$m_e = \sqrt{3} y_e v_d \frac{v}{\Lambda} \quad m_\mu = \sqrt{3} y_\mu v_d \frac{v}{\Lambda} \quad m_\tau = \sqrt{3} y_\tau v_d \frac{v}{\Lambda} \quad (8.2.27)$$

To obtain the observed mass hierarchy among the masses in eq. 8.2.27, the authors introduce an additional $U(1)_F$ symmetry, which only affects the right-handed lepton sector. In the flavour basis, the neutrino mass matrix is

$$M_\nu^f = \frac{v_u^2}{\Lambda} \begin{pmatrix} a + 2d/3 & -d/3 & -d/3 \\ -d/3 & 2d/3 & a - d/3 \\ -d/3 & a - d/3 & 2d/3 \end{pmatrix} \quad (8.2.28)$$

which is diagonalized by the transformation

$$U^T M_\nu U = \frac{v_u^2}{\Lambda}\text{diag}(a+d, a, -a+d) \tag{8.2.29}$$

with $U = U_{\text{TBM}}$. Thus TBM is achieved. Since the first paper containing A_4 as the flavour symmetry, many authors have constructed models based on A_4 and many other flavour symmetries. The model presented above is a simple case of the application of A_4 to neutrino mixing, and this can be extended to more elaborate models.

8.3 Comparison between flavour symmetries

Flavour symmetries construct the neutrino mixing matrix. This gives octant sensitivity by implementing various symmetries. These models implemented in the simulations were found in [86] and randomly on the Internet. They are listed in table 8.3.1.

Original was [86] an overview of models which predicted $\sin^2(\theta_{13})$ from various flavour symmetries and a lot of these models have been excluded since this mixing parameter is now known. The article [86] had original 86 models whereas 55 of these models have been excluded by the measurement of $\sin^2(\theta_{13})$ by more than 3σ. Additionally 4 models are nearly within the 3σ range of $\sin^2(\theta_{13})$ from a global fit result. However, only 10 models from [86] can be used in this thesis since not all models gives their preference of octant. More models have been found on the Internet which is also listed together with the other 10 models from [86]. Additional models besides the 14 listed in table **??** are found, however they all state that they can accommodate the current results from the neutrino mixing matrix. A simulation based on the current neutrino mixing matrix is given in the previous chapter, which is why they are not included in this analysis. This thesis is limited on time, which is the reason it does not include each and every flavour model.

The table 8.3.1 is divided into various columns with numbers, names and mixing parameters shown in the top. First is given a specific number to each flavour symmetry making it easier to distinguish between each model when looking at the figures showing the octant sensitivity. The next column is the actual flavour symmetry for that model and thereafter are the various predictions of mixing parameters for the flavour symmetries. The mass square differences are taken from global fits. Most models can only be realized with normal hierarchy compared to inverted hierarchy. However, there are also models which can be realized with both spectrums and models with no preference stated.

In the table there is also shown a star (*) and a dagger (†) symbol. The value of the oscillation parameter which have a * is near the outer value of the 3σ range of the global fit. So this value can still be used as an oscillation parameter since it should have the benefit of the doubt when it comes to global fits (in one global fit it is out of the 3σ band and in another global fit it is within the 3σ band). The † on the other hand means that the range listed in the table of some specific oscillation parameter contains the 3σ range and beyond from the global fit. In this case the oscillation parameter will be constrained to the 3σ range of the global fit. Global fits of neutrino oscillation data can be found here [87] and here [88].

With these models listed, they are implemented in the simulations and the octant sensitivities are shown in the plots 8.3.1 and 8.3.2. First a description of the plots itself. They are divided into two groups; one only for normal hierarchy and one for inverted hierarchy. The 4 plots in each group are given by the combination of resolution functions, so upper left (upper right) has $\sigma_E = 0.2E'_{\text{GeV}}$ and $\sigma_\theta = 0.5\sqrt{1\text{GeV}/E'_{\text{GeV}}}$ rad ($\sigma_E = 0.2E'_{\text{GeV}}$ and $\sigma_\theta = \sqrt{1\text{GeV}/E'_{\text{GeV}}}$ rad) whereas the lower left (lower right) has $\sigma_E = 2$

GeV and $\sigma_\theta = 0.5\sqrt{1\text{GeV}/E'_{\text{GeV}}}$ rad ($\sigma_E = 2$ GeV and $\sigma_\theta = \sqrt{1\text{GeV}/E'_{\text{GeV}}}$ rad). In the plot legend, each number listed on the left side of the flavour symmetry is also the number for each flavour symmetry listed in table 8.3.1. On the right side of each flavour symmetry is written a scaling factor The reason for this is simply to give a better view of the result, else all the various fits would have lied on top of each other. However, this scaling can be deceiving since the scaling factor makes either a smaller (if scaling factor is less than one) or a larger (if scaling factor is larger than one) separation than it is in reality. The scaling factors have been kept fixed through the various four plots as the resolution functions worsen. This is to see how the sensitivity changes as the resolution functions worsen without changing the scaling factor. If both the resolution functions and the scaling factor were changed, there would be no chance to determine if the reduction of the sensitivity came from the scaling factor or the worsening of the resolution functions. With the scaling factors kept fixed, the reduction of the sensitivity would be read of the plots 8.3.1 and 8.3.2 as the resolution functions worsened.

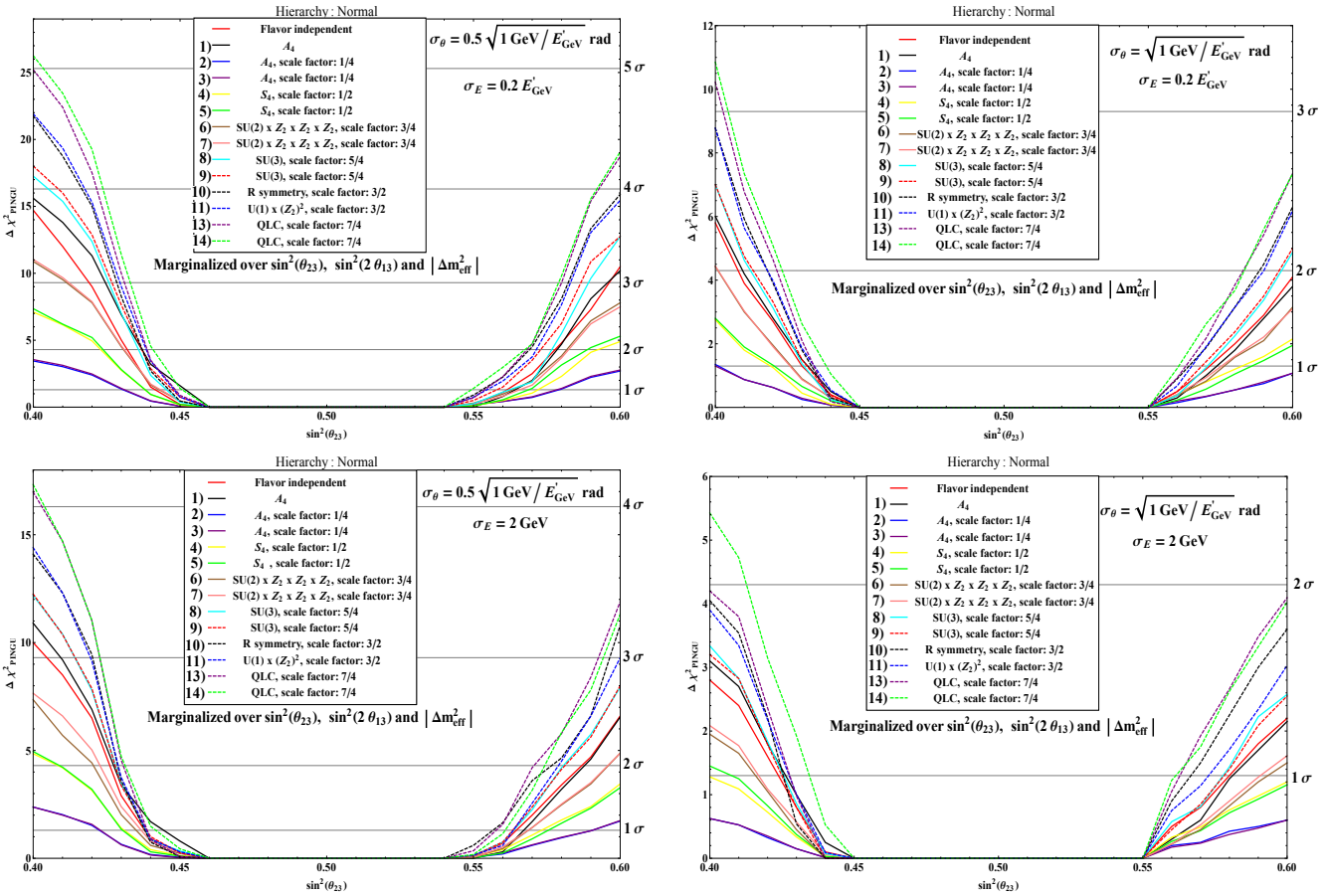

Figure 8.3.1: *$\Delta\chi^2$ for the wrong octant obtained from the PINGU data with 3 years statistics for various flavour symmetries. Mass spectrum is assumed to be normal. See appendix for larger versions.*

The one called "flavour independent" is the fit from the plots 7.9.1 in the previous chapter (the ones with the new systematic uncertainty) and shows the gain or reduction of octant sensitivity in comparison. The hierarchy is kept fixed throughout the simulations since it is believed that the hierarchy is already known at the time when the octant determination is realized. An estimation of the determination of the neutrino mass hierarchy is that it scales with number of years, so for 3 (5) years of data gives ~ 3 (~ 5) σ

C.L. [[60], [62]]. Also seen in the plots is that the "valley" becomes larger as the resolution functions worsen, so less phase space is probed.

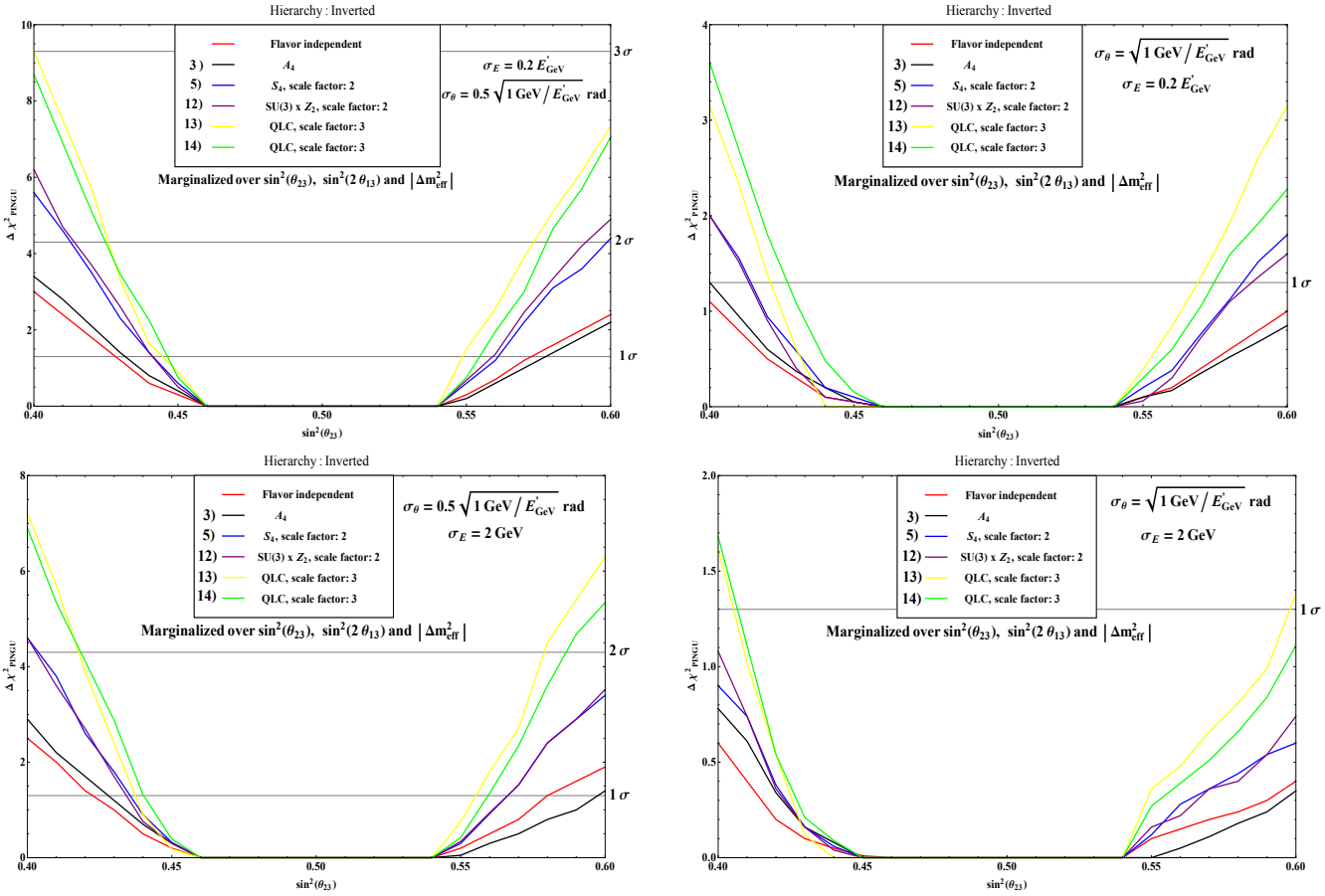

Figure 8.3.2: *$\Delta\chi^2$ for the wrong octant obtained from the PINGU data with 3 years statistics for various flavour symmetries. Mass spectrum is assumed to be inverted. See appendix for larger versions.*

8.4 Flavour symmetry comparison over multiple of years

From figures 8.3.1 and 8.3.2 can be seen that there is no significance between the various models with 3 years of data. In this section, the simulations will be made over multiple years, namely 5, 10 and 15 years after which a comparison will be made. At some point there will be a difference between the various flavour symmetries.

A qualified guess for the operational time for PINGU is 15-20 years. After it is installed, it only need fuel to keep it going. There is no physical reason why PINGU will cease to operate. The digital optical module (DOM) failure rate is exceptionally low, and the ice drifts uniformly such that there is no fear of cable shear during operation. This is the reason the simulations have been made for 15 years as the maximum of operational years. In principle it would only stop if it is not efficiently enough, there were no more science for it to probe or due to economy.

This simulation is done for fixed resolution functions, namely $\sigma_E = 0.2E'_{\mathrm{GeV}}$ and $\sigma_\theta = 0.5\sqrt{1\mathrm{GeV}/E'_{\mathrm{GeV}}}$ which is the resolution function used by the IceCube collaboration [[15], [62]]. The plots are shown the following way: In the top left corner, there is the plot with 3 years of statistics whereas in the top right corner, it has been made for 5 years

No.	Flavour symmetry	Hierarchy	$\sin^2(\theta_{23})$	$\sin^2(\theta_{12})$	$\sin^2(\theta_{13})$
1	A_4 [89]	NH	0.51-0.56	0.31	0.0026-0.034†
2	A_4 [90]	NH	0.42	0.35	0.017
3	A_4 [91]	NH or IH	0.371-0.456(NH) $\otimes$ 0.604-0.671*(IH)	0.27-0.37	0.016-0.027
4	S_4 [92]	NH	0.41-0.5	0.311	<0.030
5	S_4 [93]	NH or IH	(0.441 or 0.559)(NH) or (0.401 or 0.599)(IH)	0.329	0.025
6	SU(2) x Z_2 x Z_2 x Z_2 [94]	NH	0.51	0.26	0.014*
7	SU(2) x Z_2 x Z_2 x Z_2 [95]	NH	0.53	0.29	0.012*
8	SU(3) [96]	NH	0.44-0.56	0.29-0.38	0.024
9	SU(3) [97]	NH	0.5-0.51	0.26-0.28	0.0009-0.016*
10	R symmetry [98]	NH	0.44	0.31	0.0001-0.04†
11	U(1) x $(Z_2)^2$ [99]	NH	0.49	0.29	0.019
12	SU(3) x Z_2 [100]	IH	0.47	0.31	0.012*
13	QLC [101]		0.446	0.336	0.023
14	QLC [102]		0.378-0.388 $\otimes$ 0.612-0.623	0.194-0.5†	0.024-0.028

Table 8.3.1: *Flavour models used in simulations.*

of data. In the bottom left corner, it is 10 years of data and next to it is with 15 years of data. Again the number in the plot legend is also the number shown in table 8.3.1. The resolution functions are given in the top right corner for each plot. We keep the test hierarchy fixed to the true hierarchy displayed in the top of each plot.

Two features can be seen from the plots. First, the separation between each flavour symmetry becomes larger, meaning it will be easier to distinguish between them. As more and more years of data is included, less and less models need a scaling factor. Second, more phase space is probed for the atmospheric angle. The "valley" around $\sin^2(\theta_{23}) = 0.5$ becomes smaller as more data is included. This comes from a bigger seperation of event rates for the individual χ^2 when taking the difference between χ^2(NH)

and χ^2(IH). Including T2K and NOvA would greatly enhance the sensitivity to the octant since they both depend on the atmospheric angle θ_{23} and have sensitivity to its octant. Additional data from the reactor experiments would constrain Δm^2_{eff} which in turn would give a higher octant sensitivity and more phase space would be probed.

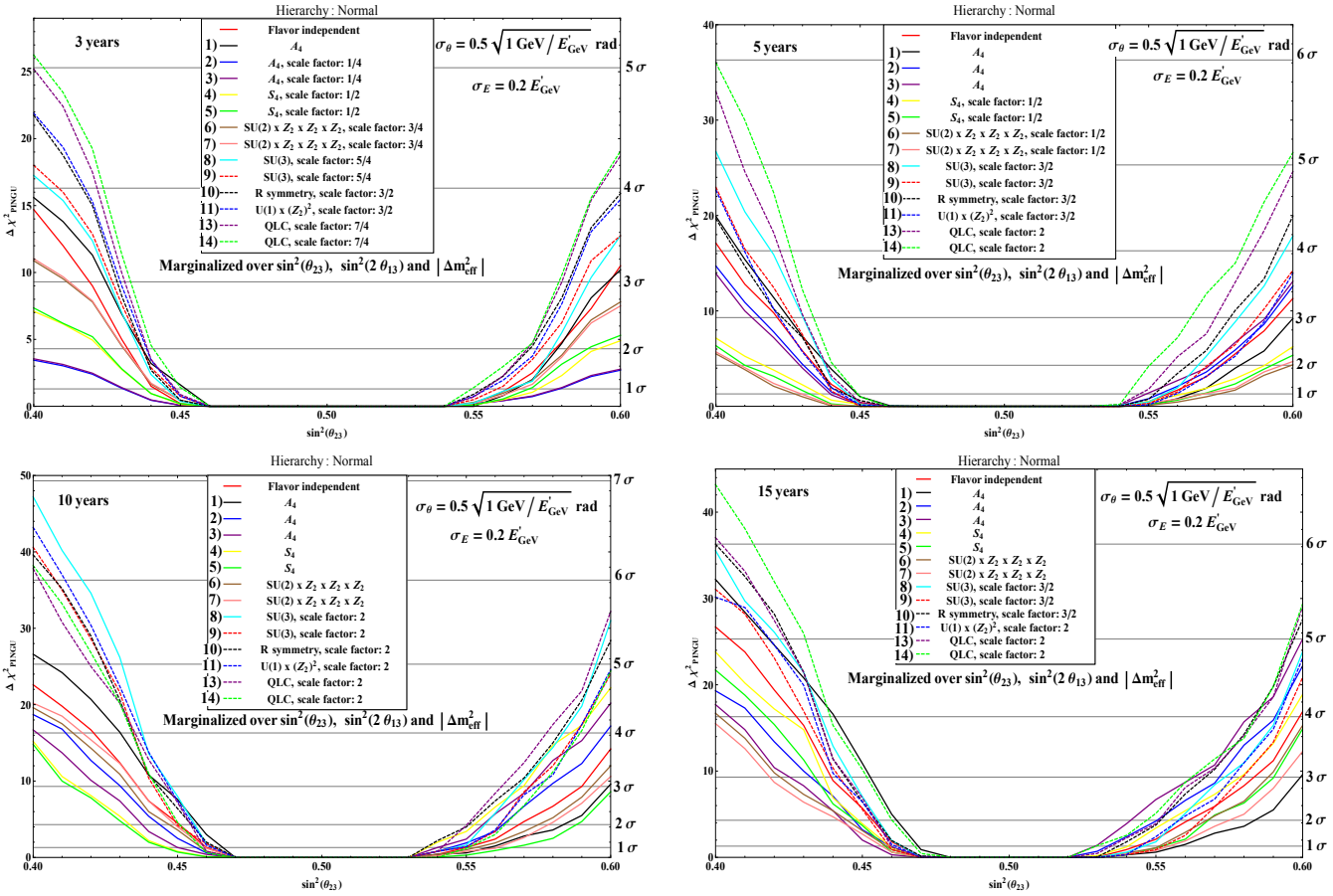

Figure 8.4.1: *$\Delta\chi^2$ for the wrong octant obtained from the PINGU data over multiple years (indicated in the left corner) for various flavour symmetries. Mass spectrum is assumed to be normal. See appendix for larger versions.*

As can be seen from the figures with 15 years of data, the "flavour independent" fit can reach above 4σ for $\sin^2(\theta_{23}) < 0.429$ and $\sin^2(\theta_{23}) > 0.599$ for normal hierarchy and 2σ for $\sin^2(\theta_{23}) < 0.415$ and $\sin^2(\theta_{23}) > 0.59$. For the flavour symmetries there are different output of confidence level depending on the true octant for the flavour symmetries. Some are above or below the "flavour independent", meaning that if it is below (above) the "flavour independent", it prefers a mixing angle θ_{23} in the first (second) octant. If it is only below, it prefers an octant sensitivity in the "valley" and the sensitivity is washed out. However, if it is above, it prefers an octant outside of the range [0.4-0.6].

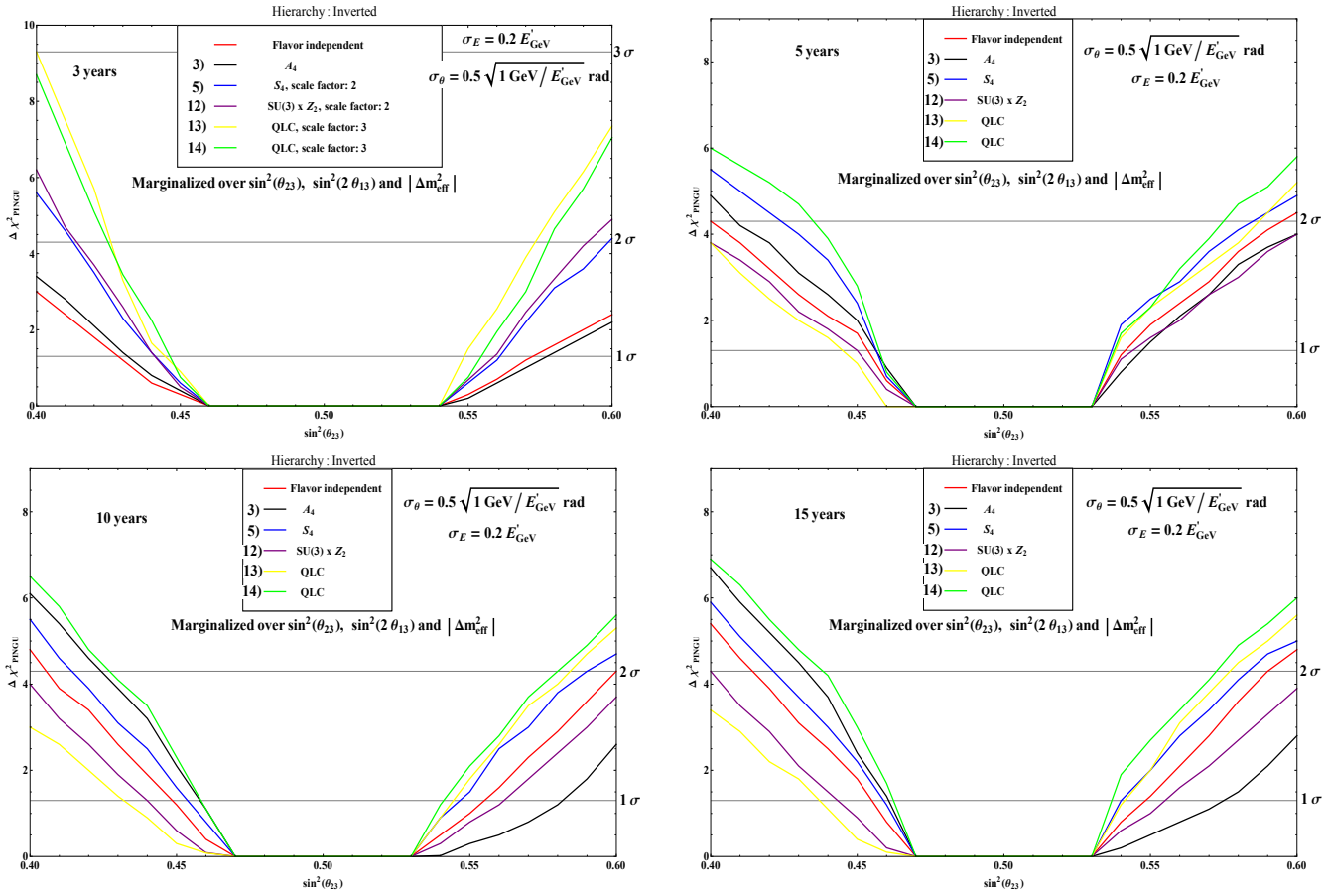

Figure 8.4.2: *$\Delta\chi^2$ for the wrong octant obtained from the PINGU data over multiple years (indicated in the left corner) for various flavour symmetries. Mass spectrum is assumed to be inverted. See appendix for larger versions.*

9

Conclusion

Since the first postulation of their existence in 1930 by Pauli, the field of neutrino physics has raised many interesting and fundamental questions. However, experiments dealing with almost non-interacting particles are naturally difficult to carry out. If neutrinos acquire their masses through new physics at some very high energy scale, as in the see-saw mechanism, this also raises big challenges for neutrino experiments. Theory must rely on very little experimental data and not many constraints can be imposed when carrying out model building. However, the many unknown aspects and the lack of hard data allow for greater liberty and creativity when working in this field.

PINGU has great potential resolve various important physics questions. This thesis focusses on the determination of the θ_{23} octant and the level of confidence depends on the resolution functions, statistics and hierarchy. With 3 years of data, PINGU is capable of determining the wrong octant at ~ 3 (~ 2) σ for normal (inverted) hierarchy, depending on the resolution functions. A careful look was also taken at the systematic uncertainties and their influence on the sensitivity to the octant determination. Two of the five uncertainties had the most influence on the sensitivity, namely those concerning the arrival angle and energy dependence of the atmospheric neutrino flux. These are the most important to control if a high significance is required. A further insight to the sensitivity to the wrong octant came from consideration of the systematic uncertainty in particle identification.

Following this analysis, a look was taken at various flavour symmetries which can realize the neutrino mixing matrix. By implementing the different flavour symmetries gave the sensitivity for each flavour symmetry to the wrong octant was obtained. With just 3 years of data, there is no significant difference between the various flavour symmetries so one cannot distinguish between the various models. With more data however, the difference between the various models becomes measurable. So PINGU can in principle constrain flavour models in future.

As is also mentioned in the thesis, the octant sensitivity can be increased through the introduction of more data from other experiments, including more information from the PINGU detector, changing the shape and values of the resolution functions, etc.

There are other ways to constrain flavour symmetries. One could have an analysis which looked at multiple (un)known neutrino oscillation parameters and see how they complement each other in this regard. However, there is still a long way to go to achieve the same precision of the mixing parameters as in the quark sector. This would ultimately lead us to the true mechanism behind neutrino mixing.

Appendices

A

Plots of octant sensitivity

These images are the same as figures 7.7.1, only larger versions for readable purpose.

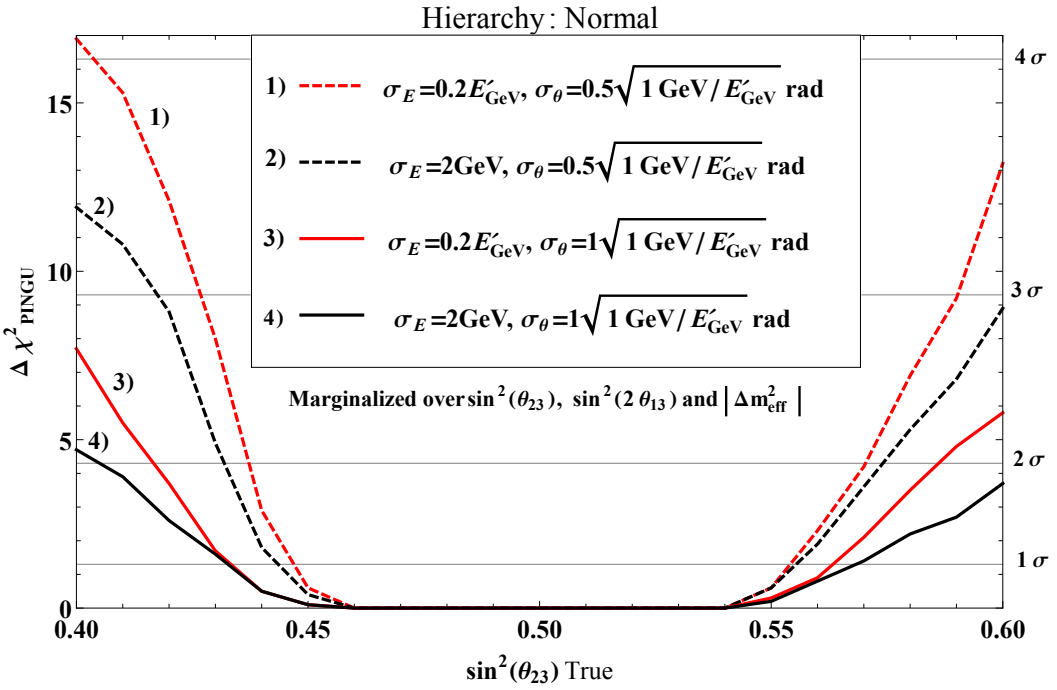

Figure 1.0.3: *$\Delta\chi^2$ for the wrong octant obtained from PINGU data with 3 years statistics, as a function of $\sin^2(\theta_{23})$(true). This plot is for normal hierarchy taken as true and χ^2 is varied over the oscillation parameters, $|\Delta m^2_{eff}|$ and $\sin^2(2\theta_{13})$ in the allow range given in table 7.2.1 and $\sin^2(\theta_{23})$ in interval [0.4-0.6], but the mass hierarchy is held fixed to the assumed true case in the fit. The four lines are for the four possible combinations for the choices of the energy and angle resolution of PINGU.*

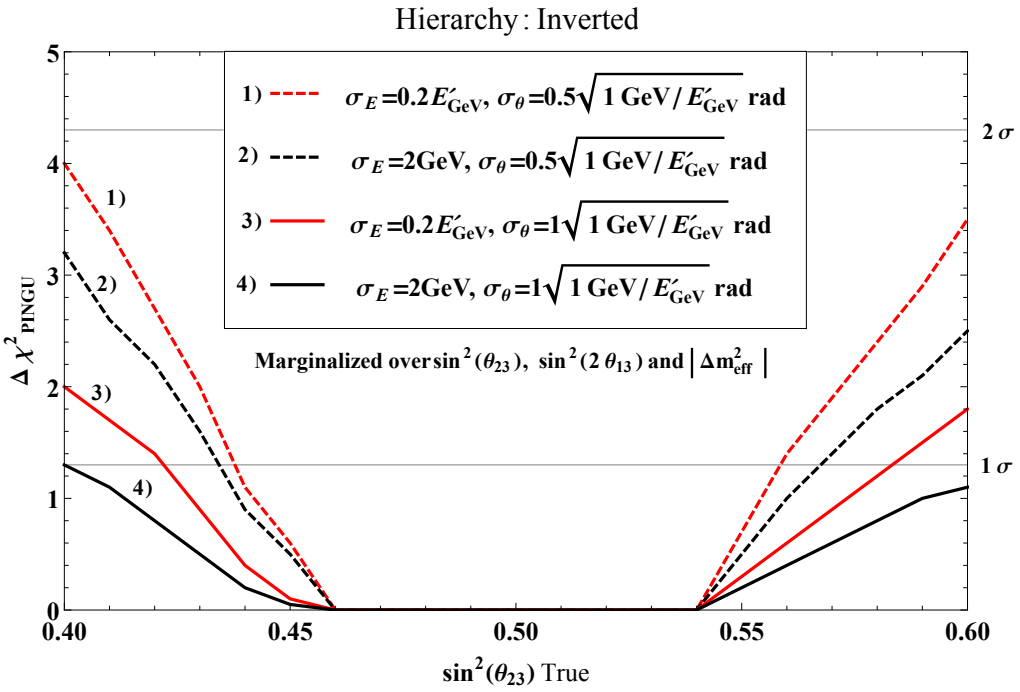

Figure 1.0.4: *The same as 1.0.3, but the true hierarchy is inverted.*

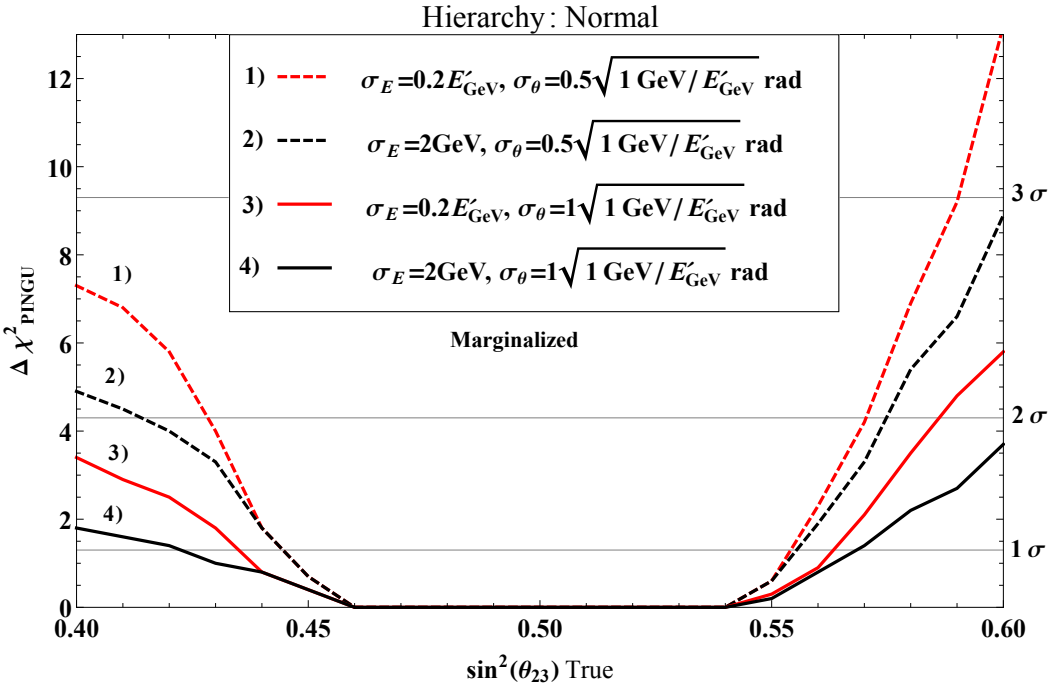

Figure 1.0.5: *The same as 1.0.3, but the* χ^2 *is not only varied over* $|\Delta m^2_{eff}|$, $\sin^2(2\theta_{13})$ *and* $\sin^2(\theta_{23})$, *but also keeping the mass hierarchy free in the fit.*

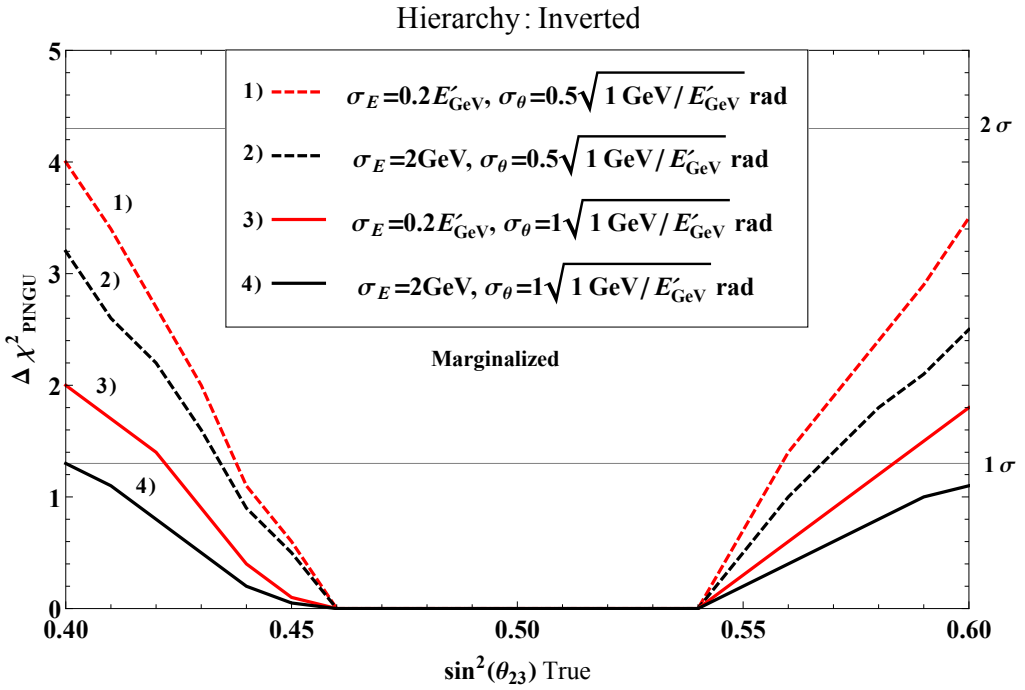

Figure 1.0.6: *The same as 1.0.5, just for inverted hierarchy.*

B

Plots of systematic uncertainties

These images are the same as figures 7.8.1, only larger versions for readable purpose.

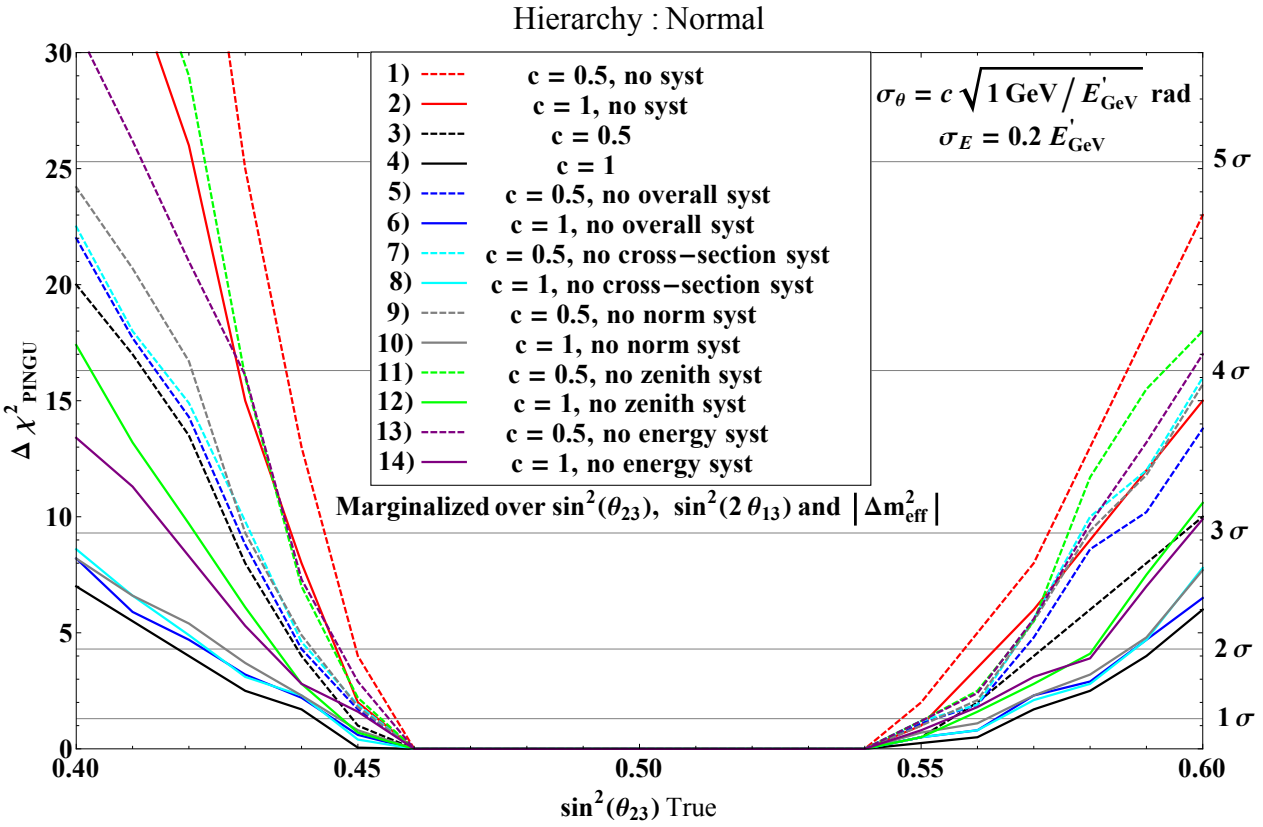

Figure 2.0.7: *Impact of systematic uncertainties on the $\Delta\chi^2$ for the wrong octant obtained from PINGU data with 3 years statistics, as a function of $\sin^2(\theta_{23})$. The assumption of the width of the resolution functions are shown in the figure legend. The test hierarchy is kept fixed at the true value for all cases whereas we vary over $|\Delta m^2_{\mathrm{eff}}|$, $\sin^2(\theta_{23})$ and $\sin^2(2\theta_{13})$. This particular plot has $\sigma_E = 0.2E'$ and $\sigma_\Theta = c\sqrt{1\,GeV/E'_{GeV}}$ where c is given in plot legend.*

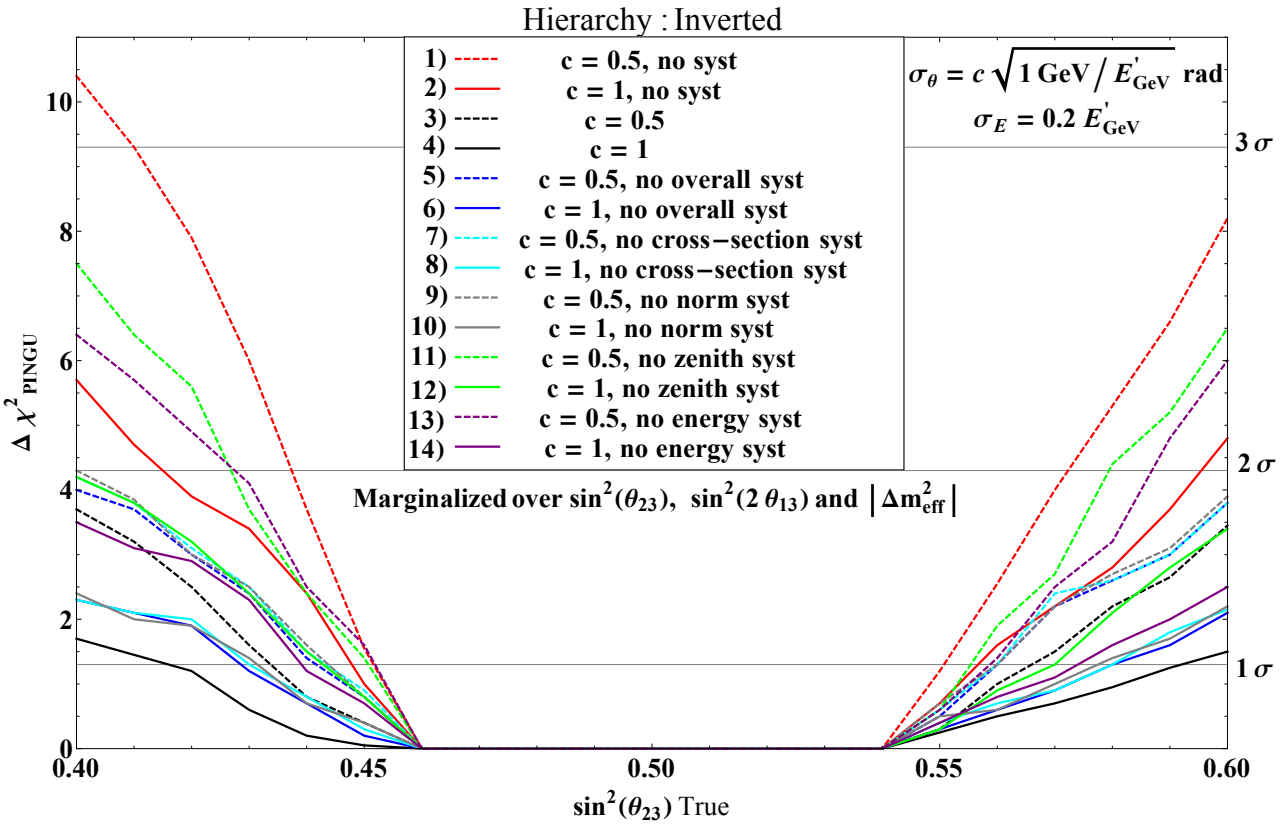

Figure 2.0.8: *Same plot as 2.0.7, but for inverted hierarchy.*

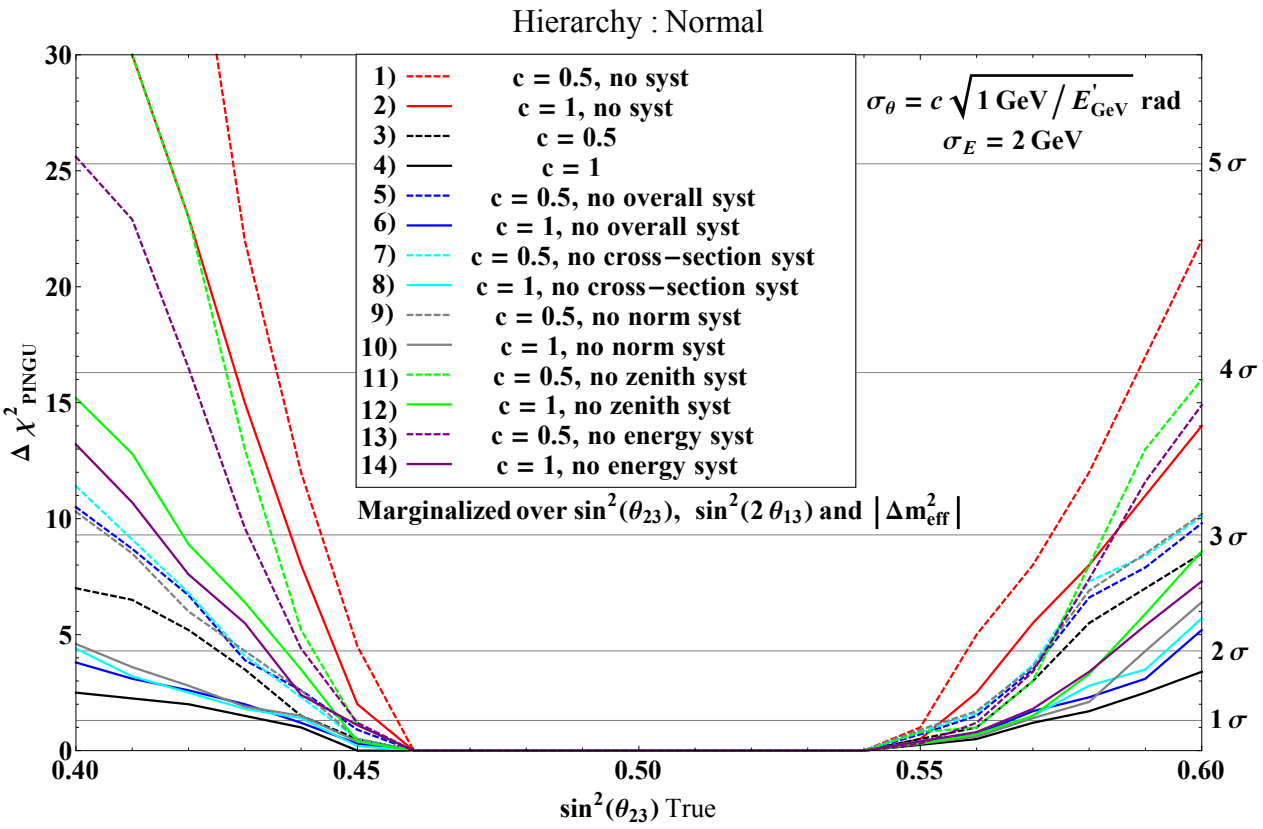

Figure 2.0.9: *Same plot as 2.0.7, but has* $\sigma_E = 2\,GeV$.

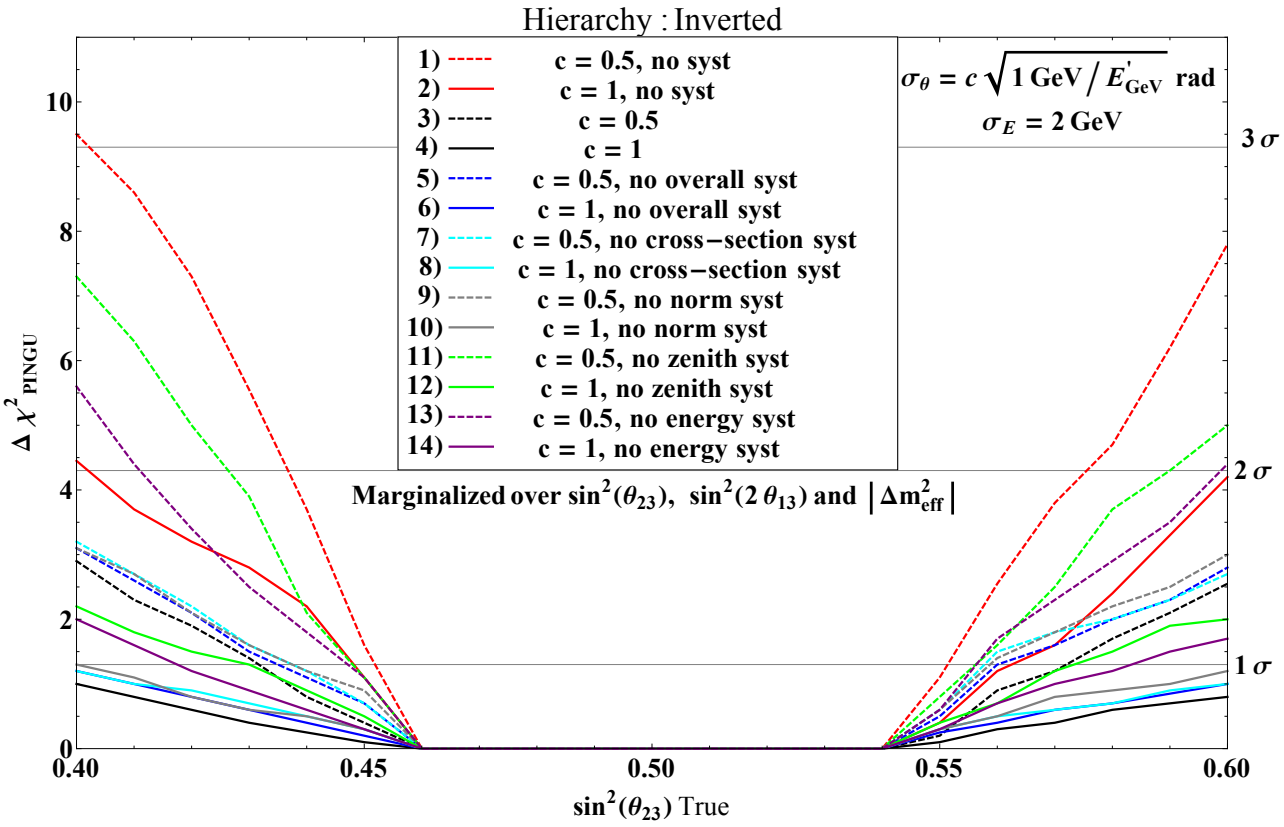

Figure 2.0.10: *Same plot as 2.0.9, but for inverted hierarchy.*

C

Plots including particle identification uncertainty

These images are the same as figures 7.9.1, only larger versions for readable purpose.

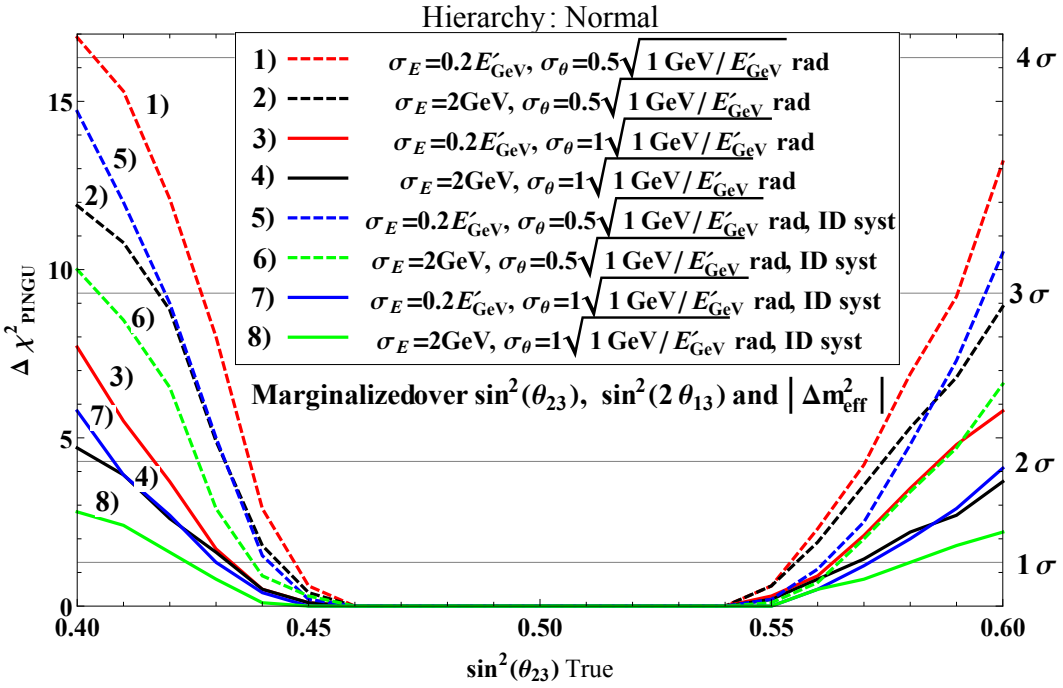

Figure 3.0.11: *$\Delta\chi^2$ for the wrong octant obtained from PINGU data with 3 years statistics, as a function of $\sin^2(\theta_{23})$(true). This plot is for normal hierarchy taken as true and χ^2 is varied over the oscillation parameters, $|\Delta m^2_{eff}|$ and $\sin^2(2\theta_{13})$ in the allow range given in table 7.2.1 and $\sin^2(\theta_{23})$ in interval [0.4-0.6], but the mass hierarchy is held fixed to the assumed true case in the fit. The four lines are for the four possible combinations for the choices of the energy and angle resolution of PINGU.*

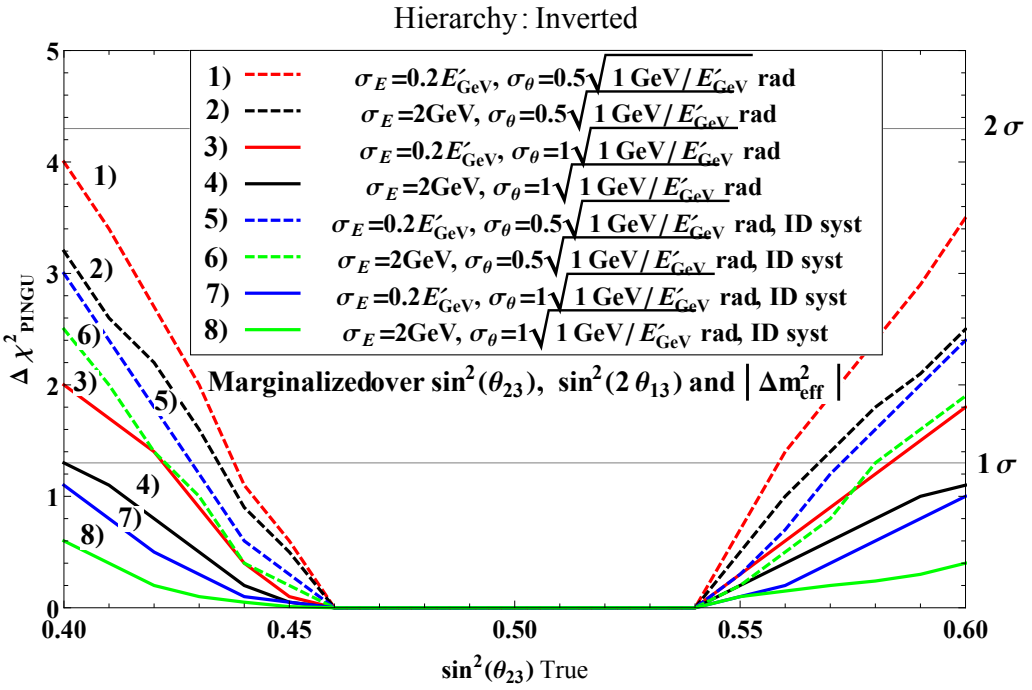

Figure 3.0.12: *The same as 3.0.11, but the true hierarchy is inverted.*

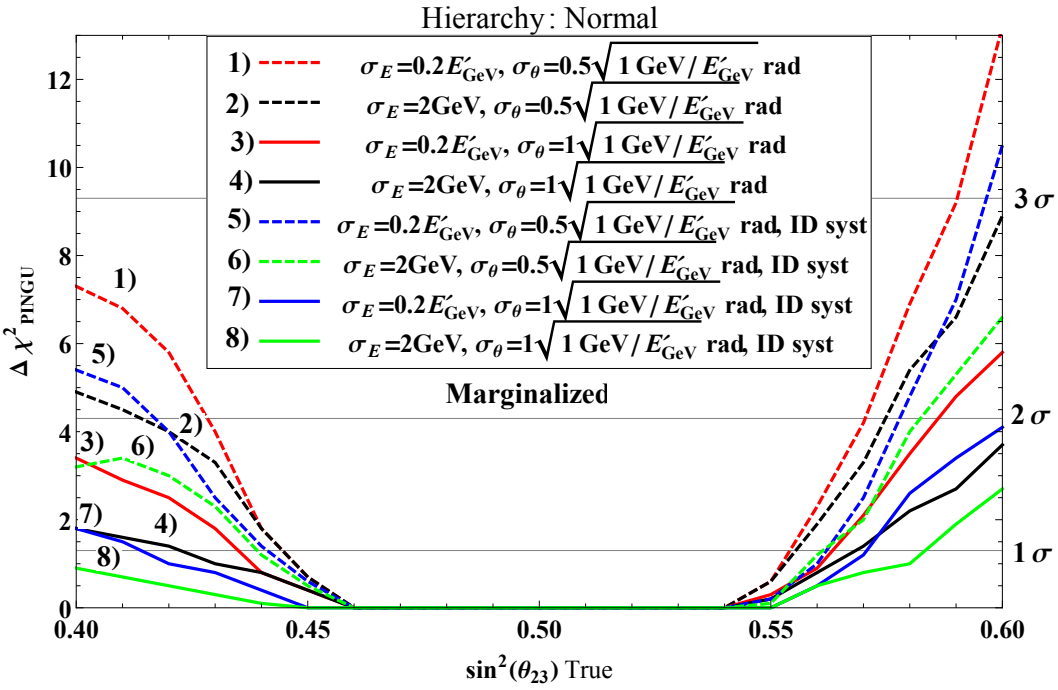

Figure 3.0.13: *The same as 3.0.11, but the* χ^2 *is not only varied over* $|\Delta m^2_{eff}|$, $\sin^2(2\theta_{13})$ *and* $\sin^2(\theta_{23})$, *but also keeping the mass hierarchy free in the fit.*

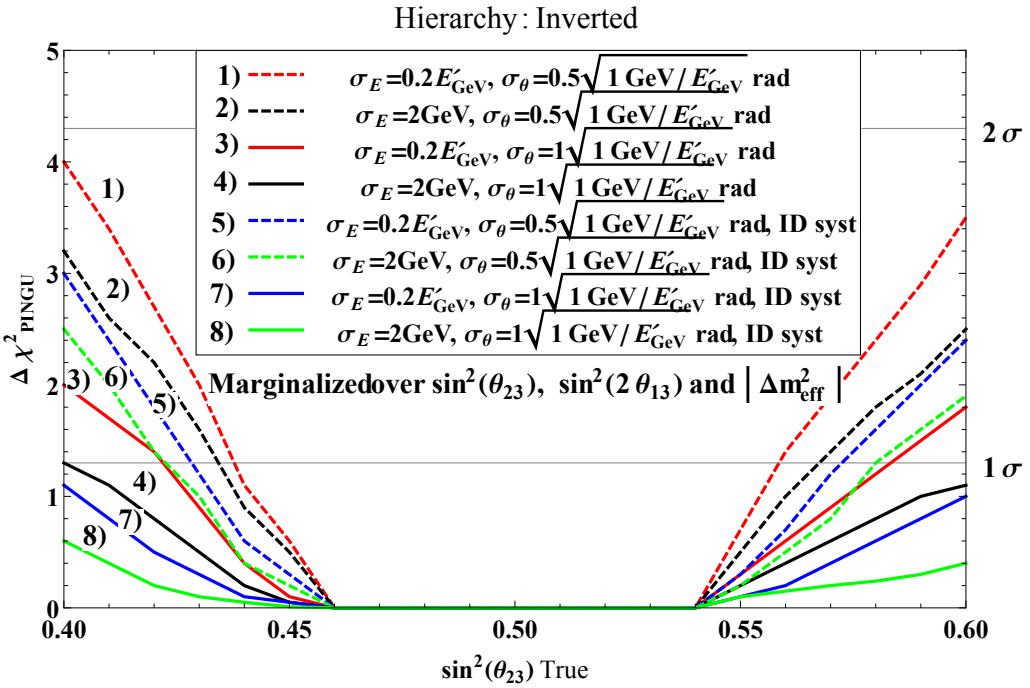

Figure 3.0.14: *The same as 3.0.13, just for inverted hierarchy.*

D

Introduction to A_4

The following is an outline of the A_4 symmetry group [81]

This group is the alternating group of order 4, and is also the group of all even permutations of four objects, isomorphic to the group of rotational symmetries of the regular tetrahedron. It is a finite, non-Abelian subgroup of SO(3) and SU(3). A_4 has 12 elements, which can be divided into 4 conjugacy classes with membership 1, 3, 4 and 4. The dimensionality theorem implies that there are 4 irreducible representations with dimension d_j such that $\sum_j d_j^2 = 12$. The only solution is $d_1 = d_2 = d_3 = 1$ and $d_4 = 3$, and the representations are labeled as $\underline{1}$, $\underline{1}'$, $\underline{1}''$ and $\underline{3}$, which means that there are three one-dimensional representations and one three-dimensional representation. The character table of A_4 is given by with $\omega = e^{2\pi i/3}$ and $\omega^2 = e^{-2\pi i/3}$. There are two bases for A_4

Class	$1C^1$	$2C^4$	$3C^4$	$4C^3$
$\chi^{[\underline{1}]}$	1	1	1	1
$\chi^{[\underline{1}']}$	1	ω	ω^2	1
$\chi^{[\underline{1}'']}$	1	ω^2	ω	1
$\chi^{[\underline{3}]}$	3	0	0	-1

Table 4.0.1: *Character table of the group A_4*

commonly used in lepton symmetry models: The Ma-Rajasekaran basis and the Altarelli-Feruglio basis. The former basis is generated by two basic permutations S and T, given by $S = (4321)$ and $T = (2314)$, where the generic permutation $(1, 2, 3, 4) \to (n_1, n_2, n_3 n_4)$ is denoted by $(n_1 n_2 n_3 n_4)$. It follows that

$$S^2 = T^3 = (ST)^3 = 1 \tag{4.0.1}$$

which defines the presentation of the group. The one-dimensional unitary representations are generated by

$$\underline{1}: \quad S = 1 \quad T = 1 \tag{4.0.2}$$

$$\underline{1}': \quad S = 1 \quad T = \omega \tag{4.0.3}$$

$$\underline{1}'': \quad S = 1 \quad T = \omega^2 \tag{4.0.4}$$

and the three-dimensional unitary representation is given by

$$S = \begin{pmatrix} 1 & 0 & 0 \\ 0 & -1 & 0 \\ 0 & 0 & -1 \end{pmatrix}, \quad T = \begin{pmatrix} 0 & 1 & 0 \\ 0 & 0 & 1 \\ 1 & 0 & 0 \end{pmatrix}. \tag{4.0.5}$$

The 3×3 matrices of the natural three-dimensional representation $\underline{3}$ are

$$C_1: \quad \begin{pmatrix} 1 & 0 & 0 \\ 0 & 1 & 0 \\ 0 & 0 & 1 \end{pmatrix} \tag{4.0.6}$$

$$C_2: \quad \begin{pmatrix} 0 & 0 & 1 \\ 1 & 0 & 0 \\ 0 & 1 & 0 \end{pmatrix}, \quad \begin{pmatrix} 0 & 0 & 1 \\ -1 & 0 & 0 \\ 0 & -1 & 0 \end{pmatrix}, \quad \begin{pmatrix} 0 & 0 & -1 \\ 1 & 0 & 0 \\ 0 & -1 & 0 \end{pmatrix}, \quad \begin{pmatrix} 0 & 0 & -1 \\ -1 & 0 & 0 \\ 0 & 1 & 0 \end{pmatrix} \tag{4.0.7}$$

$$C_3: \quad \begin{pmatrix} 0 & 1 & 0 \\ 0 & 0 & 1 \\ 1 & 0 & 0 \end{pmatrix}, \quad \begin{pmatrix} 0 & 1 & 0 \\ 0 & 0 & -1 \\ -1 & 0 & 0 \end{pmatrix}, \quad \begin{pmatrix} 0 & -1 & 0 \\ 0 & 0 & 1 \\ -1 & 0 & 0 \end{pmatrix}, \quad \begin{pmatrix} 0 & -1 & 0 \\ 0 & 0 & -1 \\ 1 & 0 & 0 \end{pmatrix} \tag{4.0.8}$$

$$C_4: \quad \begin{pmatrix} 1 & 0 & 0 \\ 0 & -1 & 0 \\ 0 & 0 & -1 \end{pmatrix}, \quad \begin{pmatrix} -1 & 0 & 0 \\ 0 & 1 & 0 \\ 0 & 0 & -1 \end{pmatrix}, \quad \begin{pmatrix} -1 & 0 & 0 \\ 0 & -1 & 0 \\ 0 & 0 & 1 \end{pmatrix} \tag{4.0.9}$$

where each matrix is a product of the generators S and T. It is evident that the characters of the $\underline{3}$ representation are simply the traces of the matrices in each class. The multiplication rules are given by

$$\underline{1} \times \underline{1} = \underline{1} \tag{4.0.10}$$

$$\underline{1}' \times \underline{1}'' = \underline{1} \tag{4.0.11}$$

$$\underline{1}'' \times \underline{1}' = \underline{1} \tag{4.0.12}$$

$$\underline{1}' \times \underline{1}' = \underline{1}'' \tag{4.0.13}$$

$$\underline{1}'' \times \underline{1}'' = \underline{1}' \tag{4.0.14}$$

$$\underline{3} \times \underline{3} = \underline{1} + \underline{1}' + \underline{1}' + \underline{3}_{as} + \underline{3}_s \tag{4.0.15}$$

where $\underline{3}_{as}$ and $\underline{3}_s$ are asymmetric and symmetric combinations respectively. If $\underline{3}_a \sim (a_1, a_2, a_3)$ and $\underline{3}_b \sim (b_1, b_2, b_3)$ are two triplets transforming by the matrices in eq. 4.0.9, then the three singlets and two triplets in the product of equations 4.0.10-4.0.15 are:

$$\underline{1} = a_1 b_1 + a_2 b_2 + a_3 b_3 \tag{4.0.16}$$

$$\underline{1}' = a_1 b_1 + \omega^2 a_2 b_2 + \omega_3 b_3 \tag{4.0.17}$$

$$\underline{1}'' = a_1 b_1 + \omega a_2 b_2 + \omega^2 a_3 b_3 \tag{4.0.18}$$

$$\underline{3}_1 \sim (a_2 b_3, a_3 b_1, a_1 b_2) \tag{4.0.19}$$

$$\underline{3}_2 \sim (a_3 b_2, a_1 b_3, a_2 b_1) \tag{4.0.20}$$

This was the Ma-Rajasekaran basis where the generator S is diagonal. However, one can also represent A_4 in a basis where T is diagonal, obtained through the unitary transformation

$$T' = V^\dagger T V = \begin{pmatrix} 1 & 0 & 0 \\ 0 & \omega & 0 \\ 0 & 0 & \omega^2 \end{pmatrix} \tag{4.0.21}$$

$$S' = V^\dagger S V = \frac{1}{3}\begin{pmatrix} -1 & 2 & 2 \\ 2 & -1 & 2 \\ 2 & 2 & -1 \end{pmatrix} \tag{4.0.22}$$

where

$$V = \frac{1}{\sqrt{3}}\begin{pmatrix} 1 & 1 & 1 \\ 1 & \omega & \omega^2 \\ 1 & \omega^2 & \omega \end{pmatrix}. \tag{4.0.23}$$

Note that the matrix V is the so-called "magic matrix", which appears in A_4 models as the unitary matrix that diagonalizes the charged lepton mass matrix. In the S', T' basis, the multiplication rules are identical to those in equations 4.0.10-4.0.15, but the product of two triplets gives the composition of the following irreducible representations:

$$\underline{1} = a_1 b_1 + a_2 b_3 + a_3 b_2 \tag{4.0.24}$$

$$\underline{1}' = a_3 b_3 + a_1 b_2 + a_2 b_1 \tag{4.0.25}$$

$$\underline{1}'' = a_2 b_2 + a_1 b_3 + a_3 b_1 \tag{4.0.26}$$

$$\underline{3}_s \sim \frac{1}{3}(2a_1 b_1 - a_2 b_3 - a_3 b_2, 2a_3 b_3 - a_1 b_2 - a_2 b_1, 2a_2 b_2 - a_1 b_3 - a_3 b_1) \tag{4.0.27}$$

$$\underline{3}_{as} \sim \frac{1}{3}(a_2 b_3 - a_3 b_2, a_1 b_2 - a_2 b_1, a_1 b_3 - a_3 b_1) \tag{4.0.28}$$

E

Plots of flavour symmetries

These images are the same as figures 8.3.1 and 8.3.2, only larger versions for readable purpose.

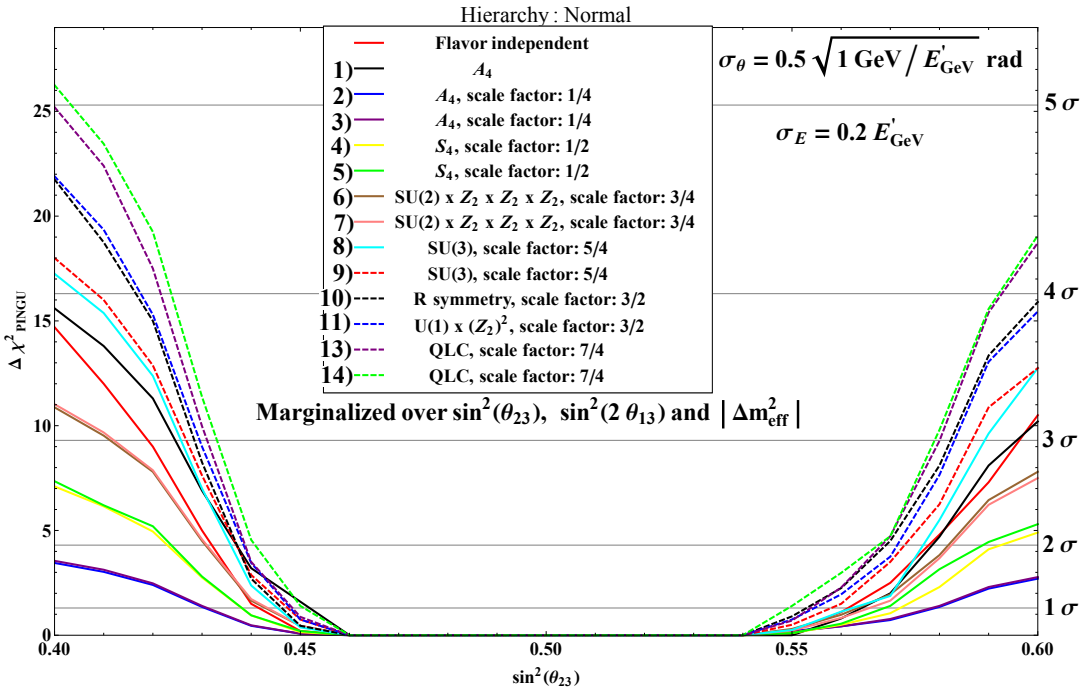

Figure 5.0.15: *$\Delta\chi^2$ for the wrong octant obtained from PINGU data with 3 years statistics for various flavour symmetries, as a function of* $\sin^2(\theta_{23})$*. This plot is for normal hierarchy taken as true and* χ^2 *is varied over the oscillation parameters,* $|\Delta m^2_{eff}|$ *and* $\sin^2(2\theta_{13})$ *in the allow range given in table 7.2.1 and* $\sin^2(\theta_{23})$ *in interval [0.4-0.6], but the mass hierarchy is held fixed to the assumed true case in the fit. The specific resolution functions are shown in the right corner.*

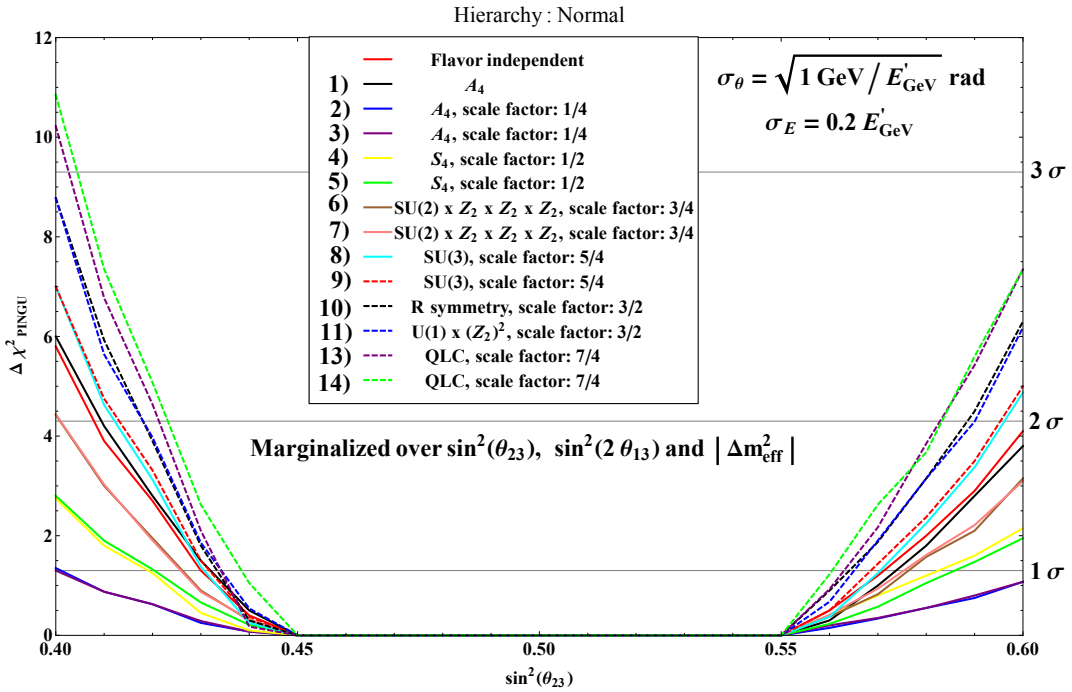

Figure 5.0.16: *Same as 5.0.15, but with a worsen angular resolution function.*

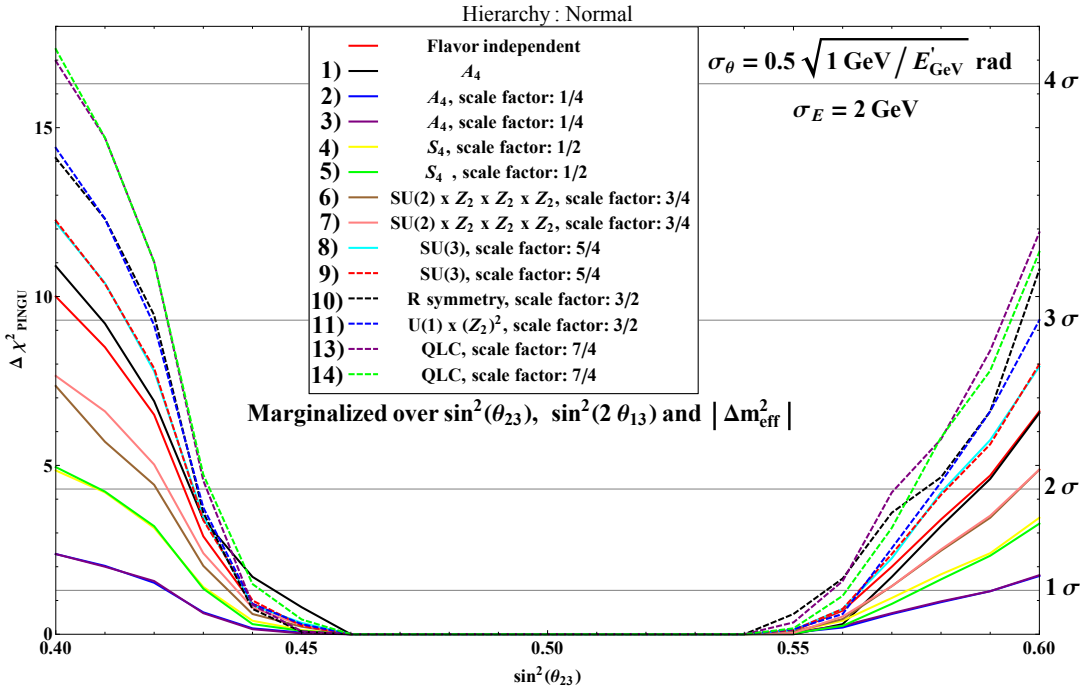

Figure 5.0.17: *Same as 5.0.15, but with a worsen energy resolution function.*

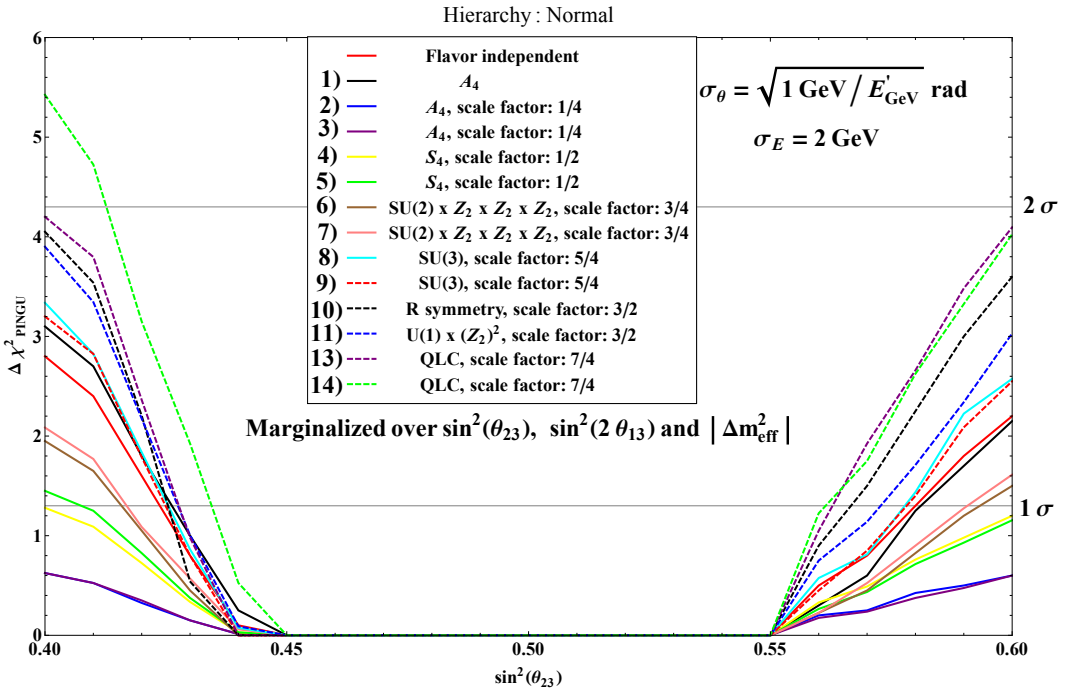

Figure 5.0.18: *Same as 5.0.15, but with both energy and angular resolution functions worsen.*

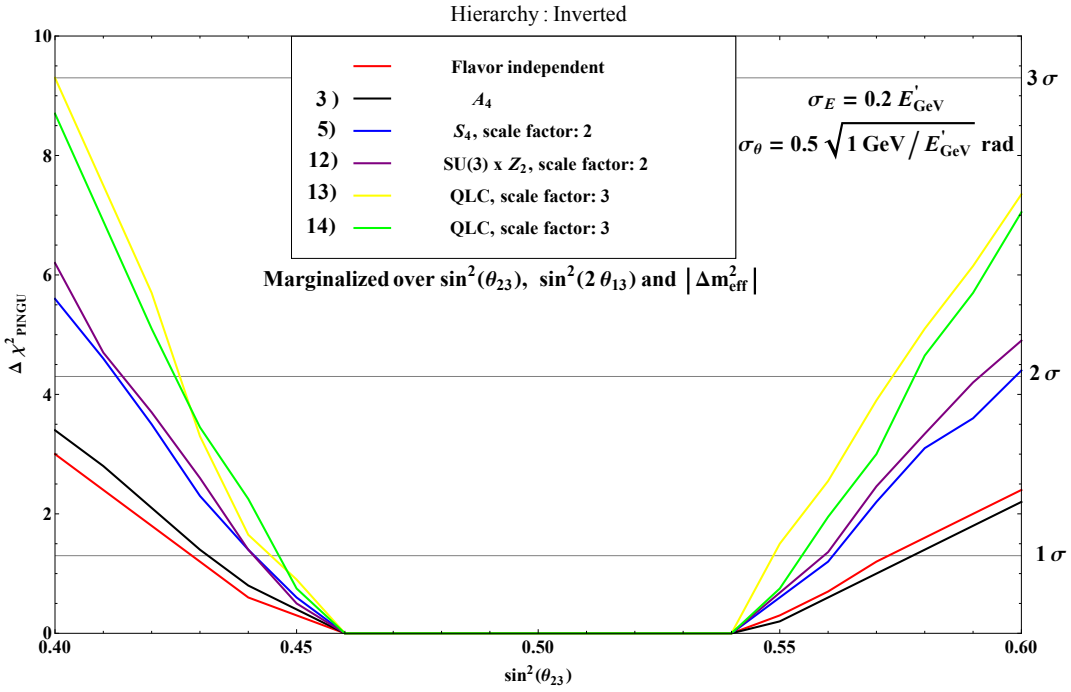

Figure 5.0.19: *Same as 5.0.15, but the true hierarchy is inverted.*

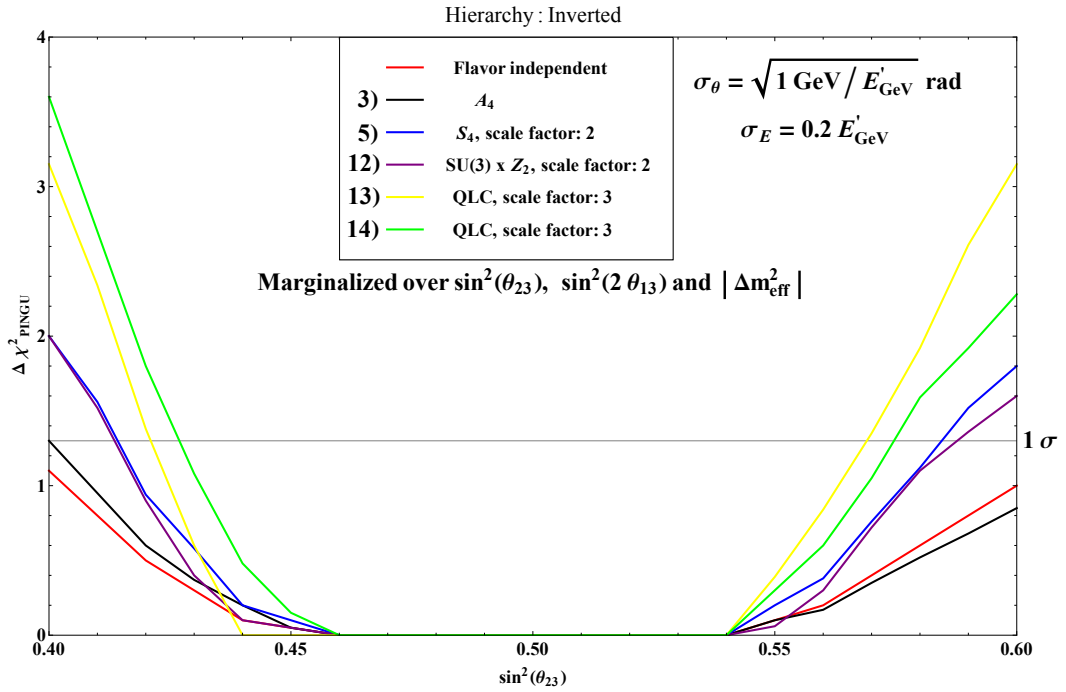

Figure 5.0.20: *Same as 5.0.19, but with a worsen angular resolution function.*

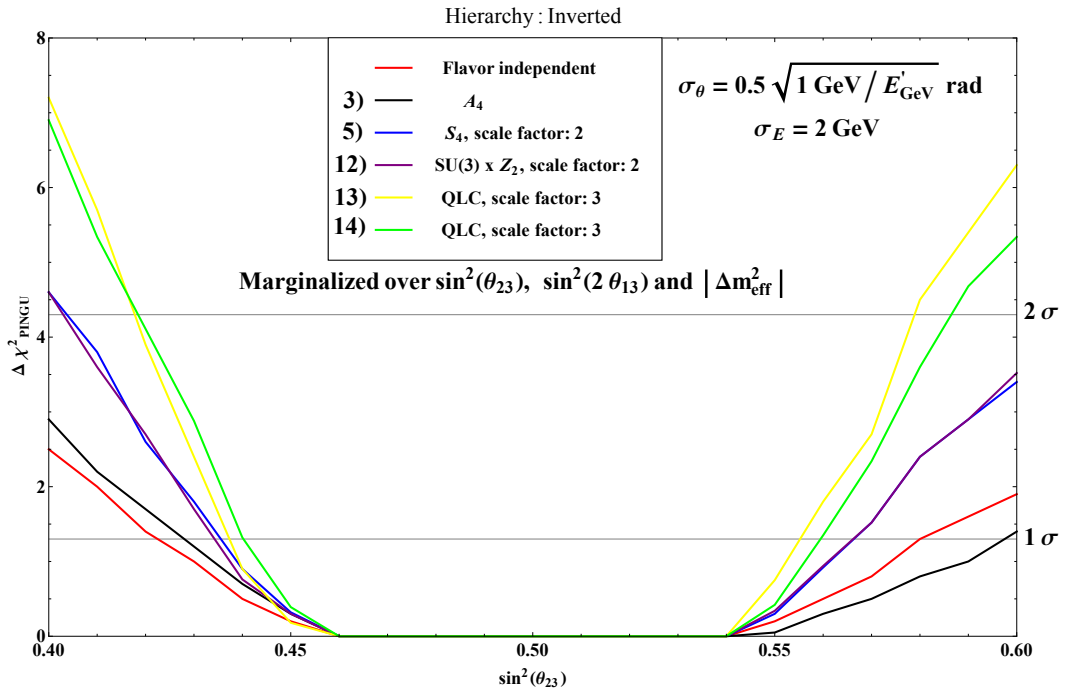

Figure 5.0.21: *Same as 5.0.19, but with a worsen energy resolution function.*

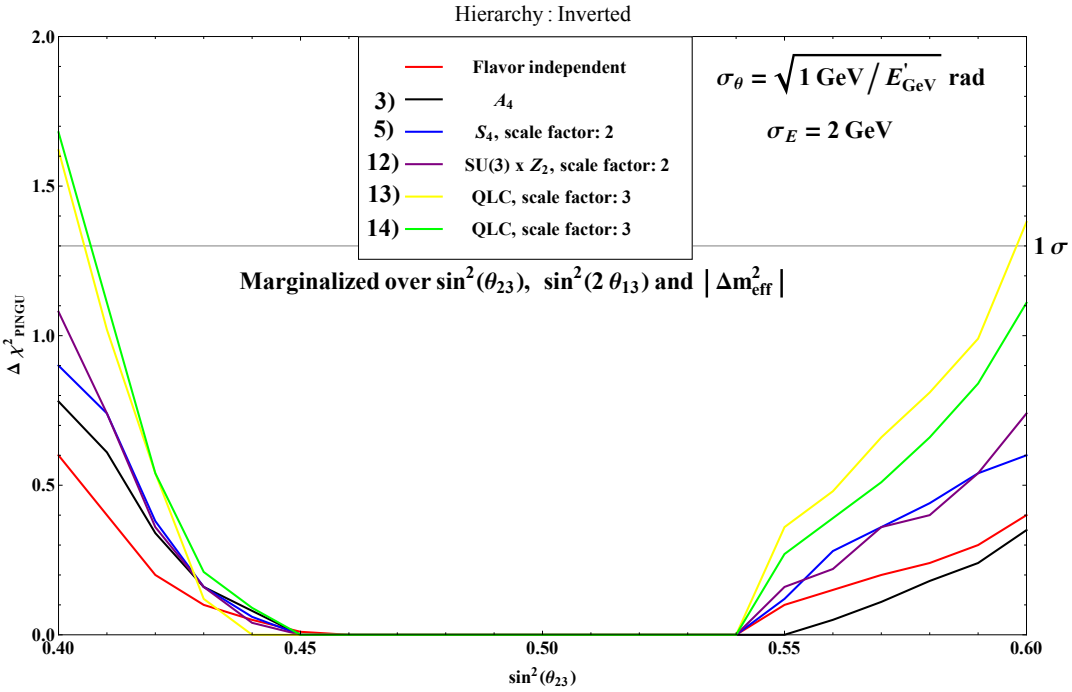

Figure 5.0.22: *Same as 5.0.19, but with both resolution functions worsen.*

F

Plots of flavour symmetries over time

These images are the same as figures 8.4.1 and 8.4.2, only larger versions for readable purpose.

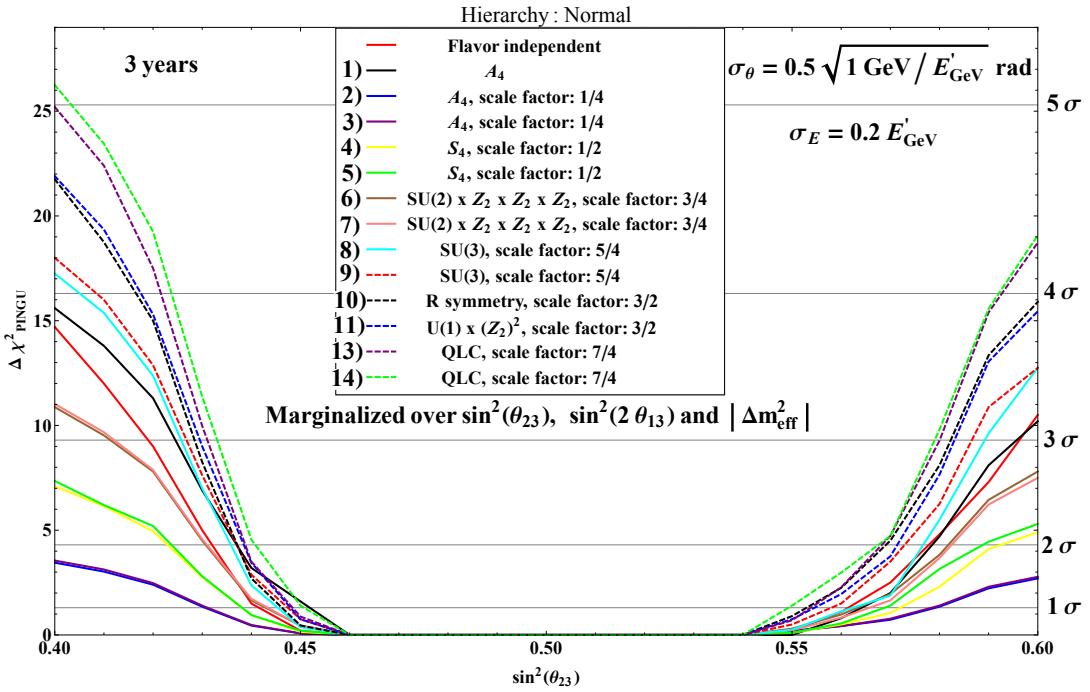

Figure 6.0.23: *$\Delta\chi^2$ for the wrong octant obtained from PINGU data for various flavour symmetries, as a function of* $\sin^2(\theta_{23})$. *This plot is for normal hierarchy taken as true and χ^2 is varied over the oscillation parameters, $|\Delta m^2_{eff}|$ and* $\sin^2(2\theta_{13})$ *in the allow range given in table 7.2.1 and* $\sin^2(\theta_{23})$ *in interval [0.4-0.6], but the mass hierarchy is held fixed to the assumed true case in the fit. The specific resolution functions are shown in the right corner whereas the number of years taken data is listed in the left corner.*

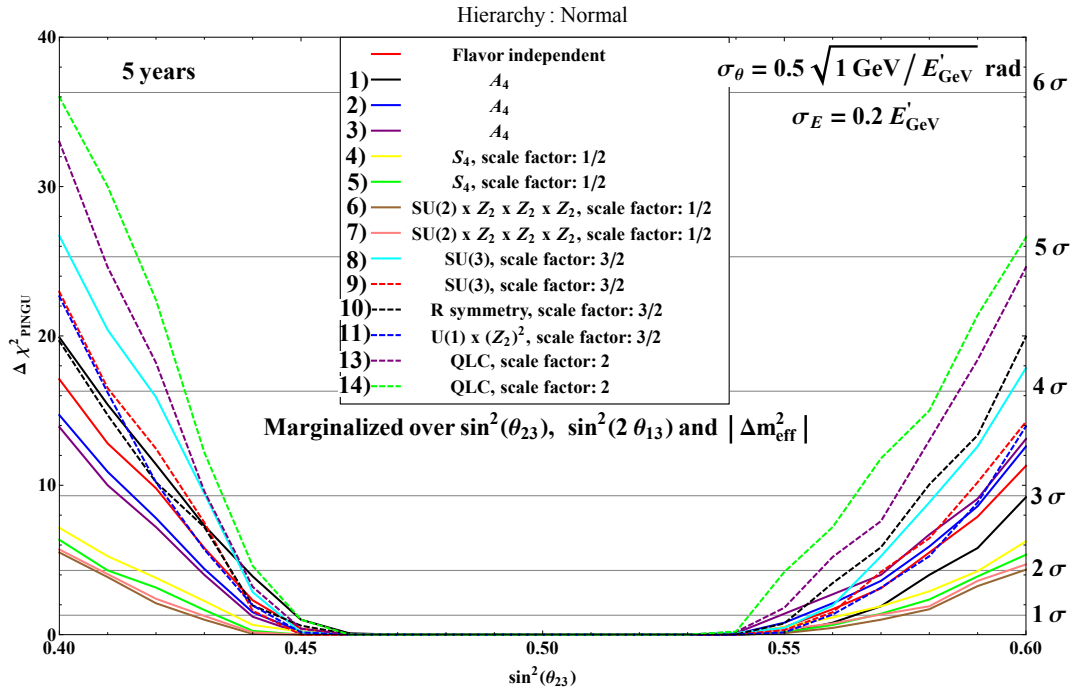

Figure 6.0.24: *Same as 6.0.23, but for 5 years of data.*

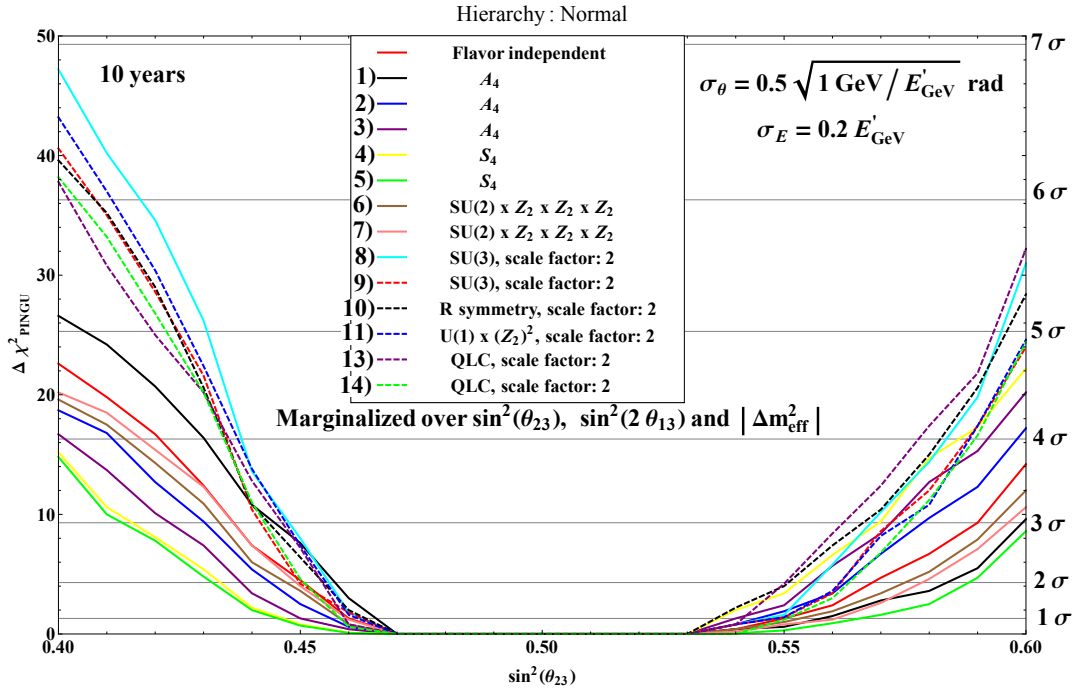

Figure 6.0.25: *Same as 6.0.23, but for 10 years of data.*

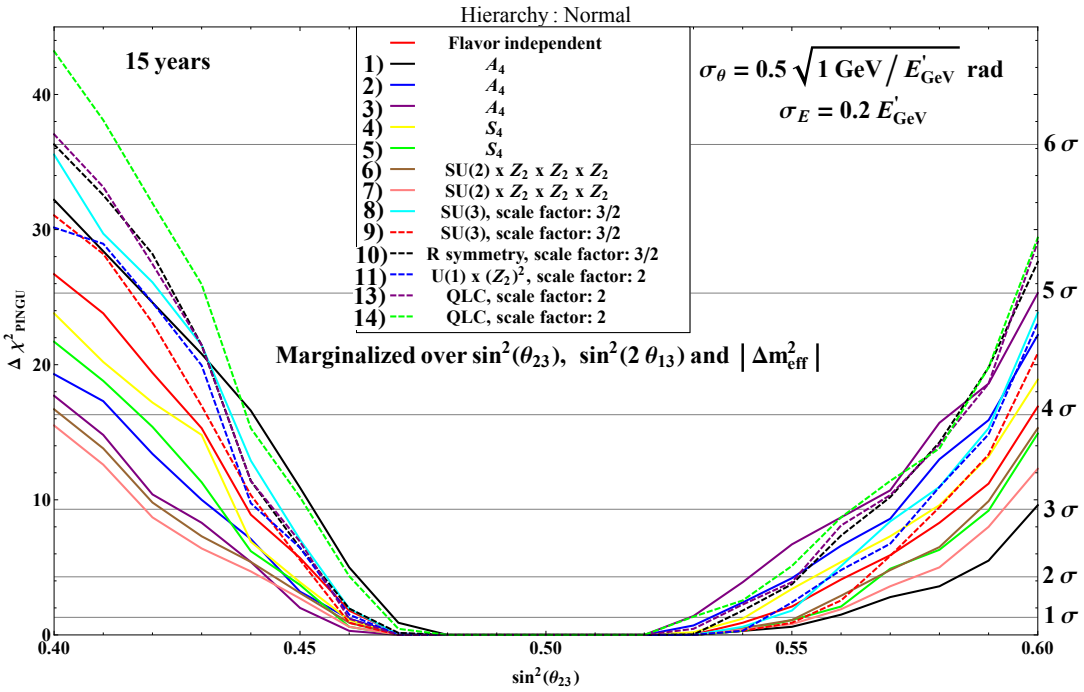

Figure 6.0.26: *Same as 6.0.23, but for 15 years of data.*

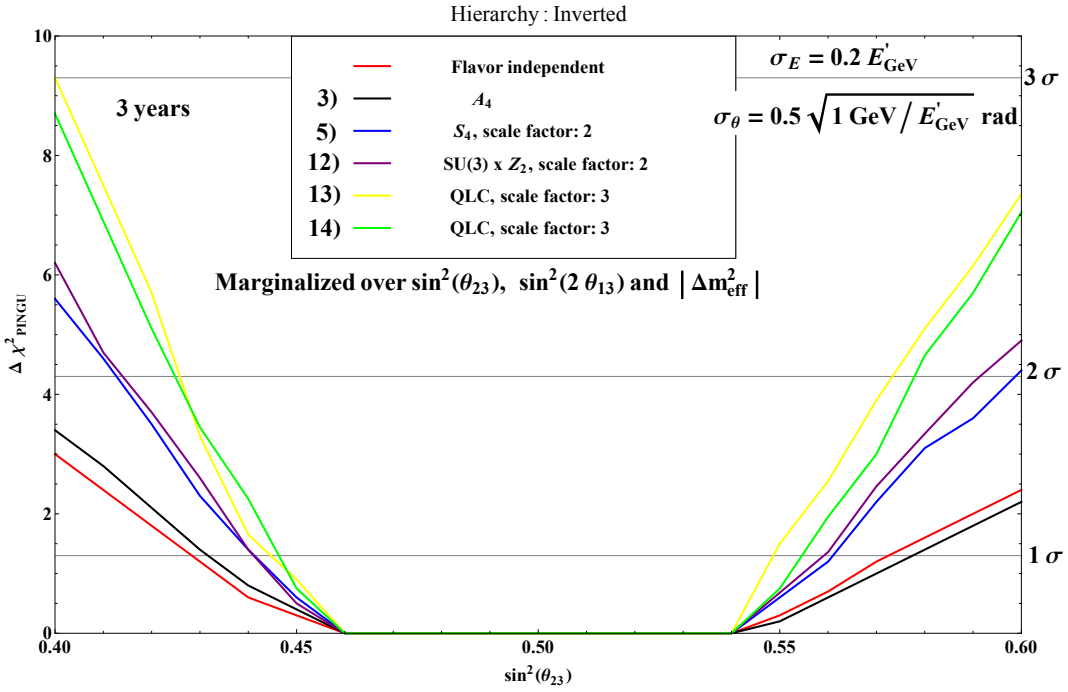

Figure 6.0.27: *Same as 6.0.23, but for inverted hierarchy.*

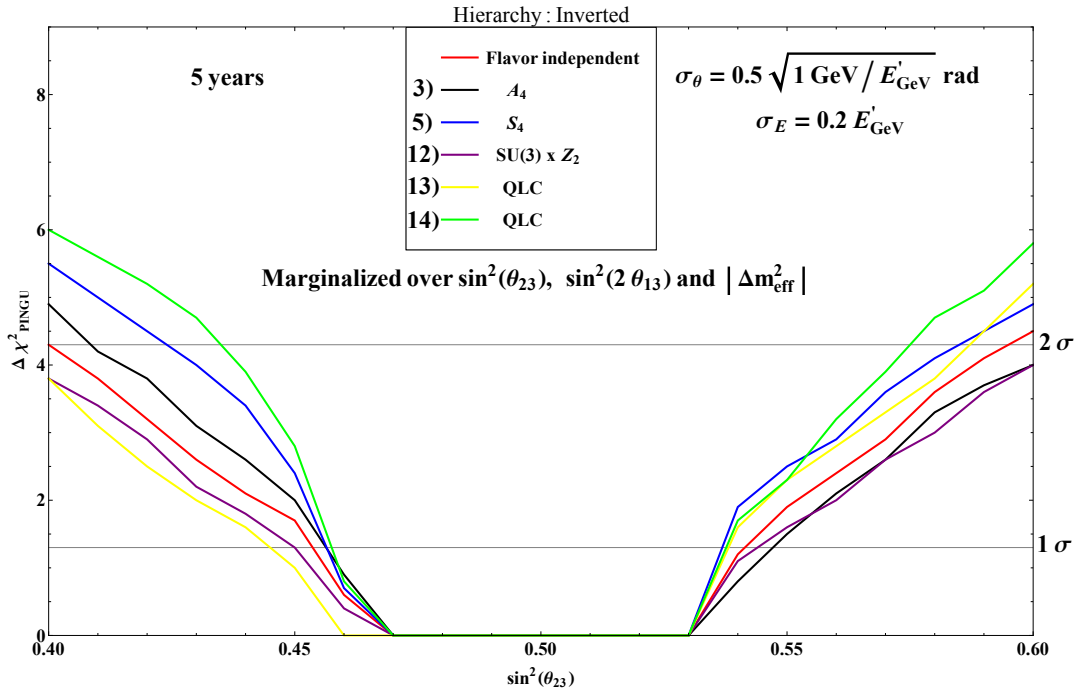

Figure 6.0.28: *Same as 6.0.27, but for 5 years of data.*

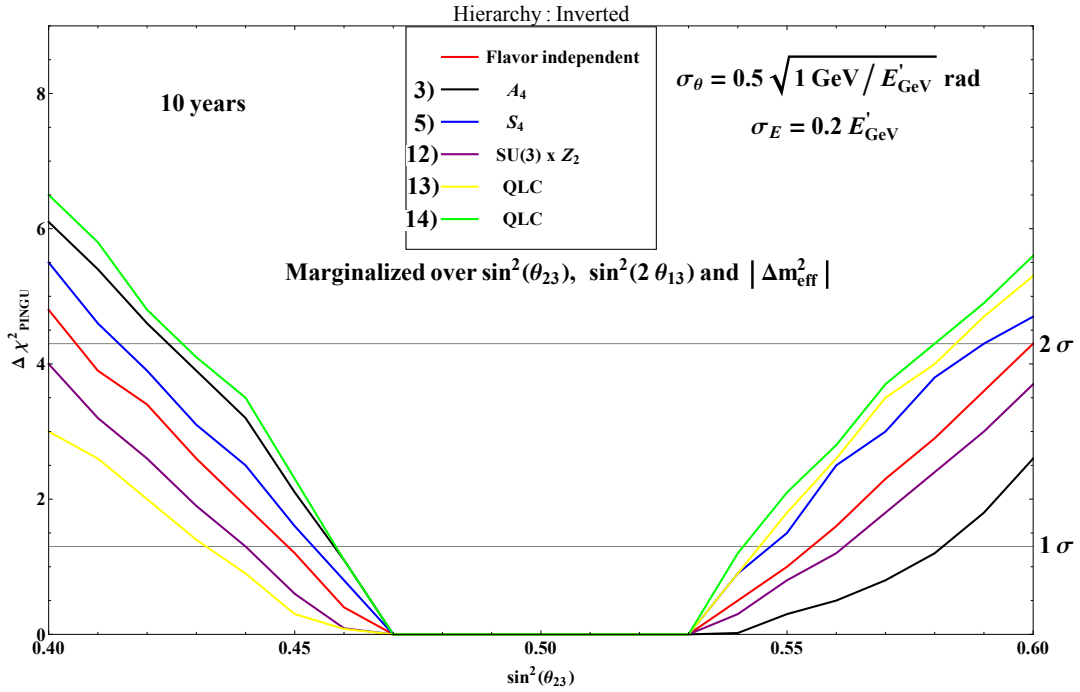

Figure 6.0.29: *Same as 6.0.27, but for 10 years of data.*

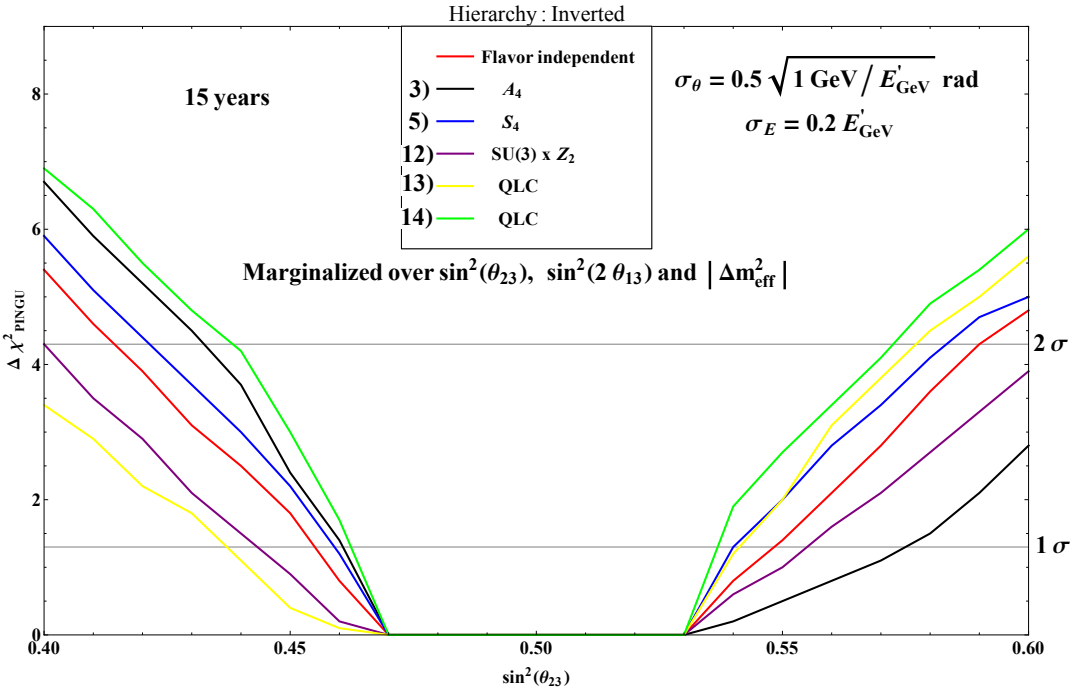

Figure 6.0.30: *Same as 6.0.27, but for 15 years of data.*

Bibliography

[1] W. Pauli *"Neutrino"*, *Cambridge Monogr. Part. Phys. Nucl. Phys Cosmol.* **14** (2000) 1.

[2] C. L. Cowan, F. Reines, F. B. Harrison, H. W. Kruse and A. D. McGuire, *"Detection of the free neutrino: A confirmation"*, *Science* **124** (1956) 103.

[3] R. Davis, D. S. Harmer and K. C. Hoffman, *"Search for Neutrinos from the Sun"*, *Phys. Rev. Lett.* **20** (1968) 1205–1209. http://link.aps.org/doi/10.1103/PhysRevLett.20.1205.

[4] **Super-Kamiokande Collaboration** Y. Fukuda *et. al.* *"Evidence for oscillation of atmospheric neutrinos"*, *Phys.Rev.Lett.* **81** (1998) 1562–1567 arXiv:hep-ex/9807003 [hep-ex].

[5] **Particle Data Group** J. Beringer *et. al.* *"Review of Particle Physics"*, *Phys. Rev. D* **86** (2012) 010001. http://link.aps.org/doi/10.1103/PhysRevD.86.010001.

[6] G. Mention, M. Fechner, T. Lasserre, T. Mueller, D. Lhuillier *et. al.* *"The Reactor Antineutrino Anomaly"*, *Phys.Rev.* **D83** (2011) 073006 arXiv:1101.2755 [hep-ex].

[7] C. Giunti, M. Laveder, Y. Li, Q. Liu and H. Long, *"Update of Short-Baseline Electron Neutrino and Antineutrino Disappearance"*, *Phys.Rev.* **D86** (2012) 113014 arXiv:1210.5715 [hep-ph].

[8] J. Abdurashitov, V. Gavrin, S. Girin, V. Gorbachev, P. Gurkina *et. al.* *"Measurement of the response of a Ga solar neutrino experiment to neutrinos from an Ar-37 source"*, *Phys.Rev.* **C73** (2006) 045805 arXiv:nucl-ex/0512041 [nucl-ex].

[9] **Collaboration for the Daya Bay** B.-Z. Hu *"New Results from the Daya Bay Reactor Neutrino Experiment"*, arXiv:1402.6439 [hep-ex].

[10] **RENO Collaboration** S.-H. Seo *"New Results from RENO"*, arXiv:1312.4111 [physics.ins-det].

[11] **Double Chooz Collaboration** Y. Abe *et. al.* *"Background-independent measurement of θ_{13} in Double Chooz"*, arXiv:1401.5981 [hep-ex].

[12] Y. G. Kudenko *"T2K observation of muon-to-electron neutrino oscillations"*, *Phys.Usp.* **56** (2014) 1120–1125.

[13] **MINOS Collaboration** P. Adamson *et. al.* *"Combined analysis of ν_μ disappearance and $\nu_\mu \to \nu_e$ appearance in MINOS using accelerator and atmospheric neutrinos"*, arXiv:1403.0867 [hep-ex].

[14] H. Minakata *"Phenomenology of future neutrino experiments with large Theta(13)"*, *Nucl.Phys.Proc.Suppl.* **235-236** (2013) 173–179 arXiv:1209.1690 [hep-ph].

[15] **IceCube-PINGU Collaboration** M. Aartsen *et. al.* *"Letter of Intent: The Precision IceCube Next Generation Upgrade (PINGU)"*, arXiv:1401.2046 [physics.ins-det].

[16] K. B. M. Mahn and M. H. Shaevitz, *"Comparisons and combinations of reactor and long-baseline neutrino oscillation measurements"*, *Int.J.Mod.Phys.* **A21** (2006) 3825–3844 arXiv:hep-ex/0409028 [hep-ex].

[17] A. Chatterjee, P. Ghoshal, S. Goswami and S. K. Raut, *"Octant sensitivity for large theta(13) in atmospheric and long baseline neutrino experiments"*, *JHEP* **1306** (2013) 010 arXiv:1302.1370 [hep-ph].

[18] S. K. Agarwalla, S. Prakash and S. U. Sankar, *"Resolving the octant of theta23 with T2K and NOvA"*, *JHEP* **1307** (2013) 131 arXiv:1301.2574 [hep-ph].

[19] E. K. Akhmedov, S. Razzaque and A. Y. Smirnov, *"Mass hierarchy, 2-3 mixing and CP-phase with Huge Atmospheric Neutrino Detectors"*, *JHEP* **1302** (2013) 082 arXiv:1205.7071 [hep-ph].

[20] E. Fermi *Z Physik* **88** (1934) 161.

[21] http://quest.ph.utexas.edu/Reviews/VA/VA.pdf.

[22] H. Goldstein, C. P. Poole and J. L. Safko, *"Classical Mechanics"*, .

[23] **ATLAS Collaboration** G. Aad *et. al.* *"Observation of a new particle in the search for the Standard Model Higgs boson with the ATLAS detector at the LHC"*, *Phys.Lett.* **B716** (2012) 1–29 arXiv:1207.7214 [hep-ex].

[24] **ATLAS Collaboration** G. Aad *et. al.* *"Evidence for the spin-0 nature of the Higgs boson using ATLAS data"*, *Phys.Lett.* **B726** (2013) 120–144 arXiv:1307.1432 [hep-ex].

[25] **CMS Collaboration** S. Chatrchyan *et. al.* *"Observation of a new boson at a mass of 125 GeV with the CMS experiment at the LHC"*, *Phys.Lett.* **B716** (2012) 30–61 arXiv:1207.7235 [hep-ex].

[26] V. Novikov, L. Okun, A. N. Rozanov and M. Vysotsky, *"Theory of Z boson decays"*, *Rept.Prog.Phys.* **62** (1999) 1275–1332 arXiv:hep-ph/9906465 [hep-ph].

[27] P. Langacker *"The Standard Model and Beyond"*, .

[28] S. M. Bilenky *"Bruno Pontecorvo and Neutrino Oscillations"*, *Advances in High Energy Physics* **vol. 2013** (2013) ID 873236 9. http://www.hindawi.com/journals/ahep/2013/873236/cta/.

[29] P. B. Pal *"Dirac, Majorana and Weyl fermions"*, *Am. J. Phys.* **79** (2011) 485–498 arXiv:1006.1718 [hep-ph].

[30] E. Ma *"Neutrino Mass: Mechanisms and Models"*, arXiv:0905.0221 [hep-ph].

[31] S. F. King and C. Luhn, *"Neutrino Mass and Mixing with Discrete Symmetry"*, *Rept.Prog.Phys.* **76** (2013) 056201 arXiv:1301.1340 [hep-ph].

[32] S. M. Boucenna, S. Morisi and J. W. F. Valle, *"The low-scale approach to neutrino masses"*, arXiv:1404.3751 [hep-ph].

[33] W. Winter *"Lectures on neutrino phenomenology"*, *Nucl.Phys.Proc.Suppl.* **203-204** (2010) 45–81 arXiv:1004.4160 [hep-ph].

[34] **MINOS Collaboration** P. Adamson *et. al.* *"Measurement of Neutrino and Antineutrino Oscillations Using Beam and Atmospheric Data in MINOS"*, *Phys.Rev.Lett.* **110** (2013) 251801 arXiv:1304.6335 [hep-ex].

[35] **KamLAND Collaboration** K. Eguchi *et. al.* *"First results from KamLAND: Evidence for reactor anti-neutrino disappearance"*, *Phys.Rev.Lett.* **90** (2003) 021802 arXiv:hep-ex/0212021 [hep-ex].

[36] **Super-Kamiokande Collaboration** Y. Takeuchi *"Results from Super-Kamiokande"*, *Nucl.Phys.Proc.Supl.* **229-232** (2012) 79–84 arXiv:1112.3425 [hep-ex].

[37] **SNO Collaboration** A. W. Poon *"Solving the solar neutrino problem 2 km underground: The Sudbury neutrino observatory"*, arXiv:nucl-ex/0312001 [nucl-ex].

[38] J. Linder *"Derivation of neutrino matter potentials induced by earth"*, *Am.J.Phys.* (2005) arXiv:hep-ph/0504264 [hep-ph].

[39] G. Bellini, L. Ludhova, G. Ranucci and F. Villante, *"Neutrino oscillations"*, *Advances in High Energy Physics* (2013) 191960 arXiv:1310.7858 [hep-ph].

[40] H. Zaglauer and K. Schwarzer, *"The mixing angles in matter for three generations of neutrinos and the MSW mechanism"*, *Z. Phys. C - Particles and Fields* **40** (1998) 2 273–282. http://dx.doi.org/10.1007/BF01555889.

[41] T. Kuo and J. Pantaleone, *"Neutrino oscillations in matter"*, *Rev. Mod. Phys.* **61** (1989) 937.

[42] J. B. et al. (Particle Data Group) *Phys. Rev.* **D86** (2012) 010001. http://pdg.lbl.gov.

[43] http://www.int.washington.edu/PHYS554/2011/chapter9_11.pdf.

[44] T. Gaisser and M. Honda, *"Flux of atmospheric neutrinos"*, *Ann.Rev.Nucl.Part.Sci.* **52** (2002) 153–199 arXiv:hep-ph/0203272 [hep-ph].

[45] V. Agrawal, T. K. Gaisser, P. Lipari and T. Stanev, *"Atmospheric neutrino flux above 1 GeV"*, *Phys. Rev. D* **53** (1996) 3 1314–1323. http://link.aps.org/doi/10.1103/PhysRevD.53.1314.

[46] S. Tavernier *"Experimental techniques in nuclear and particle physics - springer"*, .

[47] M. Honda, T. Kajita, K. Kasahara and S. Midorikawa, *"Improvement of low energy atmospheric neutrino flux calculation using the JAM nuclear interaction model"*, *Phys.Rev.* **D83** (2011) 123001 arXiv:1102.2688 [astro-ph.HE].

[48] T. K. Gaisser *"Cosmic rays and particle physics"*, .

[49] Y. Pal and B. Peters, *"Meson production at high energies and the propagation of cosmic rays through the atmosphere"*, *Mat. Fys. Medd. Dan. Vid. Selsk.* **33** (1964) 15. http://www.sdu.dk/media/bibpdf/Bind%2030-39%5CBind%5Cmfm-33-15.pdf.

[50] J. Formaggio and G. Zeller, *"From eV to EeV: Neutrino Cross Sections Across Energy Scales"*, *Rev.Mod.Phys.* **84** (2012) 1307 arXiv:1305.7513 [hep-ex].

[51] A. M. Dziewonski and D. L. Anderson, *"Preliminary reference Earth model"*, *Physics of the Earth and Planetary Interiors* **25** (1981) 4 297 – 356. "http://www.sciencedirect.com/science/article/pii/0031920181900467.

[52] E. K. Akhmedov, M. Maltoni and A. Y. Smirnov, *"1-3 leptonic mixing and the neutrino oscillograms of the Earth"*, *JHEP* **0705** (2007) 077 arXiv:hep-ph/0612285 [hep-ph].

[53] S. Choubey and A. Ghosh, *"Determining the Octant of θ_{23} with PINGU, T2K, NOνA and Reactor Data"*, *JHEP* **1311** (2013) 166 arXiv:1309.5760 [hep-ph].

[54] A. Ghosh and S. Choubey, *"Measuring the Mass Hierarchy with Muon and Hadron Events in Atmospheric Neutrino Experiments"*, *JHEP* **1310** (2013) 174 arXiv:1306.1423 [hep-ph].

[55] A. Ghosh, T. Thakore and S. Choubey, *"Determining the Neutrino Mass Hierarchy with INO, T2K, NOvA and Reactor Experiments"*, *JHEP* **1304** (2013) 009 arXiv:1212.1305 [hep-ph].

[56] R. Gandhi, P. Ghoshal, S. Goswami and S. U. Sankar, *"Mass hierarchy determination for $\theta_{13} = 0$ and atmospheric neutrinos"*, *Mod.Phys.Lett.* **A25** (2010) 2255–2266 arXiv:0905.2382 [hep-ph].

[57] H. Nunokawa, S. J. Parke and R. Zukanovich Funchal, *"Another possible way to determine the neutrino mass hierarchy"*, *Phys.Rev.* **D72** (2005) 013009 arXiv:hep-ph/0503283 [hep-ph].

[58] M. Ghosh, P. Ghoshal, S. Goswami and S. K. Raut, *"Can atmospheric neutrino experiments provide the first hint of leptonic CP violation?"*, *Phys.Rev.* **D89** (2014) 011301 arXiv:1306.2500 [hep-ph].

[59] M. Sajjad Athar, M. Honda, T. Kajita, K. Kasahara and S. Midorikawa, *"Atmospheric neutrino flux at INO, South Pole and Pyhäsalmi"*, *Phys.Lett.* **B718** (2013) 1375–1380 arXiv:1210.5154 [hep-ph].

[60] W. Winter *"Neutrino mass hierarchy determination with IceCube-PINGU"*, *Phys.Rev.* **D88** (2013) 1, 013013 arXiv:1305.5539 [hep-ph].

[61] M. Blennow and T. Schwetz, *"Determination of the neutrino mass ordering by combining PINGU and Daya Bay II"*, *JHEP* **1309** (2013) 089 arXiv:1306.3988 [hep-ph].

[62] **IceCube and PINGU** M. Aartsen *et. al.* *"PINGU Sensitivity to the Neutrino Mass Hierarchy"*, *ArXiv e-prints* (2013) arXiv:1306.5846 [astro-ph.IM].

[63] D. Cowen *"talk at Snowmass Cosmic Frontier Workshop"*, . https://indico.fnal.gov/getFile.py/access?contribId=89&sessionId=52&resId=0&materialId=slides&confId=6199.

[64] M. M. Devi, T. Thakore, S. K. Agarwalla and A. Dighe, *"Enhancing sensitivity to neutrino parameters at INO combining muon and hadron information"*, arXiv:1406.3689 [hep-ph].

[65] D. Forero, M. Tortola and J. Valle, *"Neutrino oscillations refitted"*, arXiv:1405.7540 [hep-ph].

[66] **IceCube Collaboration** M. Aartsen *et. al.* *"Measurement of the Atmospheric ν_e flux in IceCube"*, *Phys.Rev.Lett.* **110** (2013) 15, 151105 arXiv:1212.4760 [hep-ex].

[67] *"Private talk: ic79 ν_μ flux"*, .

[68] A. Schukraft *"Search for a diffuse neutrino flux with IceCube"*, *Master thesis* (2013). http://darwin.bth.rwth-aachen.de/opus3/volltexte/2013/4689/pdf/4689.pdf.

[69] **The IceCube Collaboration** M. Aartsen *et. al.* *"Search for a diffuse flux of astrophysical muon neutrinos with the IceCube 59-string configuration"*, *Phys.Rev.* **D89** (2014) 062007 arXiv:1311.7048 [astro-ph.HE].

[70] http://genie.hepforge.org/manuals/GENIE_PhysicsAndUserManual_20130615.pdf.

[71] http://www.genie-mc.org/.

[72] C. Andreopoulos, A. Bell, D. Bhattacharya, F. Cavanna, J. Dobson *et. al.* *"The GENIE Neutrino Monte Carlo Generator"*, *Nucl.Instrum.Meth.* **A614** (2010) 87–104 arXiv:0905.2517 [hep-ph].

[73] F. Capozzi, G. Fogli, E. Lisi, A. Marrone, D. Montanino *et. al.* *"Status of three-neutrino oscillation parameters, circa 2013"*, arXiv:1312.2878 [hep-ph].

[74] **MINOS Collaboration** P. Adamson *et. al.* *"Measurement of the neutrino mass splitting and flavor mixing by MINOS"*, *Phys.Rev.Lett.* **106** (2011) 181801 arXiv:1103.0340 [hep-ex].

[75] http://www-numi.fnal.gov/PublicInfo/forscientists.html.

[76] **T2K Collaboration** K. Abe *et. al.* *"Measurement of Neutrino Oscillation Parameters from Muon Neutrino Disappearance with an Off-axis Beam"*, *Phys.Rev.Lett.* **111** (2013) 211803 arXiv:1308.0465 [hep-ex].

[77] S. F. King, A. Merle, S. Morisi, Y. Shimizu and M. Tanimoto, *"Neutrino Mass and Mixing: from Theory to Experiment"*, arXiv:1402.4271 [hep-ph].

[78] E. K. Akhmedov, R. Johansson, M. Lindner, T. Ohlsson and T. Schwetz, *"Series expansions for three flavor neutrino oscillation probabilities in matter"*, *JHEP* **0404** (2004) 078 arXiv:hep-ph/0402175 [hep-ph].

[79] P. Ramond *"Group theory: A physicist's survey"*, .

[80] M. Holthausen, K. S. Lim and M. Lindner, *"Lepton Mixing Patterns from a Scan of Finite Discrete Groups"*, *Phys.Lett.* **B721** (2013) 61–67 arXiv:1212.2411 [hep-ph].

[81] https://openaccess.leidenuniv.nl/bitstream/handle/1887/18506/03.pdf?sequence=10.

[82] P. Harrison, D. Perkins and W. Scott, *"Tri-bimaximal mixing and the neutrino oscillation data"*, *Phys.Lett.* **B530** (2002) 167 arXiv:hep-ph/0202074 [hep-ph].

[83] C. I. Low and R. R. Volkas, *"Tri-bimaximal mixing, discrete family symmetries, and a conjecture connecting the quark and lepton mixing matrices"*, *Phys.Rev.* **D68** (2003) 033007 arXiv:hep-ph/0305243 [hep-ph].

[84] G. Altarelli and F. Feruglio, *"Tri-bimaximal neutrino mixing from discrete symmetry in extra dimensions"*, *Nucl.Phys.* **B720** (2005) 64–88 arXiv:hep-ph/0504165 [hep-ph].

[85] G. Altarelli *"Lectures on models of neutrino masses and mixings"*, arXiv:0711.0161 [hep-ph].

[86] C. H. Albright *"Overview of Neutrino Mixing Models and Ways to Differentiate among Them"*, arXiv:0905.0146 [hep-ph].

[87] M. Gonzalez-Garcia, M. Maltoni, J. Salvado and T. Schwetz, *"Global fit to three neutrino mixing: critical look at present precision"*, *JHEP* **1212** (2012) 123 arXiv:1209.3023 [hep-ph].

[88] D. Forero, M. Tortola and J. Valle, *"Global status of neutrino oscillation parameters after Neutrino-2012"*, *Phys.Rev.* **D86** (2012) 073012 arXiv:1205.4018 [hep-ph].

[89] B. Adhikary and A. Ghosal, *"Constraining CP violation in a softly broken A4 symmetric model"*, *Phys. Rev. D* **75** (2007) 073020. http://link.aps.org/doi/10.1103/PhysRevD.75.073020.

[90] R. G. Moorhouse *"Fermion masses from SO(10) Hermitian matrices"*, *Phys. Rev. D* **77** (2008) 053006. http://link.aps.org/doi/10.1103/PhysRevD.77.053006.

[91] Y. Ahn, S. K. Kang and C. Kim, *"Spontaneous CP Violation in A_4 Flavor Symmetry and Leptogenesis"*, *Phys.Rev.* **D87** (2013) 11, 113012 arXiv:1304.0921 [hep-ph].

[92] H. Zhang *"Flavor S(4) x Z(2) symmetry and neutrino mixing"*, *Phys.Lett.* **B655** (2007) 132–140 arXiv:hep-ph/0612214 [hep-ph].

[93] C. Luhn *"Trimaximal TM_1 neutrino mixing in S_4 with spontaneous CP violation"*, *Nucl.Phys.* **B875** (2013) 80–100 arXiv:1306.2358 [hep-ph].

[94] M.-C. Chen and K. Mahanthappa, *"Fermion masses and neutrino oscillations in SO(10) x SU(2)(F)"*, arXiv:hep-ph/0409165 [hep-ph].

[95] S. Bertolini and M. Malinsky, *"On CP violation in minimal renormalizable SUSY SO(10) and beyond"*, *Phys.Rev.* **D72** (2005) 055021 arXiv:hep-ph/0504241 [hep-ph].

[96] I. de Medeiros Varzielas and G. G. Ross, *"SU(3) family symmetry and neutrino bi-tri-maximal mixing"*, *Nucl.Phys.* **B733** (2006) 31–47 arXiv:hep-ph/0507176 [hep-ph].

[97] Z. Berezhiani and F. Nesti, *"Supersymmetric SO(10) for fermion masses and mixings: Rank-1 structures of flavor"*, *JHEP* **0603** (2006) 041 arXiv:hep-ph/0510011 [hep-ph].

[98] Q. Shafi and Z. Tavartkiladze, *"Supersymmetric SO(10) and a prediction for θ_{13}"*, *Physics Letters B* **633** (2006) 4 595. http://www.sciencedirect.com/science/article/pii/S0370269305018125.

[99] X.-d. Ji, Y.-c. Li and R. Mohapatra, *"An SO(10) GUT model with lopsided mass matrix and neutrino mixing angle θ_{13}"*, *Phys.Lett.* **B633** (2006) 755–760 arXiv:hep-ph/0510353 [hep-ph].

[100] B. Stech and Z. Tavartkiladze, *"Generation symmetry and E6 unification"*, *Phys. Rev. D* **77** (2008) 076009. http://link.aps.org/doi/10.1103/PhysRevD.77.076009.

[101] J. Harada *"Non-maximal θ_{23}, large θ_{13} and tri-bimaximal θ_{12} via quark-lepton complementarity at next-to-leading order"*, *Europhys.Lett.* **103** (2013) 21001 arXiv:1304.4526 [hep-ph].

[102] Y. Koide and H. Nishiura, *"Possible Deviation from Exact Tribimaximal Mixing"*, *Phys.Lett.* **B669** (2008) 24–27 arXiv:0808.0370 [hep-ph].